XVIII IAG/USP Advanced School on Astrophysics: Observational Strategies for Exoplanet Science

Andrew Szentgyorgyi
Harvard-Smithsonian Center for Astrophysics

Universidad de Sao Paulo, 26 Feb 2018

Introduction

Observational Techniques for Exoplanet Science

- Astronomy is an observational science – what we see depend on how we look at things
- Available methods for discovering and characterizing exoplanets:
  - Precise radial velocity (PRV) technique (Spectroscopy / Indirect)
  - Transit technique (Photometry / Indirect)
  - Transit timing variations
  - Microlensing
  - Direct imaging (Adaptive optic coronography / Direct)
  - Astrometry
  - Pulsar timing
  - Eclipsing binaries

Techniques likely to be used on the GMT

- The field is currently dominated by PRV and transit technique
  - PRV measures exoplanet mass (*m*) and orbital eccentricity.
  - Actually Sin (*i*)×m product, where *i* is inclination angle of orbit.
  - Transit measures exoplanet radius (*R*) and determines *i.*
  - Inclination might potentially be measured by astrometry
  - The "best" exoplanets are those where mass and radius are both measureable → yield the density of the exoplanet.
  - At present, *R* can only be measured by the transit method.
  - If PRV & transit measurements are possible, *m,* orbital elements & *R* are known.

The Precision Radial Velocity (PRV) Technique

The PRV Method

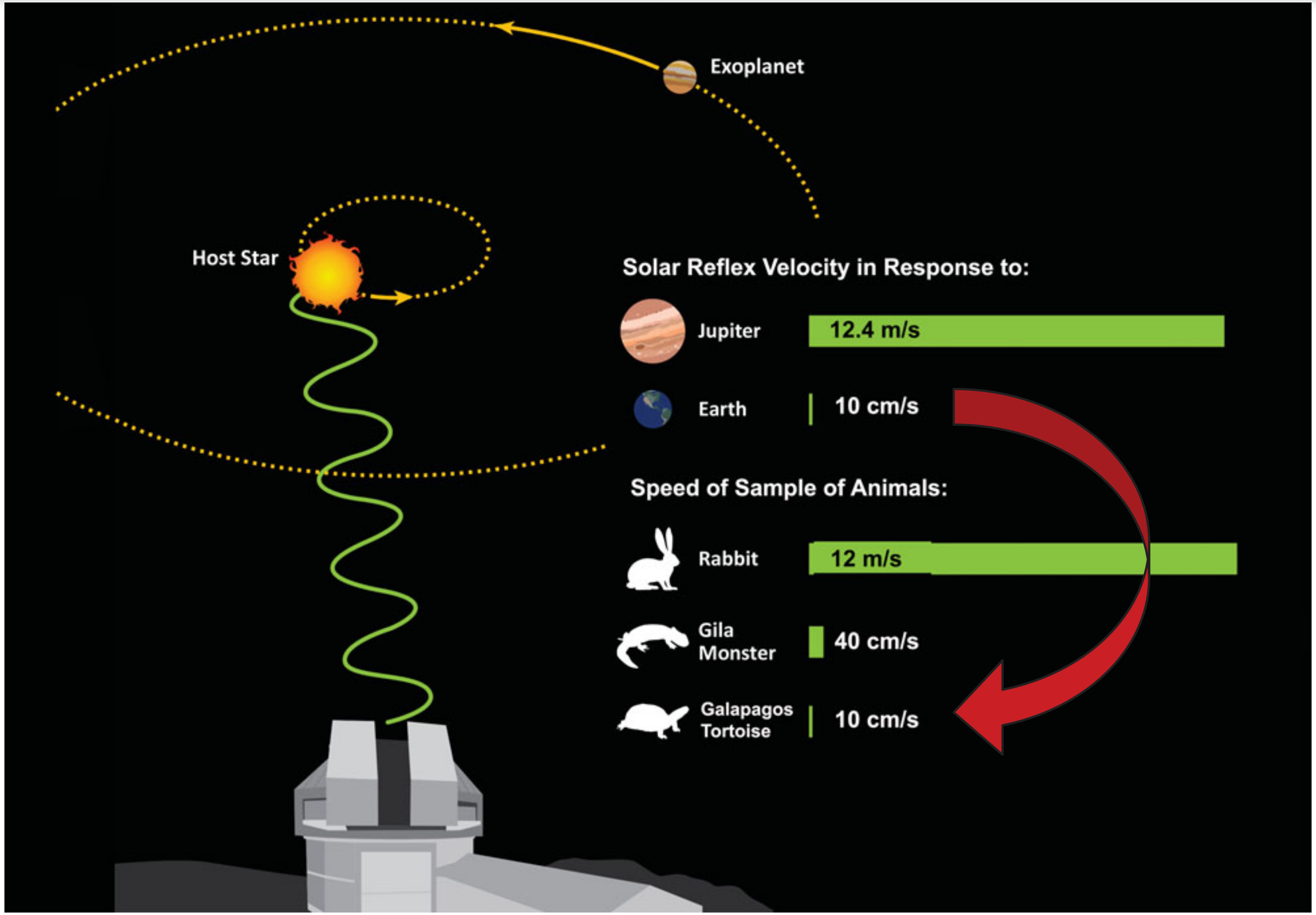

- A star and planet orbit their common barycenter
- Stars re much more massive than planets, so the reflex motion of the star is very small.

How Fast is 10 cm/sec?

The PRV Method

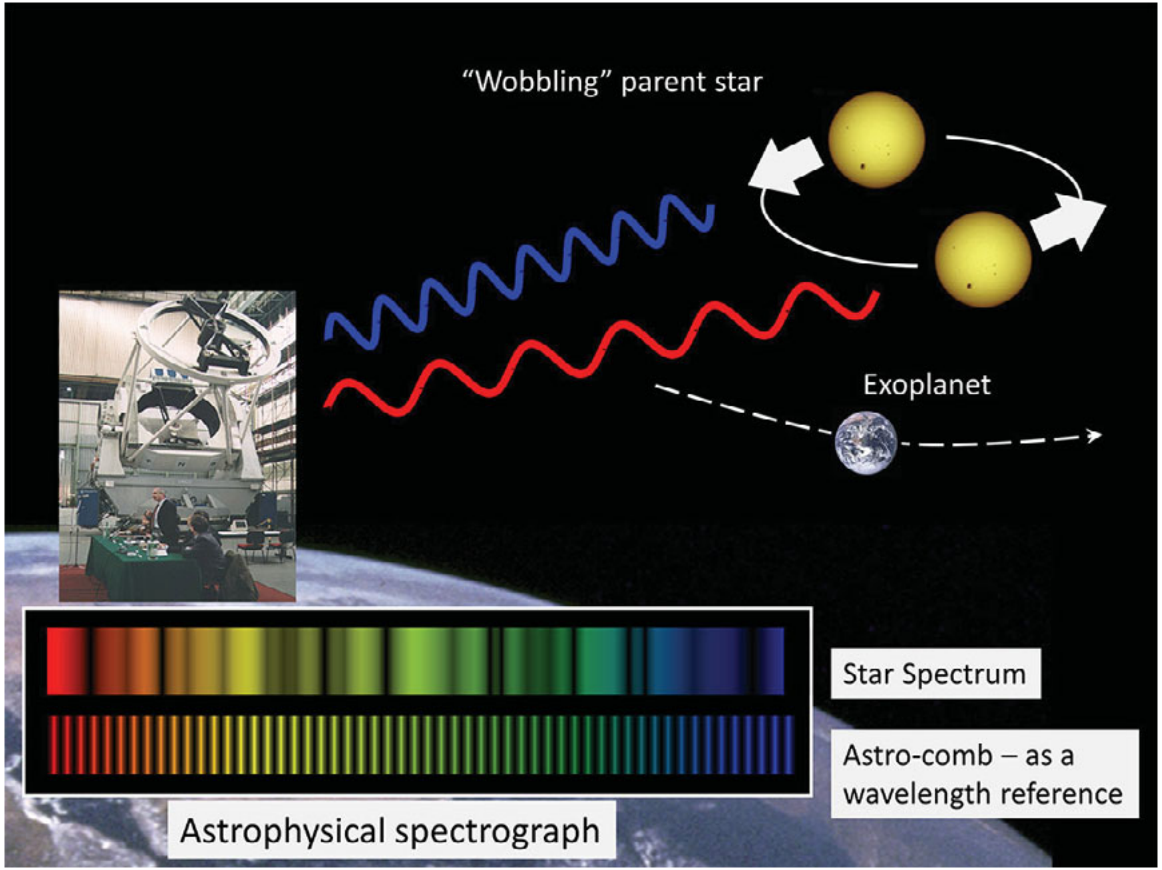

- The PRV method is indirect
- The Doppler shift is very small, ~ a shift of 1 silicon atom diameter for 10 cm/sec
  - Requires ultrastable instrumentation and exquisite wavelength calibrators

The PRV Method – The Movie

The PRV Method – The Movie

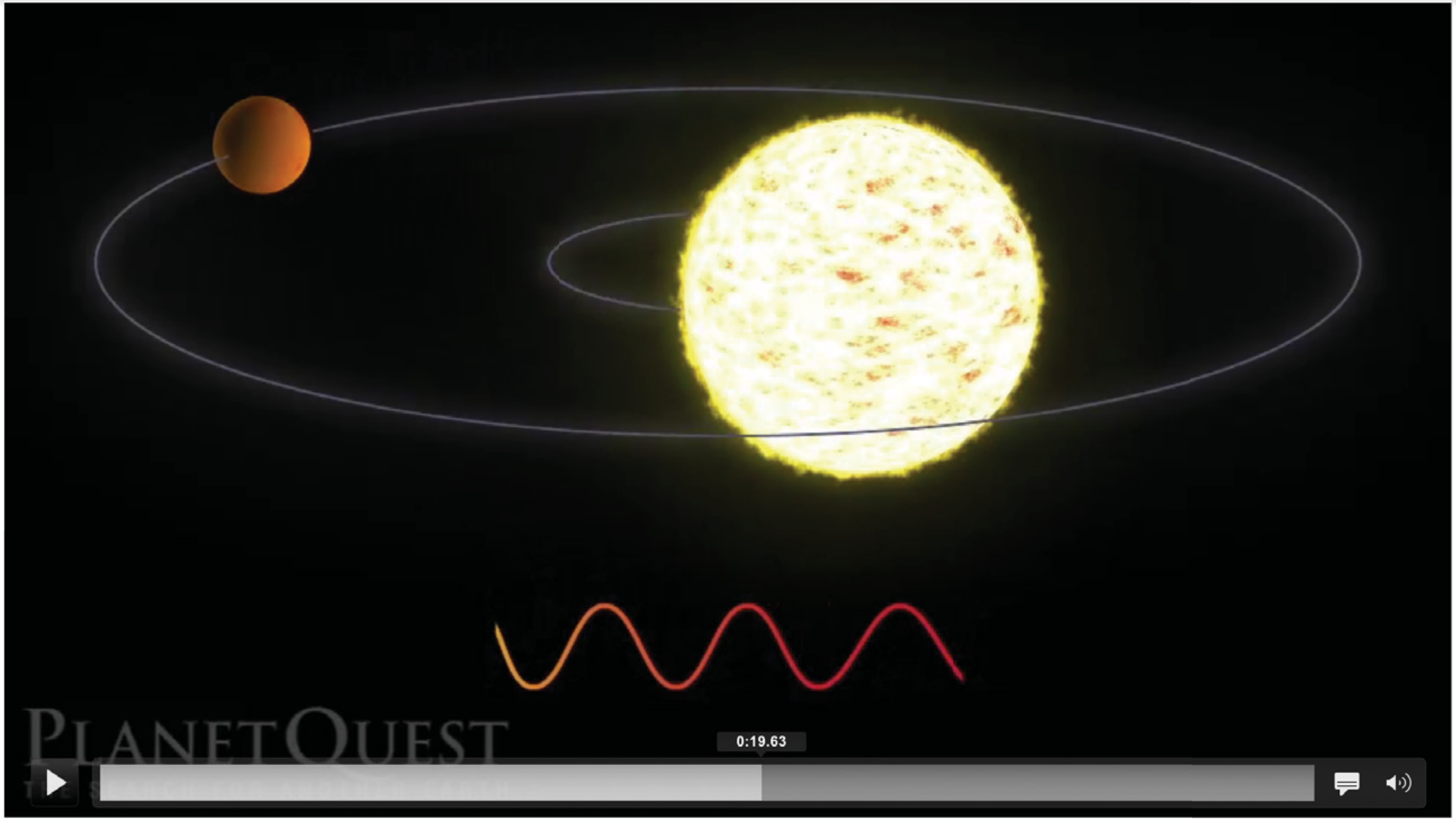

m Sin(i) Degeneracy

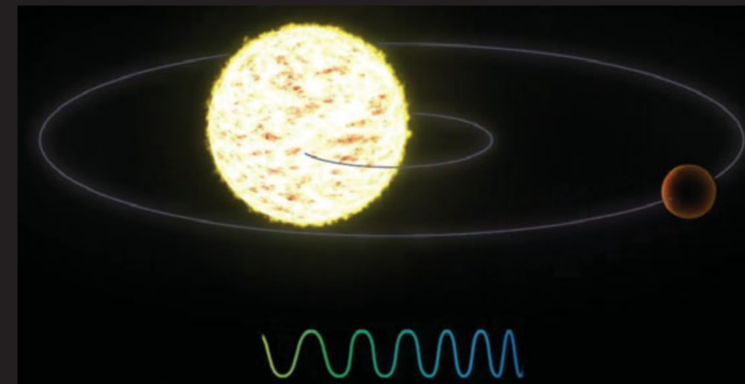

No mass determination
i = 0, m Sin(i) = 0

Ambiguous
mass determination
i = ?, m Sin(i) = ?

Ideal mass determination
i ~ 90°, m Sin(i) ~ m

Some Stellar Types Are Better for PRV Than Other

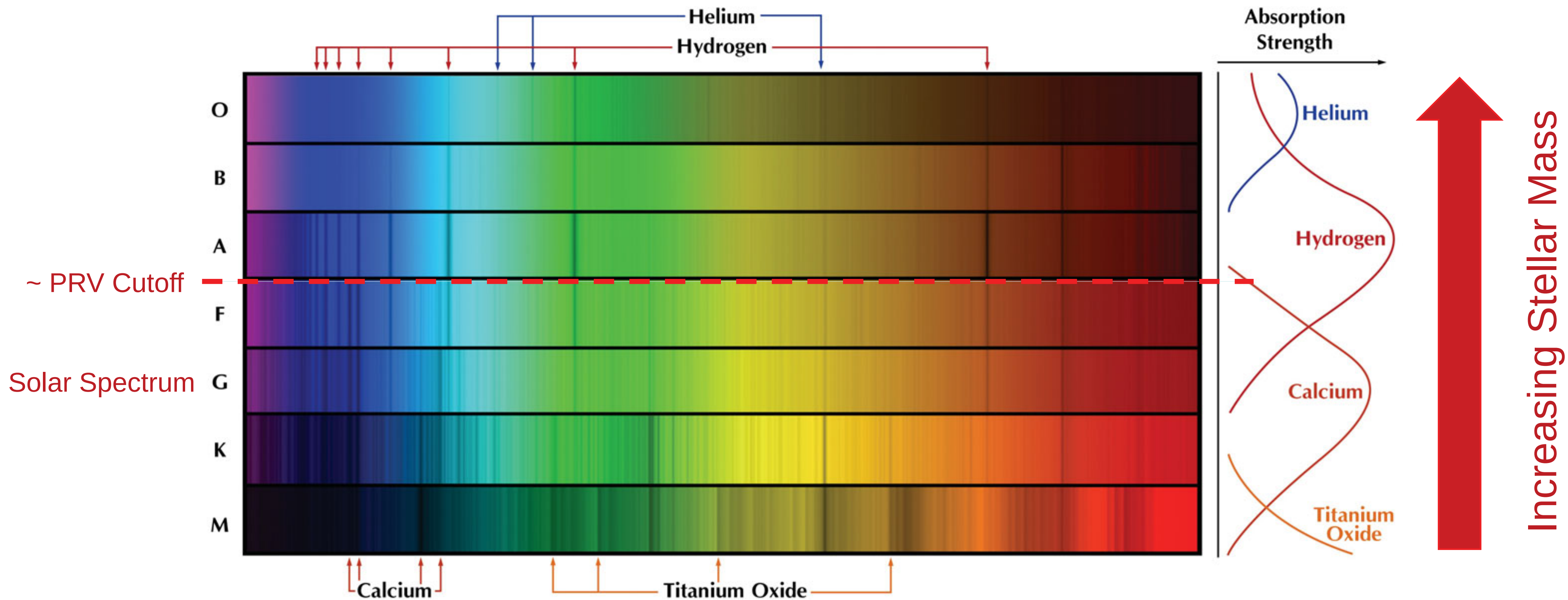

RV Precision $\propto \sqrt{N_{Lines\ Measured}}$ & Line Width

Raw Echelle Spectrograph

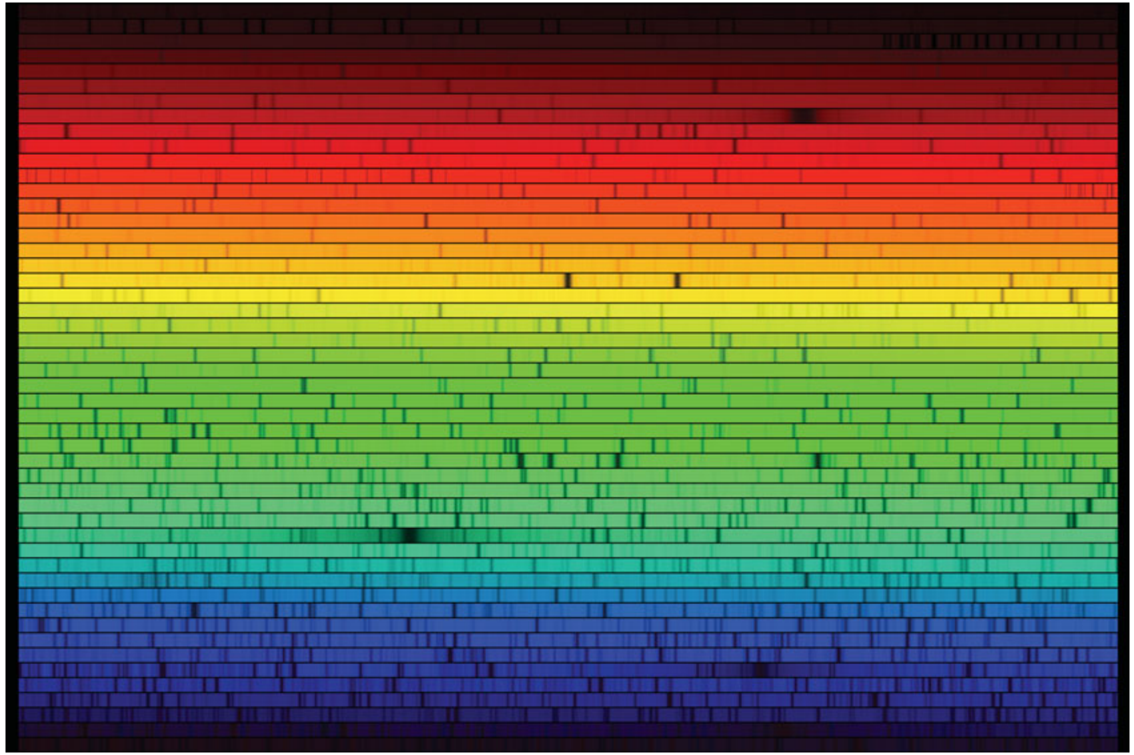

- PRV observations made with echelle spectrograph which record high resolution (R~100,000) spectra
- The data is recorded at the spectrograph focal plane with a rectangular detector
  - Usually a charged-coupled device (CCD) array
- Spectrum is “folded” optically by a cross disperer to fit the spectrum on a detector array

Reduced Echelle Spectrograph Data

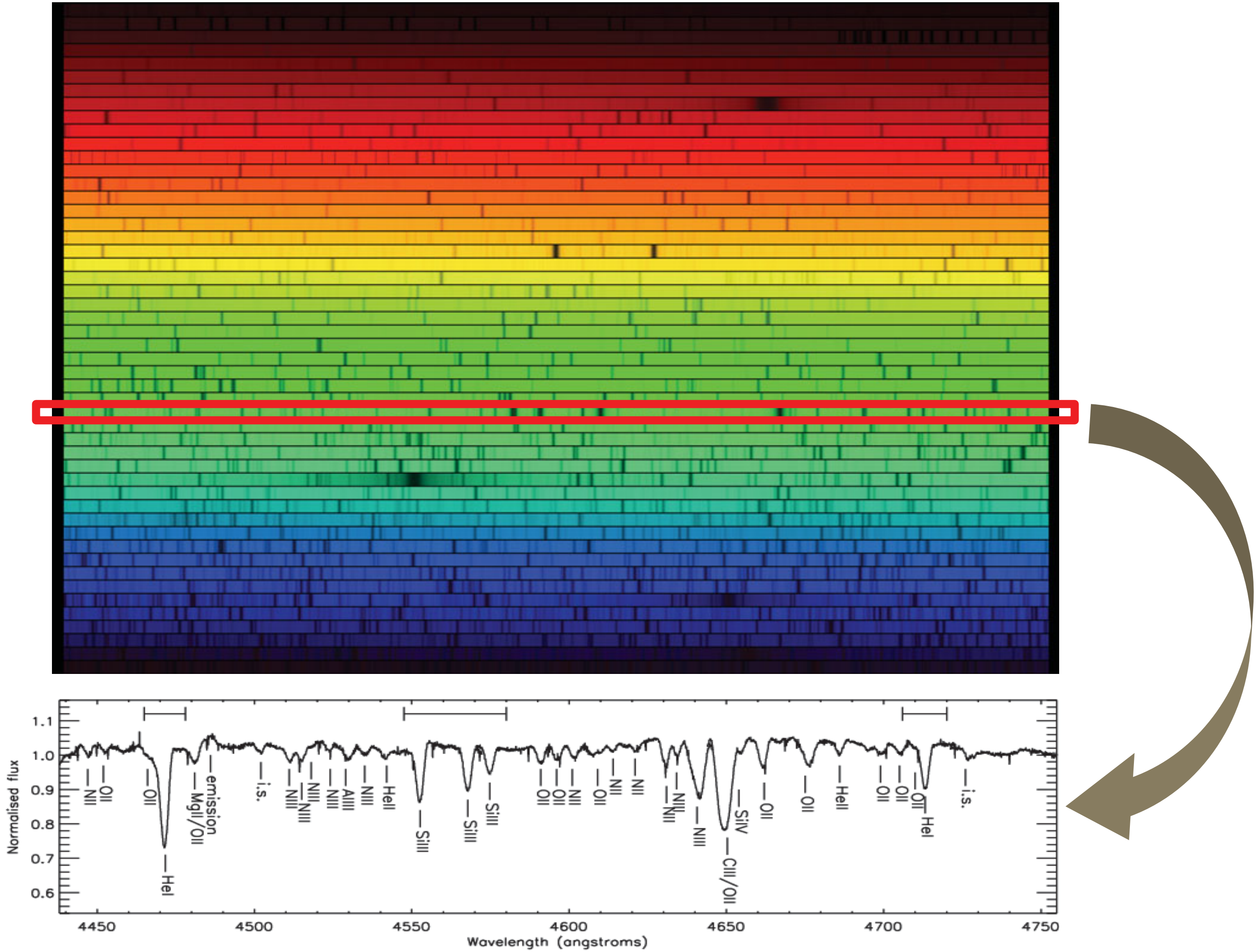

Finding Earth 2.0

- A important goal for the GMT is to find a rocky exoplanet orbiting a solar type star (F,G or K) in the star's habitable zone, where the water is in liquid phase at planetary surface temperature.
- A stepping stone to finding life on other worlds and perhaps extraterrestrial intelligence.
- The required RV precision to make this measurement is 10 cm/sec.
- The current record precision is ~ 56 cm/sec with HARPS on the La Silla 3.6 m telescope (HD20974).
    - The GMT has 38 time the area of the La Silla 3.6 m.
    - The GMT PRV instrument (G-CLEF) is being design to achieve the required precision.

The Problem of Stellar Jitter for PRV

Stars Have “Jitter”

Most stars, especially the Sun, have photospheric features which are dynamic on all time scales:

- Starspots
- Granulation
- Pulsation
- Plages

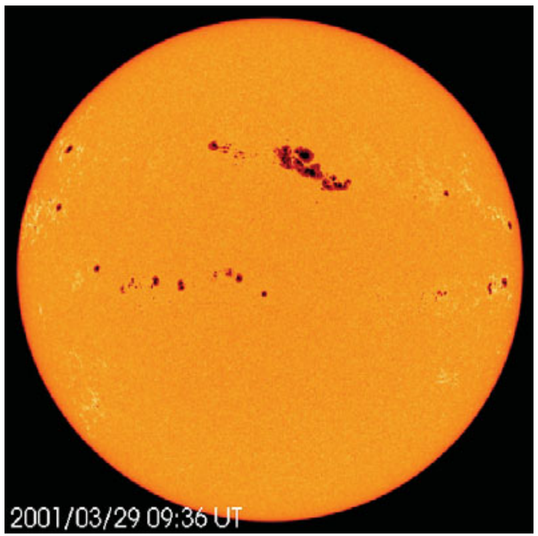

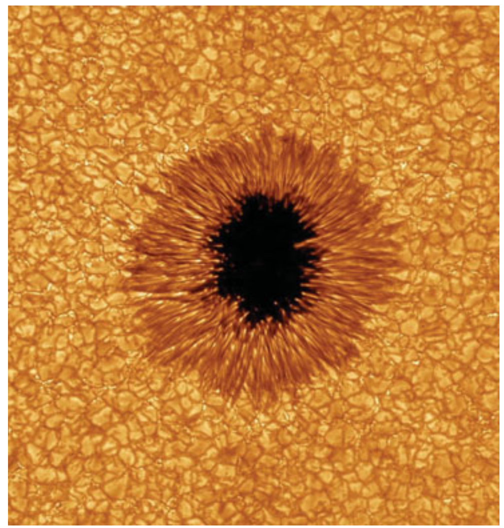

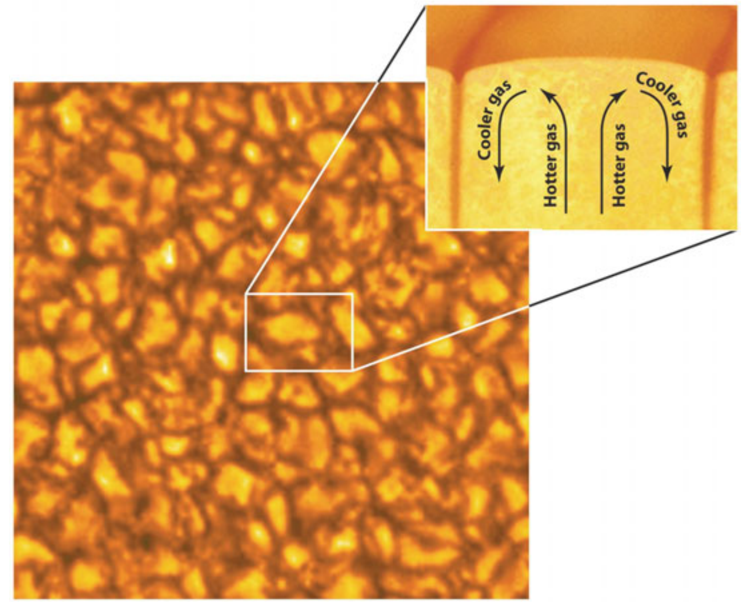

Stellar Activity Looks Very Different at Different Wavelenths

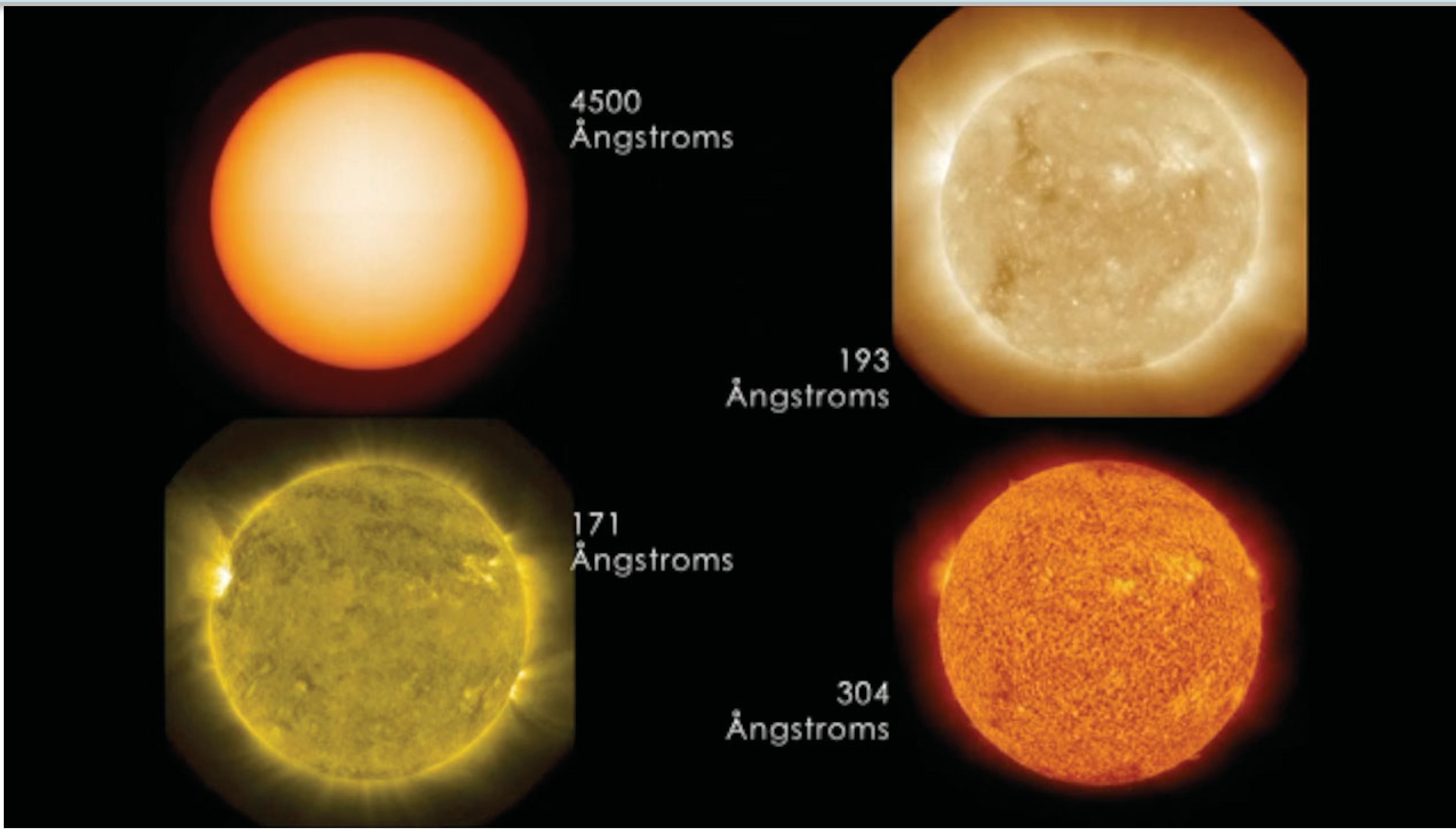

Stellar Spots Effective Exoplanet Impostors

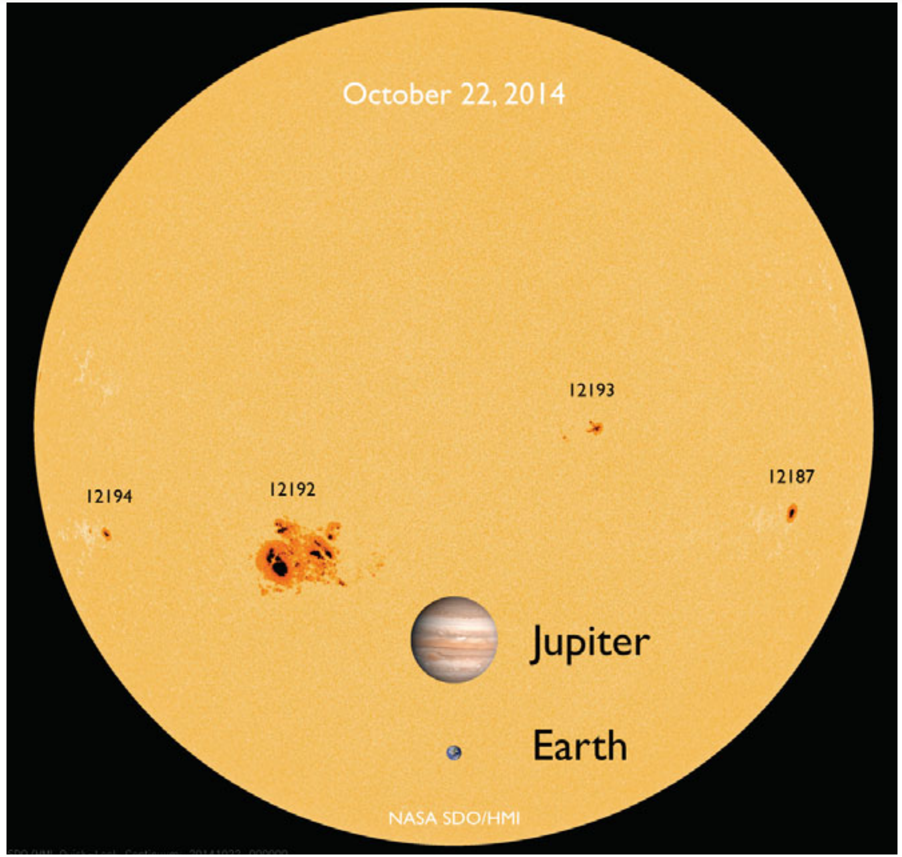

Scale sizes similar to exoplanet occulting disks
Stellar rotation periods are similar to orbital periods
Activity is a stochastic and diagnostics are often ambiguous

Cyclical Nature of Sunspots

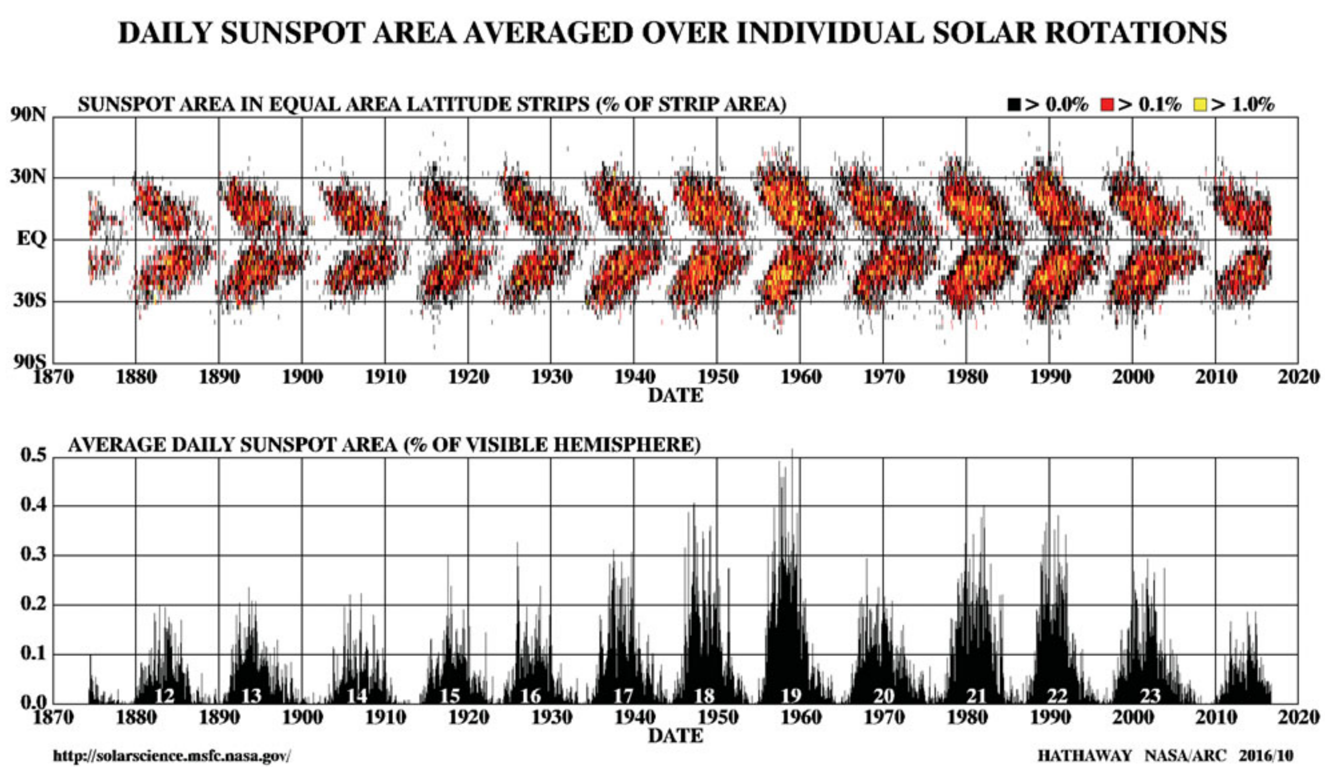

- Sunspots are cyclical
- Latitude distribution exhibits well know “butterfly” pattern
- Spots are not persistent
  - Long time averaging ultimately distinguishes spots from exoplanet transits.

Cyclical Nature of Sunspots

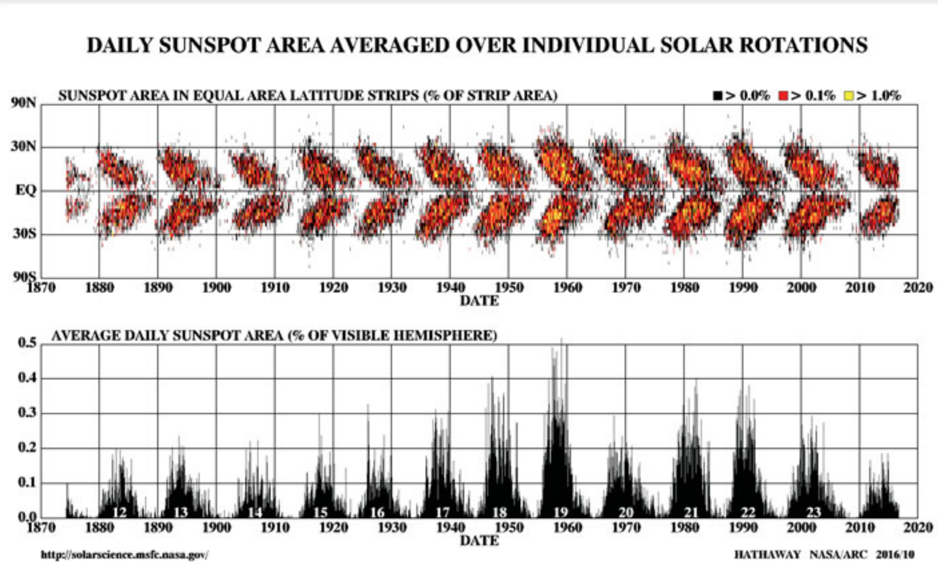

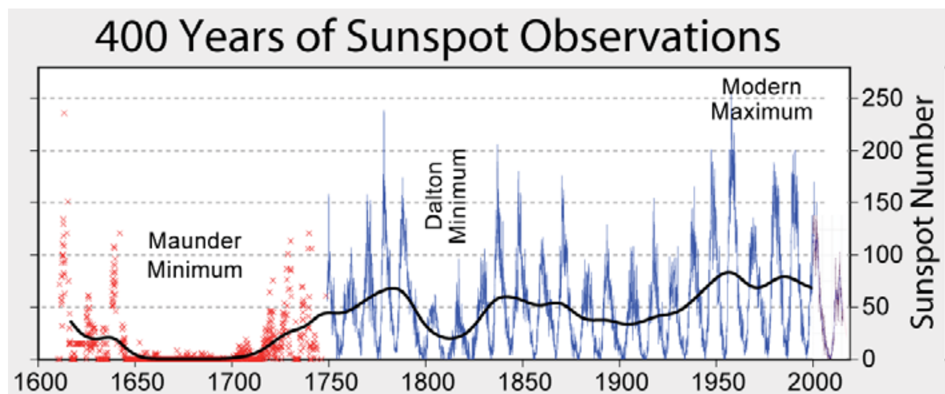

However temporal structure is at best, quasiperiodic

The Pathological Case of HD154345

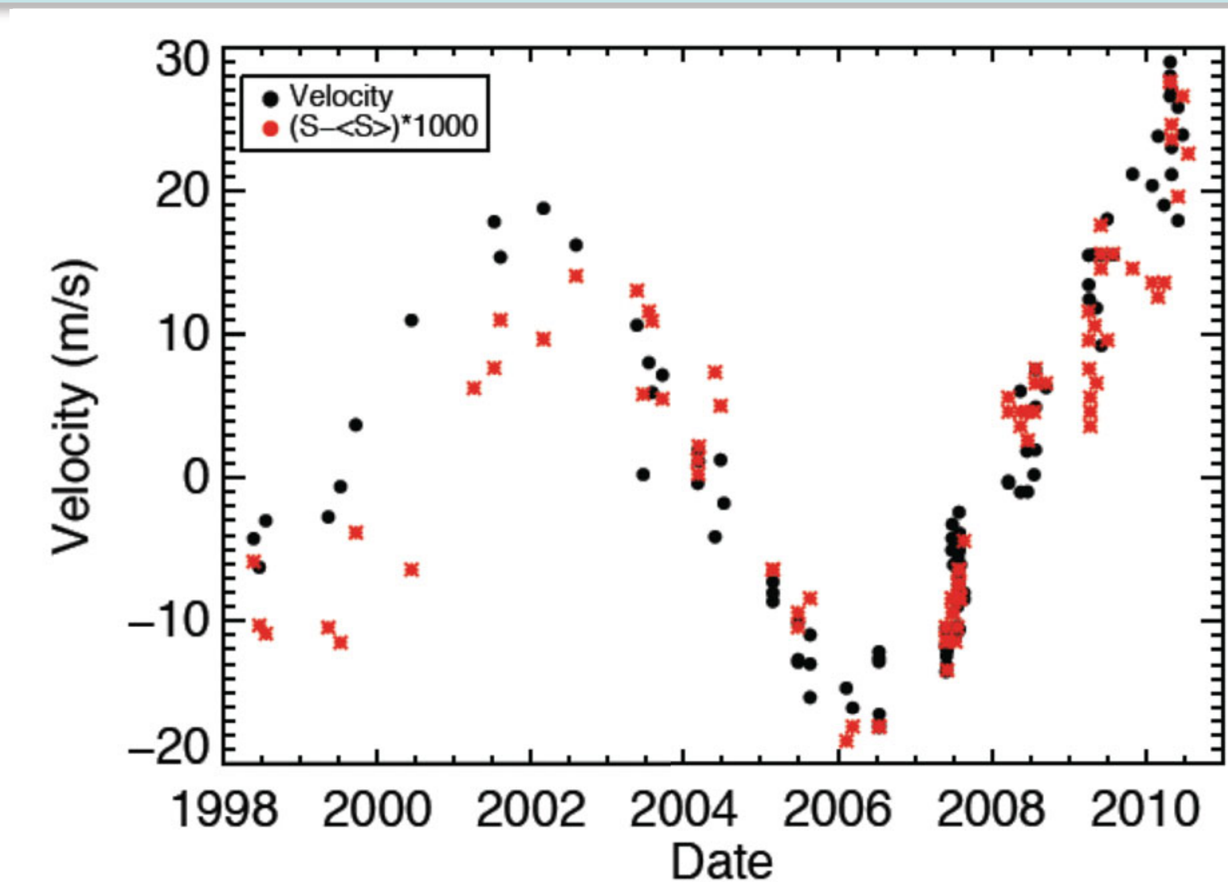

- Existence of first true Jupiter analogue discovered (Wright et al, 2007)
  - m = 0.95 $m_{♃}$, P = 9.2 y ($P_{♃}$ = 11.9 y)
- Confirmed despite strong activity (P_{Act} = 9 y, Wright et al 2008)

2012 – Existence of HD154345b retracted (Wright, 2012)

(Slides from Wright presentation 2014)

Studying Pulsations in the Brightest Star

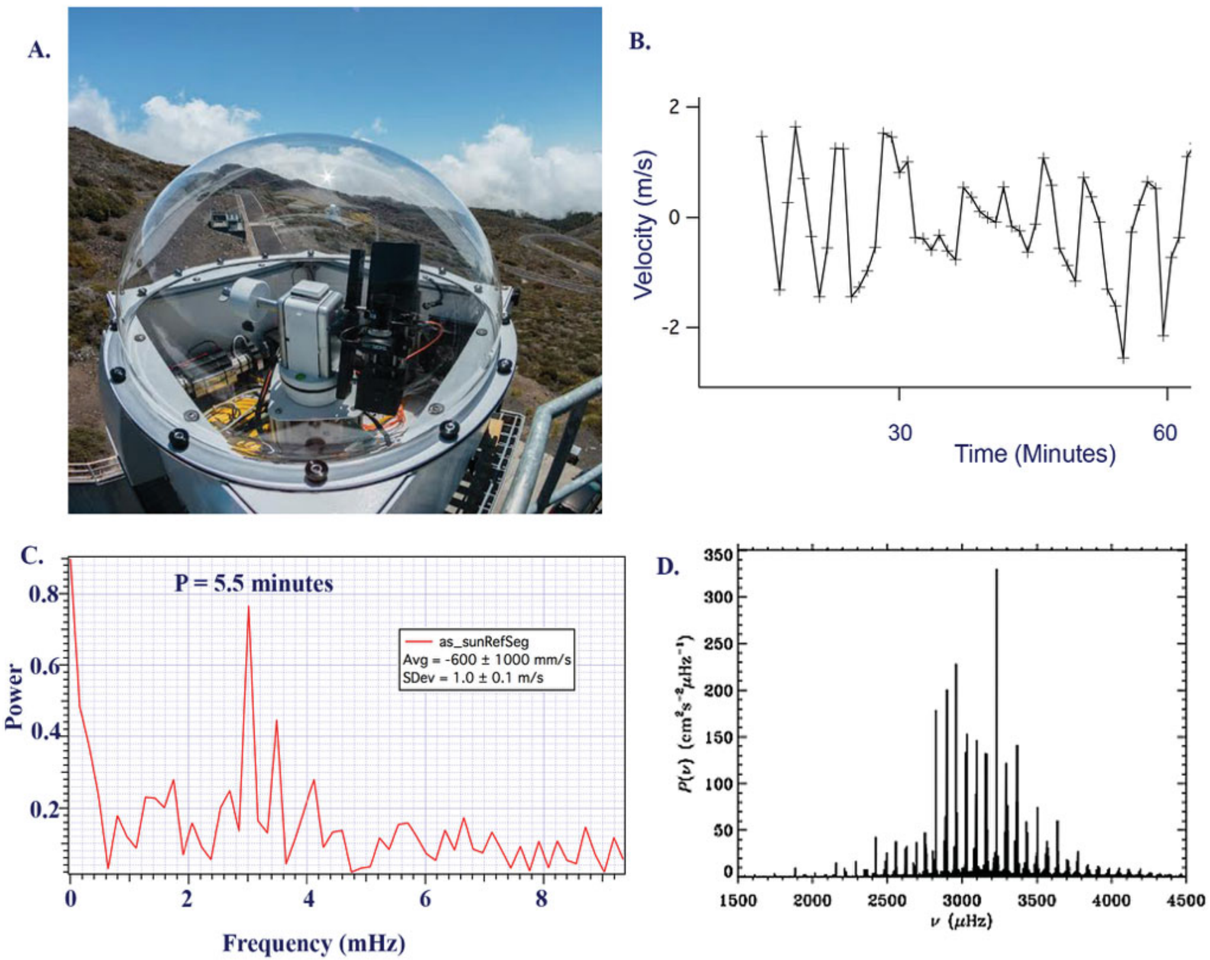

Figure 3-3: *Panel A:* a 3" aperture solar telescope that is currently deployed at the TNG and feeds HARPS-N to search for the RV signal of Venus in Solar spectra. *Panel B.:* A 1-hour time series of 20 second integrations taken with the solar telescope. The 5-minute oscillation period of the Sun is immediately evident in the time series and may be subtracted from the data. *Panel C.:* Fourier transform of 2-hour time series that data in Panel B. was extracted from. *Panel D.:* Power spectrum from BiSON experiment showing fine-structure splitting of p-modes of Sun. The phasing and amplitude of any time series – like that in Panel B. - will depend on instantaneous beating of these modes, which must be determined observationally.

Gaussian Processes Are Highly Successful for Modeling Stellar Jitter

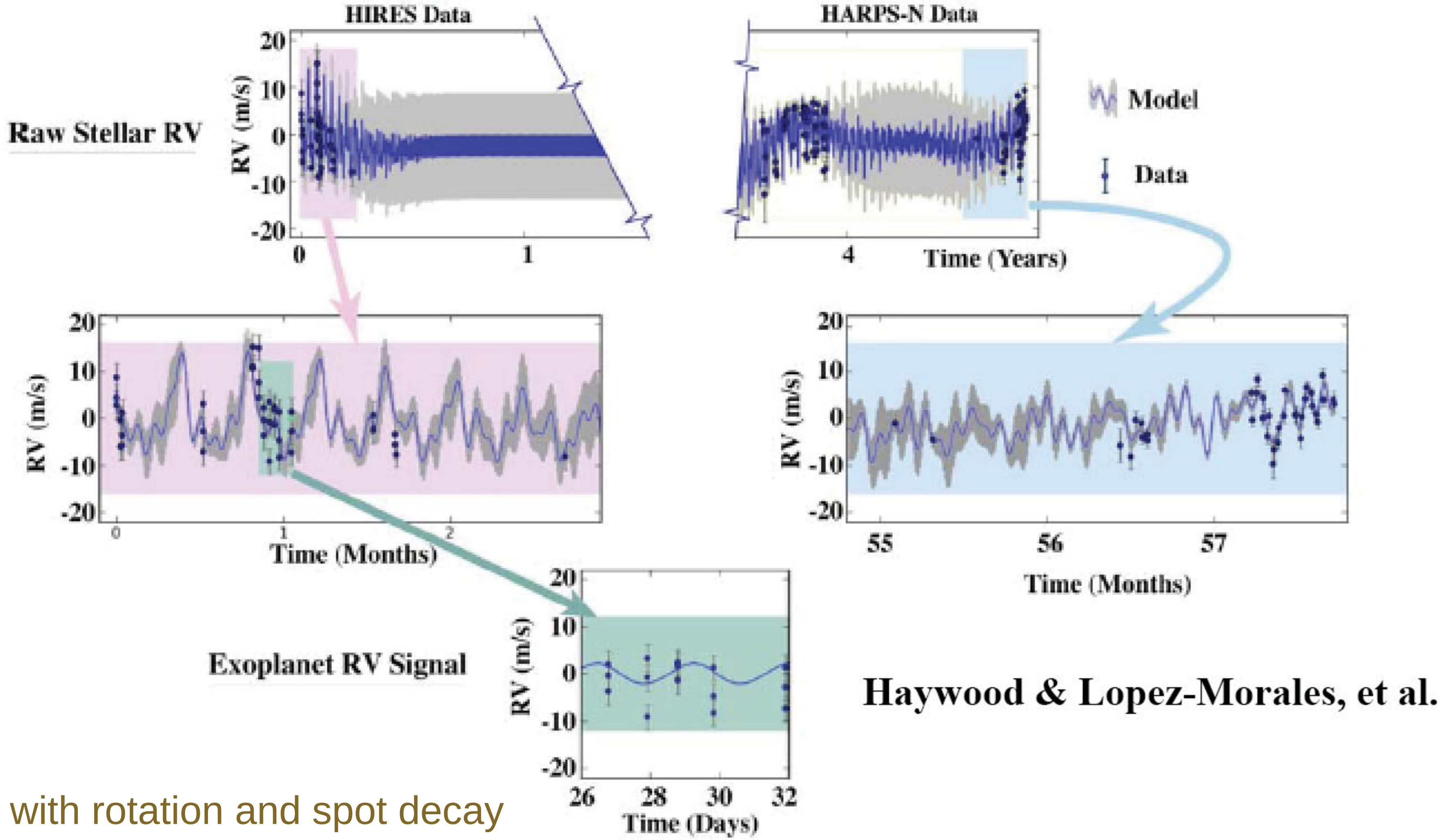

Black Dots: Data
Blue Line: GP Fit with rotation and spot decay
Grey Band: 1σ GP model dispersion

Also: RV Measurements Determine Orbital Elements

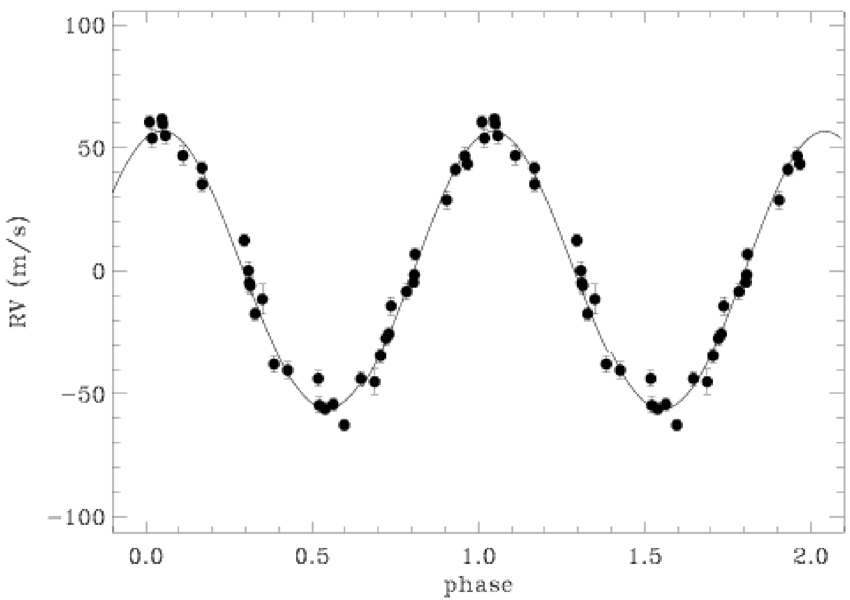

Circular Orbit

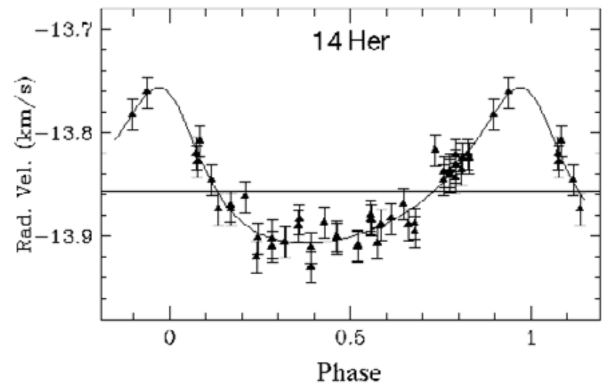

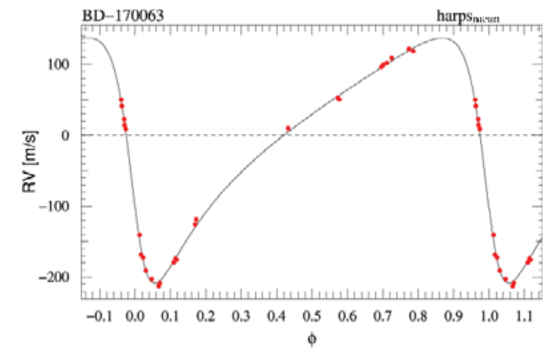

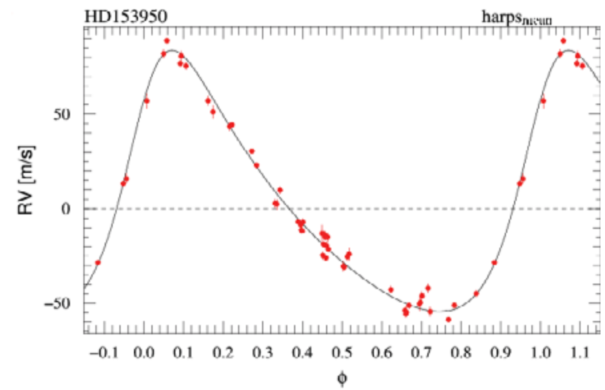

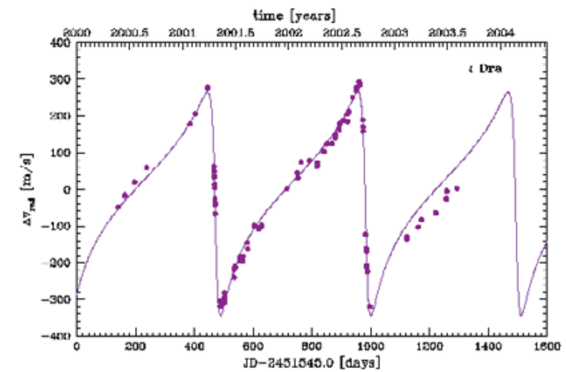

Elliptical Orbits

Exoplanet Impostors from Stellar Rotation

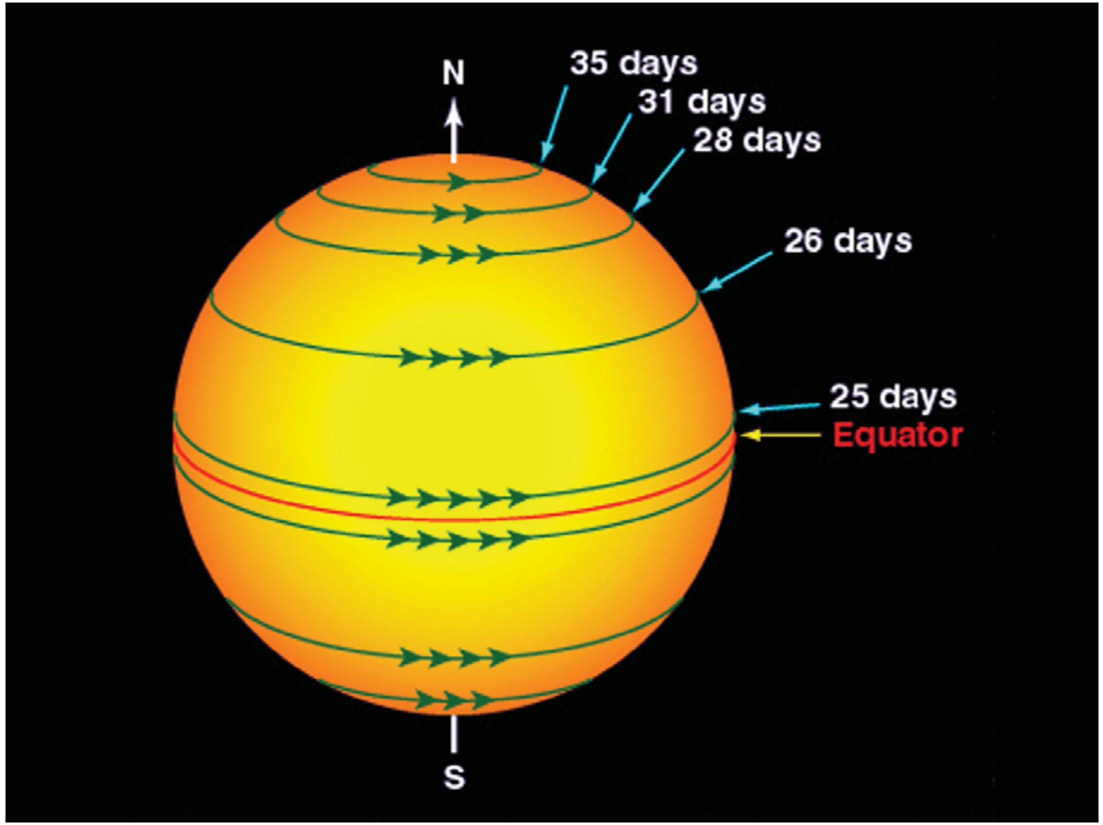

- All stars rotate
- Solar rotation depends on latitude

PRV Measurements Measure Orbital Inclination w.r.t. Stellar Rotation

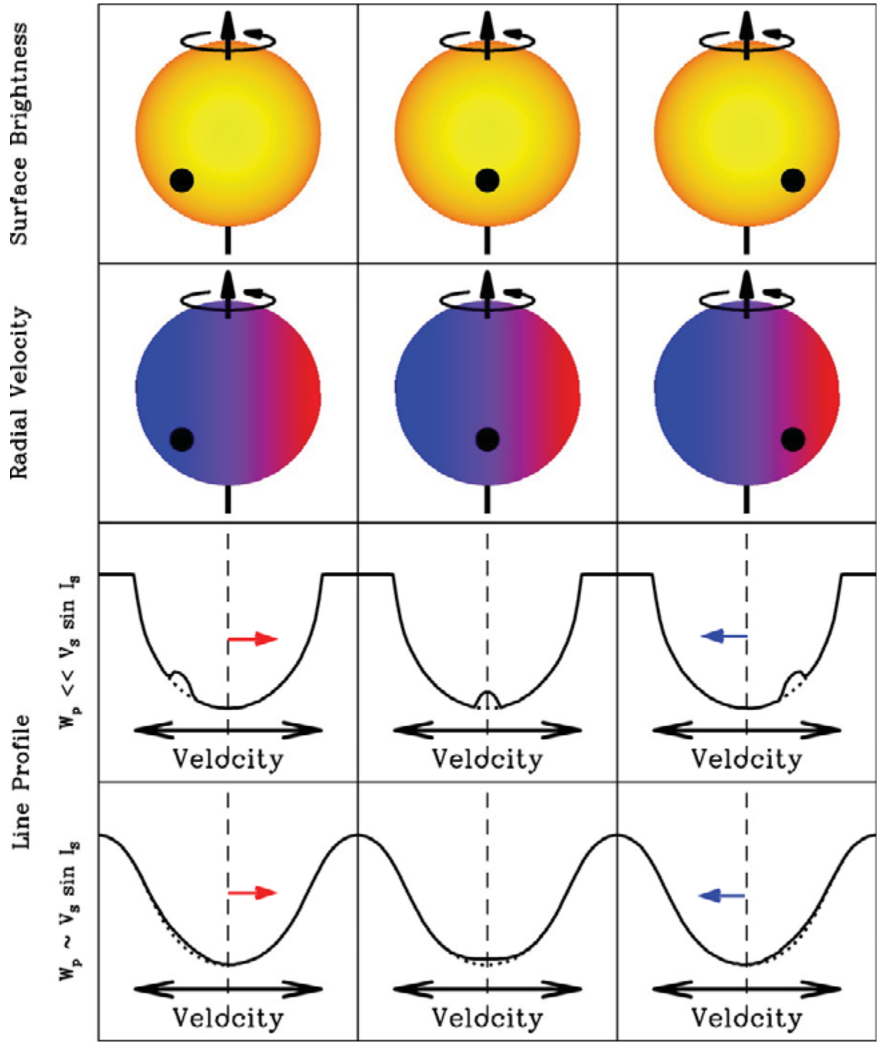

- The side of the star coming toward us is bluer than the middle.
- The side receding is redder.
- If a planet covers up part of the blue side, the star is redder and vice versa.

Rossiter - McLaughlin Effect

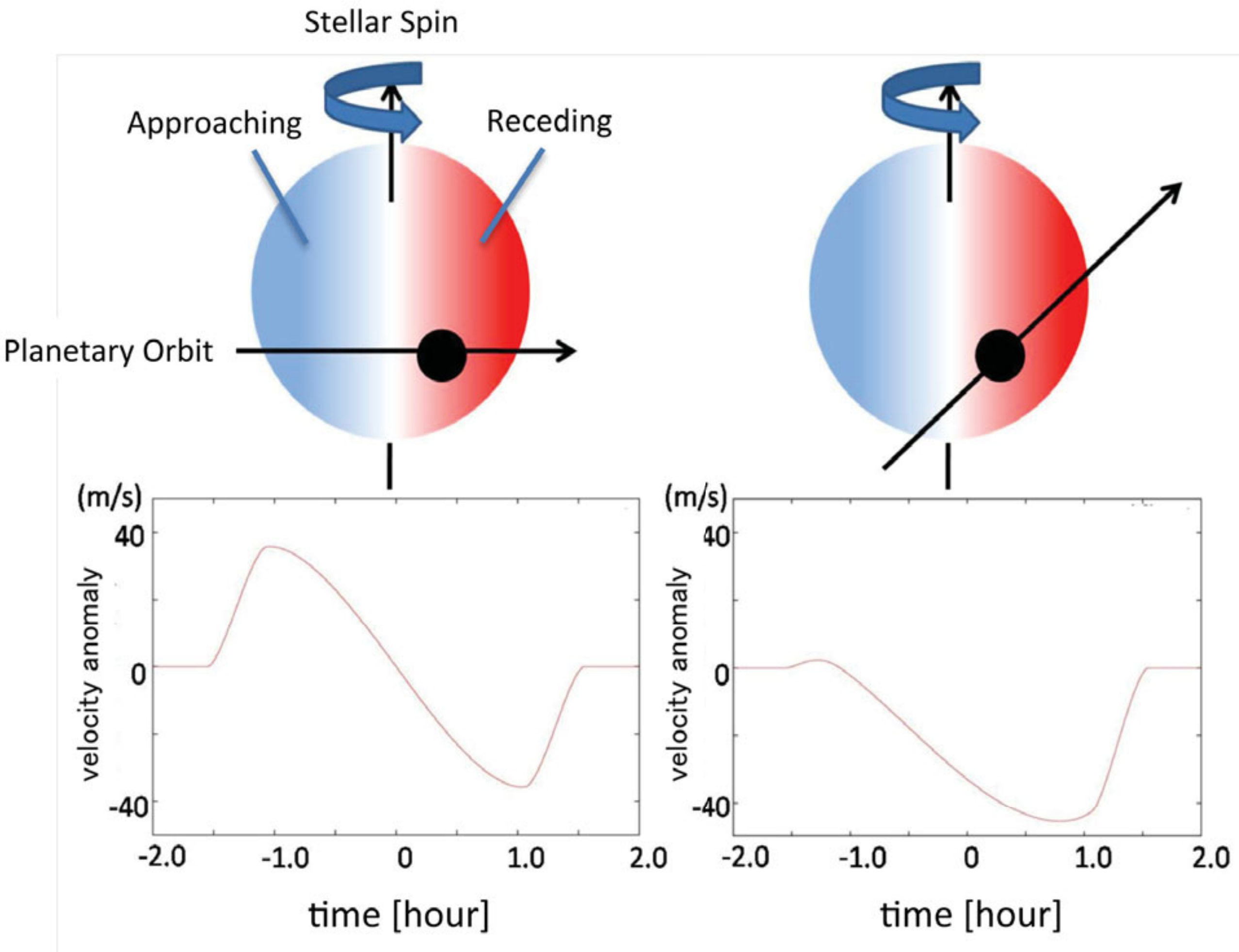

- The shape of the radial velocity curve during transit tells us how the planet crosses the stellar disk.
- It tells us the relative alignment of the spin axis of the star and the orbital axis of the exoplanet

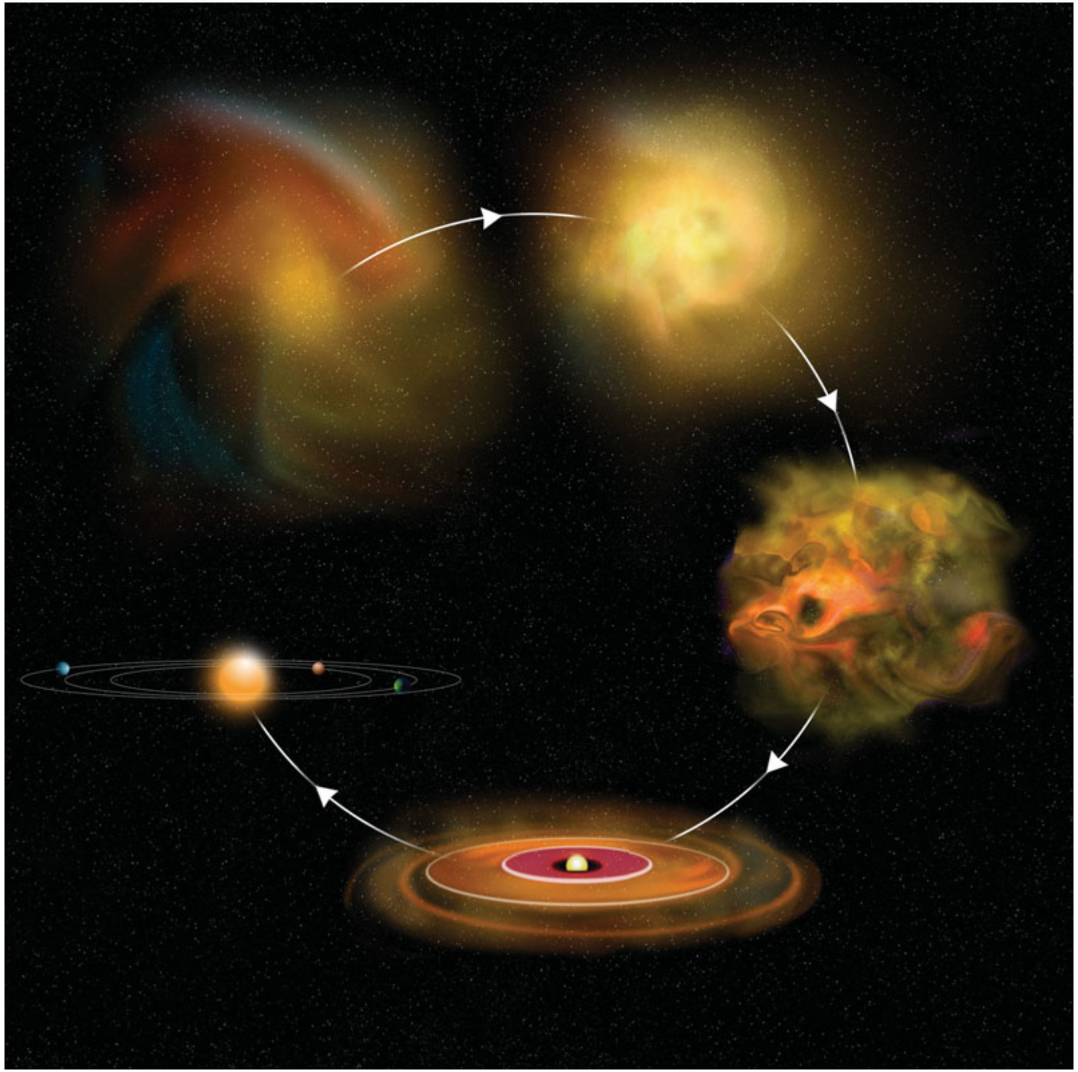

- Most evidence suggests planets formed out of disks of matter left over when a star forms
- It is reasonable to expect the stellar spin and planet orbital angular momenta vectors will be well-aligned.
- Departures from this alignment are symptoms of new dynamics.

The Strange Case of GJ 436b

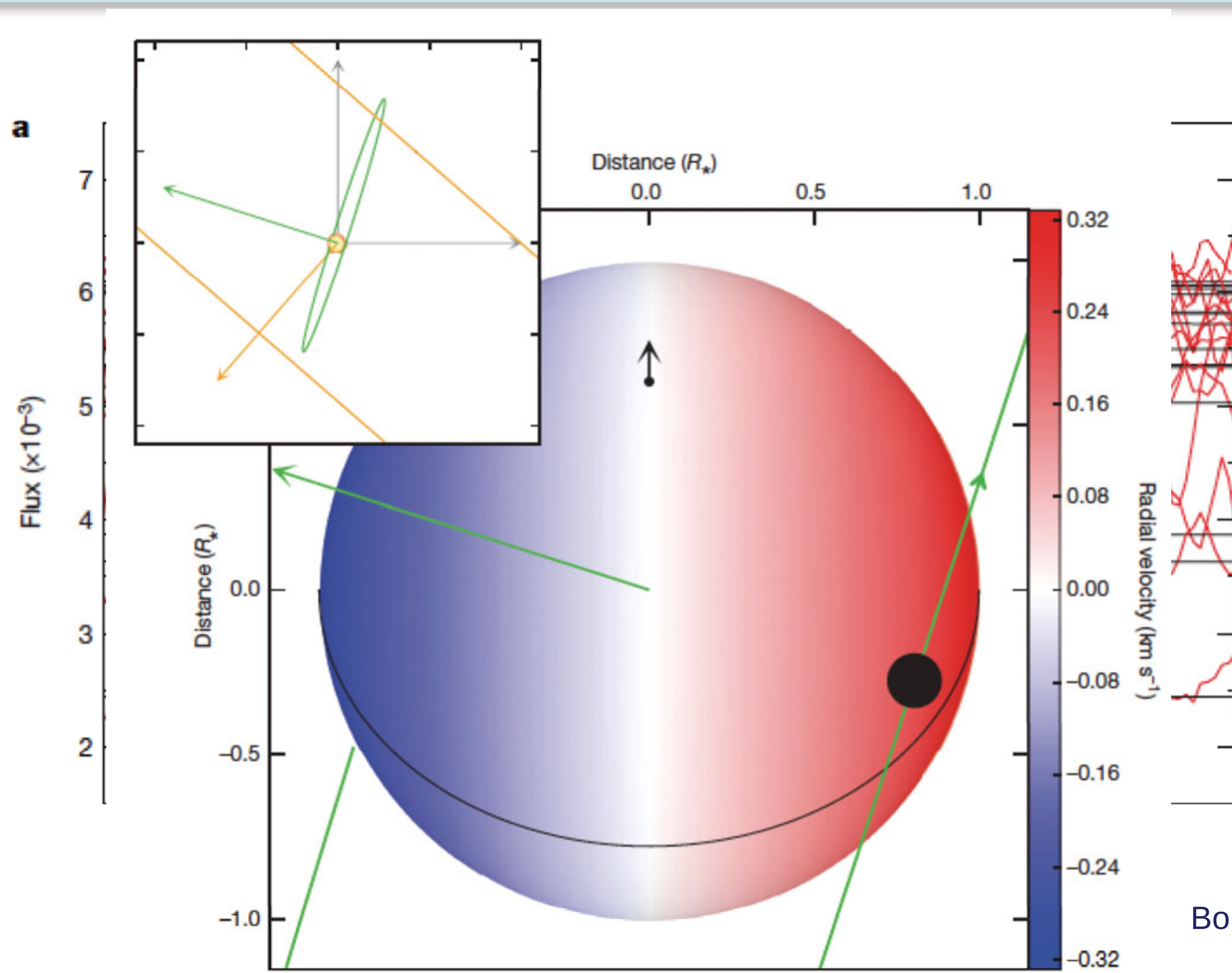

Borrier, et al., Nature, 2018

The Transit Technique

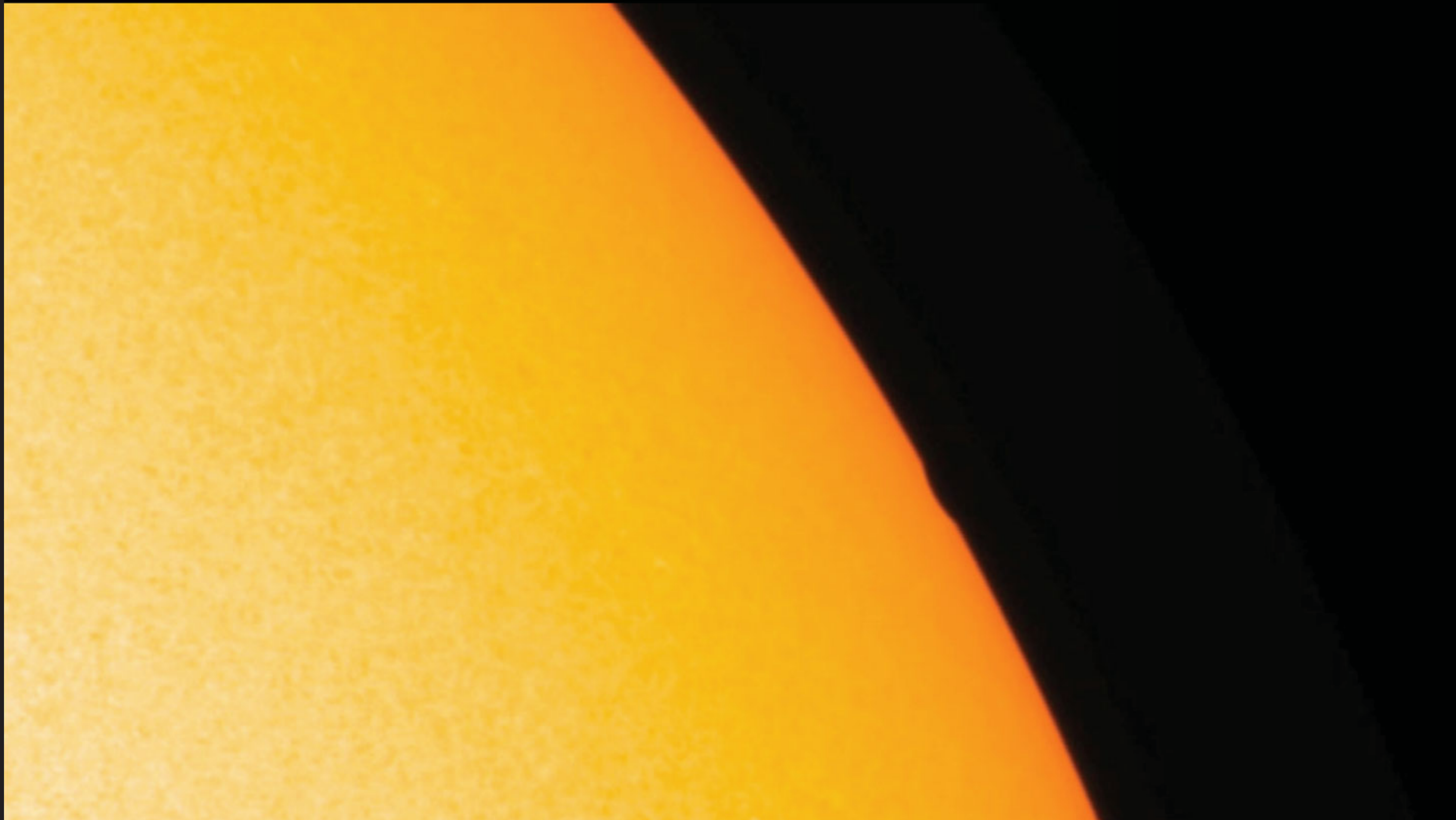

Some Prominent Transit Telescopes

Hungarian Automated Telescopes (HATS)

HATS are a geographically distributed network of small telescope

Kepler

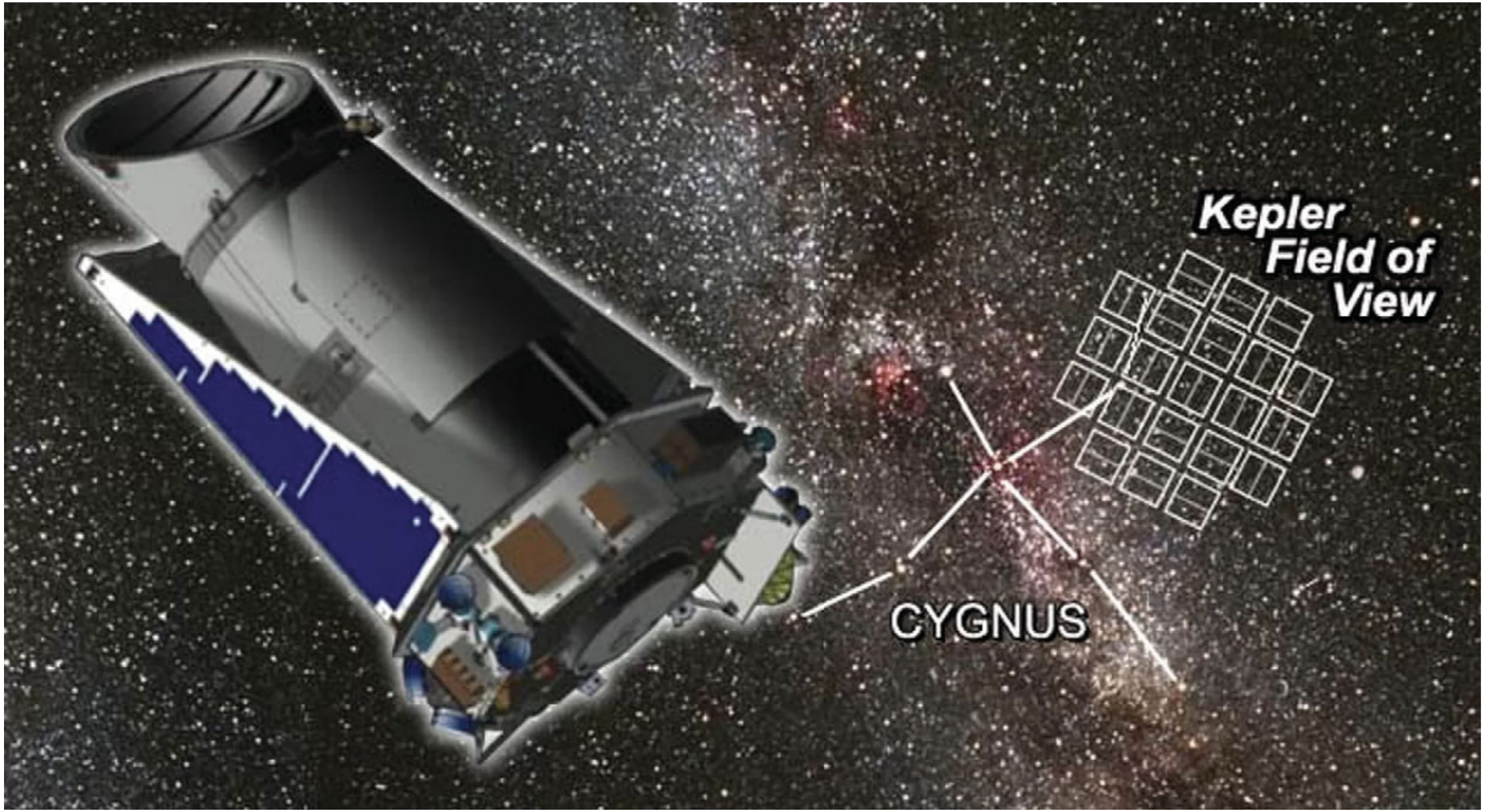

Kepler "Stared" at a ~100^2 deg field of view for ~3 years

Exoplanet Discovery Rate Pre-/Post-Kepler

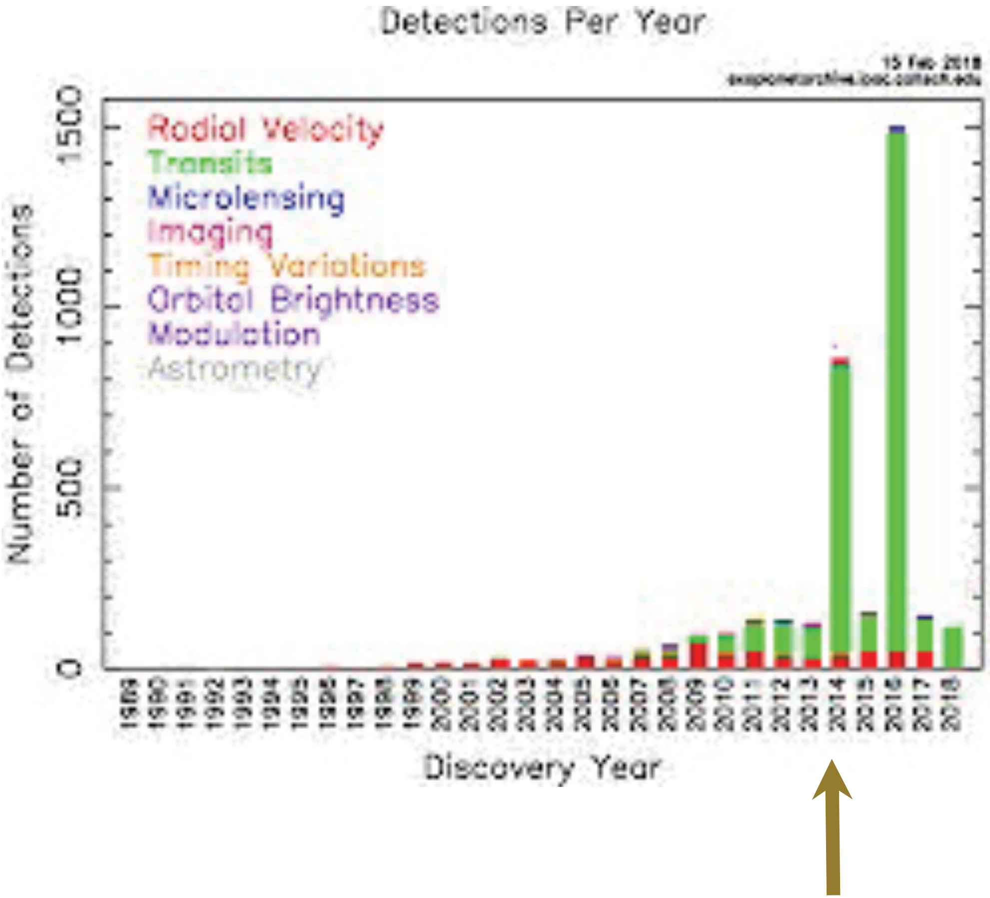

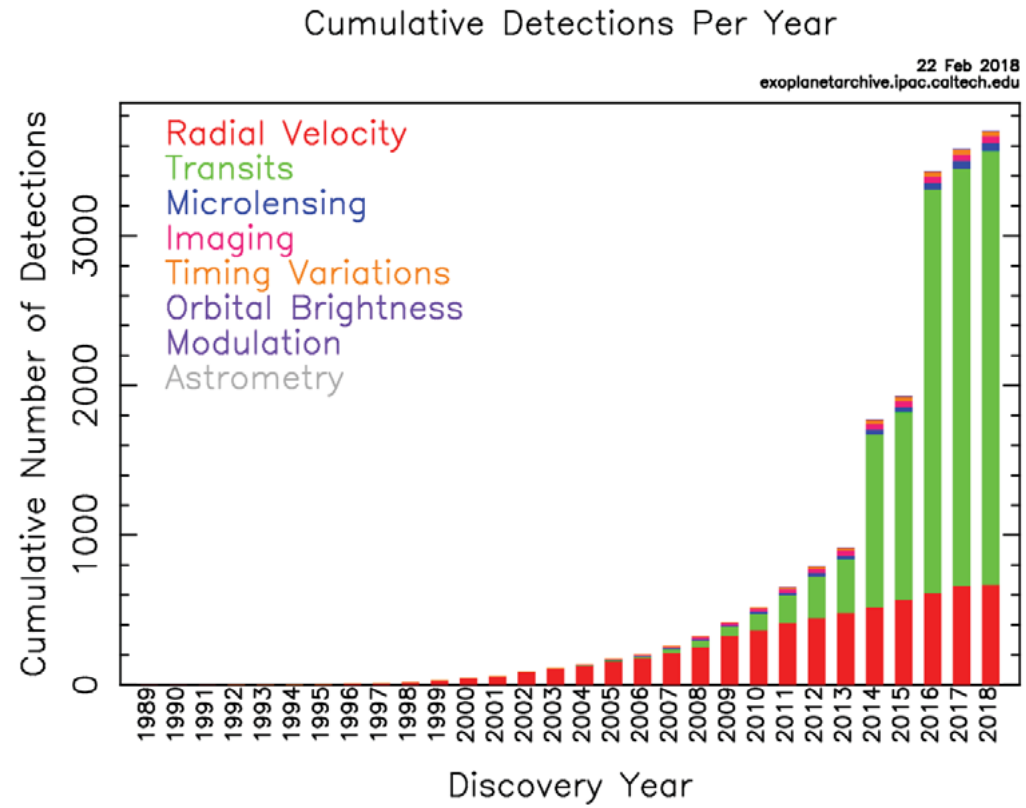

Kepler Data Release

TESS

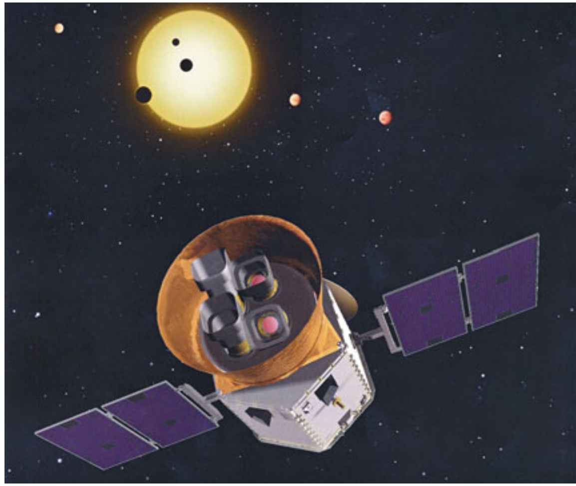

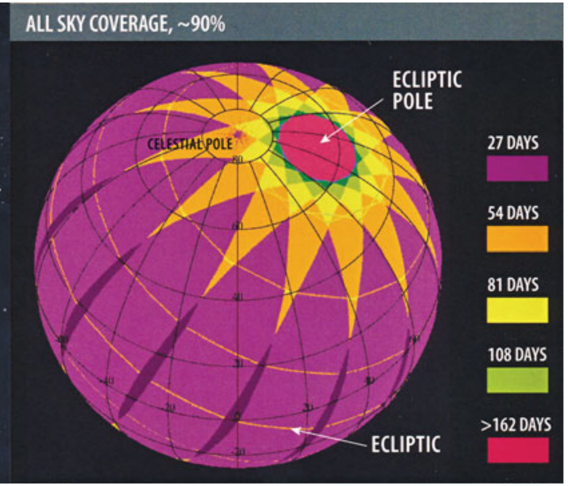

- TESS The Transiting Exoplanet Survey Satellite.
- Will find the brightest (best) exoplanetary systems.
- Launch in April 2018.
- Catalogue will become somewhat before ~G-CLEF 1st light.

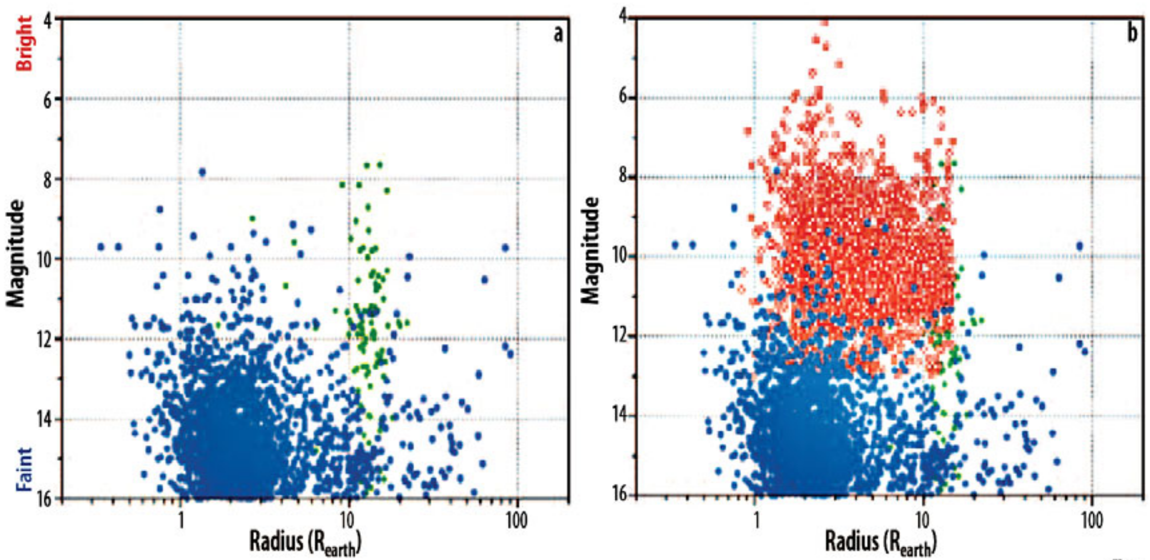

Comparison of brightness of Kepler discoveries (plotted in blue), ground-based transit surveys (in green) and the expected TESS yield (in red)

CHEOPS

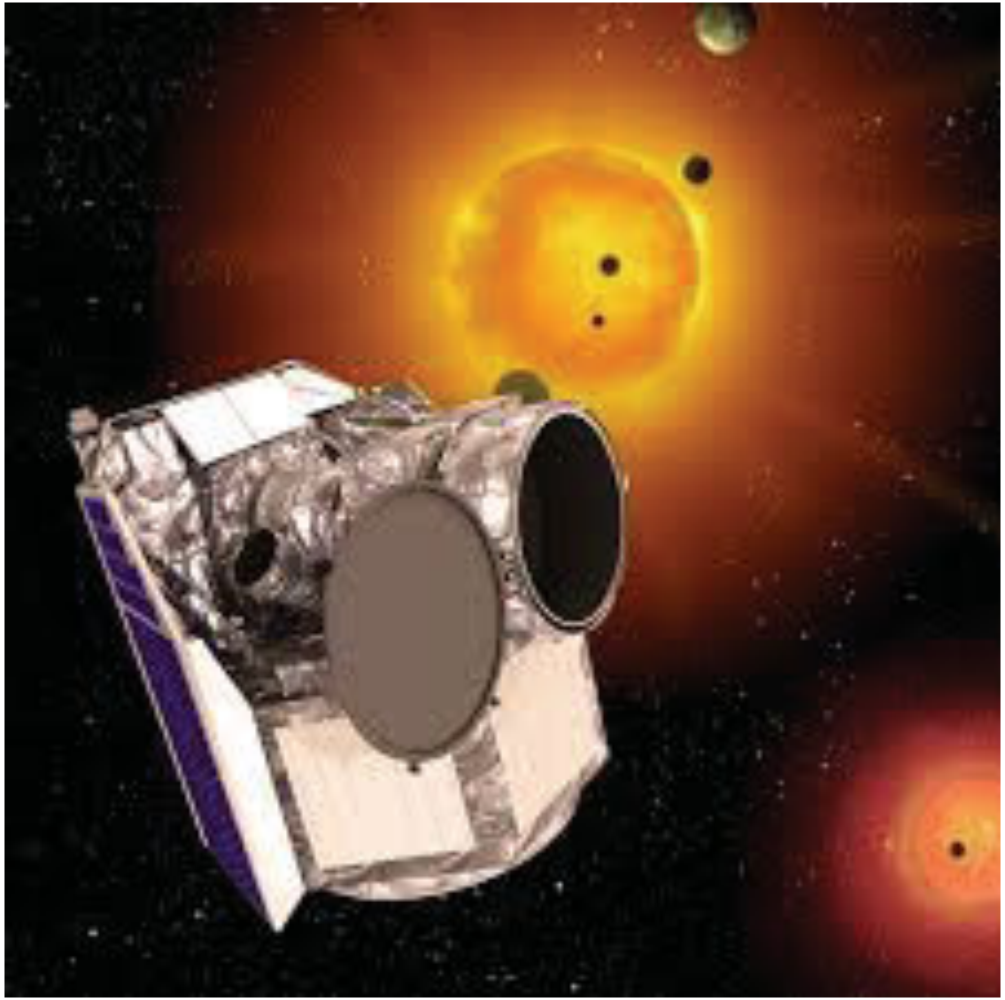

- CHaracterizing ExOPlanets Satellite.
- ESA S-class Cosmic Visions Program.
- Launch in late 2018.
- 30 cm aperture Ritchey-Chretien telescope.
- To provide accurate radius measurements of exoplanets with mass measurements by PRV.
- Can search for extremely shallow transits.

PLATO

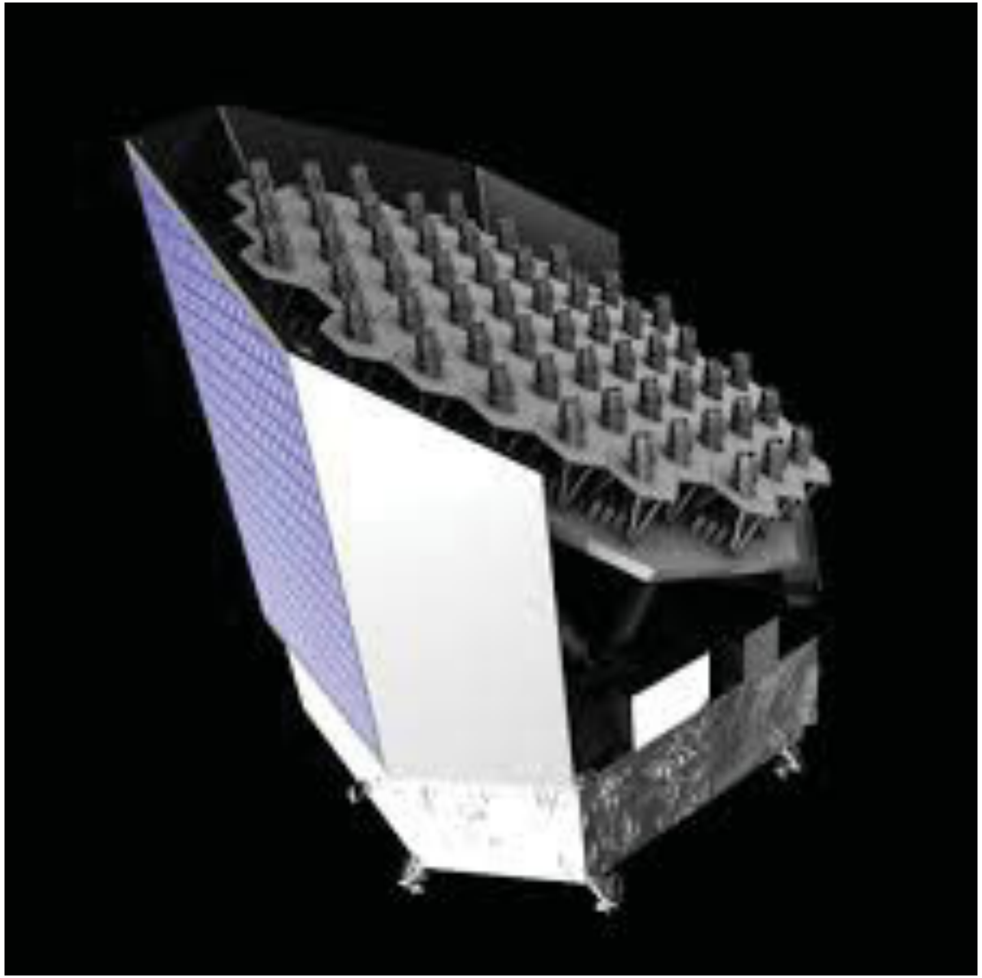

- Planetary Transits and Oscillations of stars (PLATO).
- ESA medium class Cosmic Vision mission.
- Launch in 2026.
- 26 small telescopes to observe 300,000-1,000,000 stars for transits.
- Stars in 4 < M < 11 band

Necessary Photometric Precision Achieved By Massive Differential Photometry

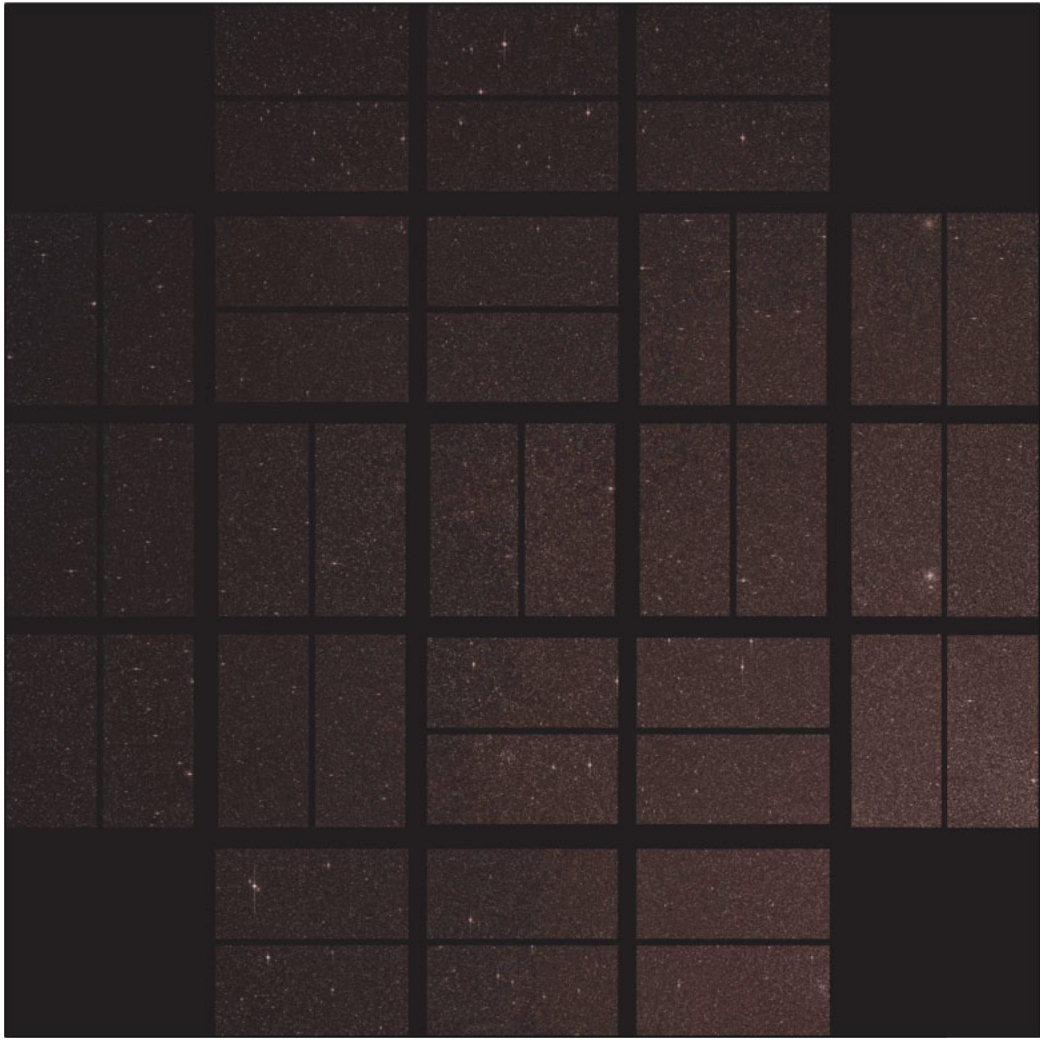

- The necessary photometric precision cannot be achieved absolutely.
  - Measures must be comparative, i.e. differential.
- By comparing many stars, very high differential precision is achievable.
- Precision grows as approximately $\sqrt{n_{Stars}}$ where $nStars$ is the number of stars measured simultaneously.
- Kepler photometered 120,000 stars at a time.
- With no diurnal gaps.
- And no atmospheric scintillation.

PRV & Transit Method

- Transit method measures the radius of an exoplanet
- PRV has intrinsic *Sin (i)* degeneracy → can only measure *m Sin (i)*
- Transit detection constrains orbital inclination tightly → $i \approx 0°$
- Mass, radius and orbital elements are known exactly for transiting systems
- Kepler detected 3000+ exoplanet candidates, many (most) not yet confirmed by PRV.
- TESS mission (launch 2018) will find 1000s of bright transit exoplanet
  - Amenable to follow–on studies of atmospheric composition, energy circulation, opacity, &c.

Transit Timing Variations

Transit Timing/Duration and Binary Star Detection

- When a transiting planet is solitary, the times of transits will be highly regular.
- If there are other unseen, non-transiting planets, they will perturb the orbit of the transiting planet.
- The times of transit will be shifted in time slighlty.
- Timing variations in transit planets can be used to infer the presence of non-transiting exoplanet in exo-solar system.

Transit Timing Variations of the Solar System

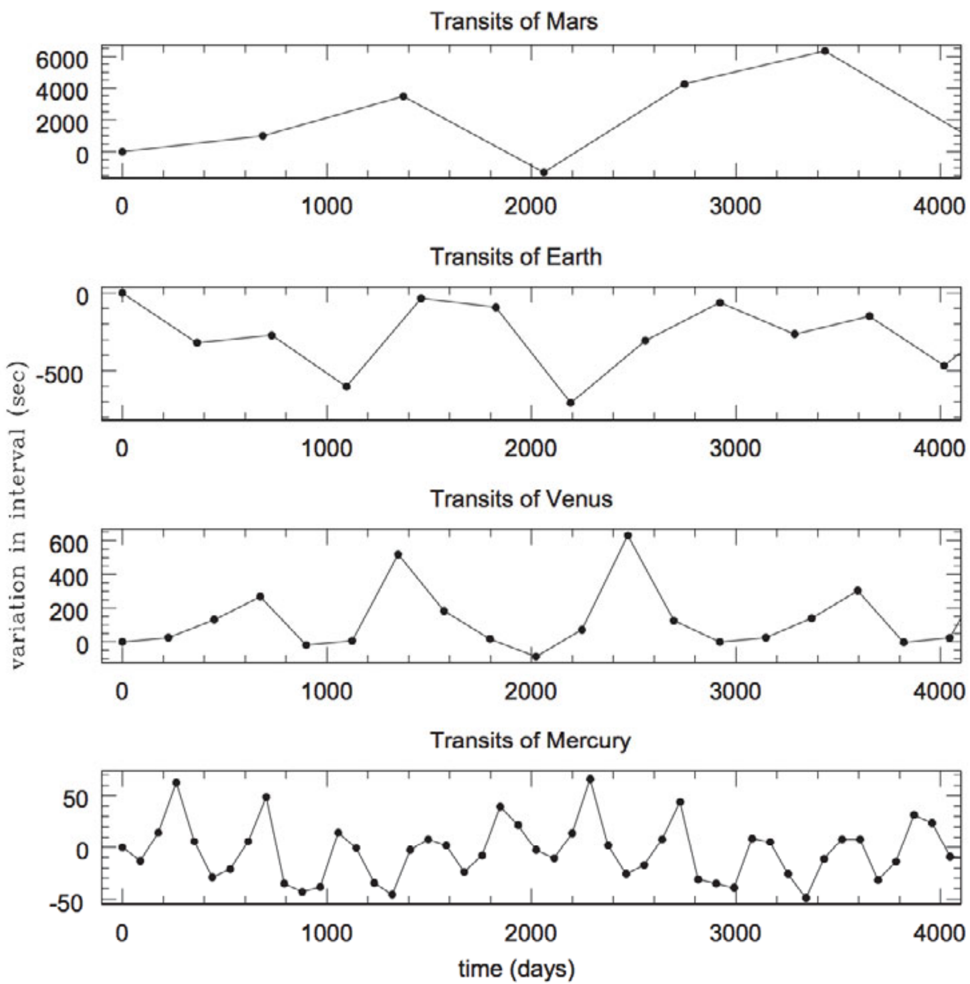

Results of an imaginary transit timing variations in transit observations of the Solar System made by ET's living on an exoplanet.

The Kepler-19 System: A Transiting 2.2 $R_\oplus$ Planet and a Second Planet Detected via Transit Timing Variations

Sarah Ballard[1], Daniel Fabrycky[2], Francois Fressin[1], David Charbonneau[1], Jean-Michel Desert[1], Guillermo Torres[1], Geoffrey Marcy[3], Christopher J. Burke[4], Howard Isaacson[3], Christopher Henze[4], Jason H. Steffen[5], David R. Ciardi[6], Steven B. Howell[7,4], William D. Cochran[8], Michael Endl[8], Stephen T. Bryson[4], Jason F. Rowe[4], Matthew J. Holman[1], Jack J. Lissauer[4], Jon M. Jenkins[9], Martin Still[4], Eric B. Ford[10], Jessie L. Christiansen[4], Christopher K. Middour[4], Michael R. Haas[4], Jie Li[9], Jennifer R. Hall[11], Sean McCauliff[11], Natalie M. Batalha[12], David G. Koch[4], William J. Borucki[4]

We present the discovery of the Kepler-19 planetary system, which we first identified from a 9.3-day periodic transit signal in the *Kepler* photometry. From high-resolution spectroscopy of the star, we find a stellar effective temperature $T_{\rm eff}$=5541 ± 60 K, a metallicity [Fe/H]=−0.13 ± 0.06, and a surface gravity log(g)=4.59 ± 0.10. We combine the estimate of $T_{\rm eff}$ and [Fe/H] with an estimate of the stellar density derived from the photometric light curve to deduce a stellar mass of $M_\star = 0.936 \pm 0.040\ M_\odot$ and a stellar radius of $R_\star = 0.850 \pm 0.018\ R_\odot$ (these errors do not include uncertainties in the stellar models). We rule out the possibility that the transits result from an astrophysical false positive by first identifying the subset of stellar blends that reproduce the precise shape of the light curve. Using the additional constraints from the measured color of the system, the absence of a secondary source in the high-resolution spectrum, and the absence of a secondary source in the adaptive optics imaging, we conclude that the planetary scenario is more than three orders of magnitude more likely than a blend. The blend scenario is independently disfavored by the achromaticity of the transit: we measure a transit depth with *Spitzer* at 4.5 μm of 547^{+113}_{-110} ppm, consistent with the depth measured in the *Kepler* optical bandpass of 567±6 ppm (corrected for stellar limb-darkening). We determine a physical radius of the planet Kepler-19b of $R_p = 2.209 \pm 0.048\ R_\oplus$; the uncertainty is dominated by uncertainty in the stellar parameters. From radial-velocity observations of the star, we find an upper limit on the planet mass of 20.3 $M_\oplus$, corresponding to a maximum density of 10.4 g cm^{-3}. We report a significant sinusoidal deviation of the transit times from a predicted linear ephemeris, which we conclude is due to an additional perturbing body in the system. We cannot uniquely determine the orbital parameters of the perturber, as various dynamical mechanisms match the amplitude, period, and shape of the transit timing signal and satisfy the host star's radial velocity limits. However, the perturber in these mechanisms has period $\lesssim 160$ days and mass $\lesssim 6 M_{Jup}$, confirming its planetary nature as Kepler-19c. We place limits on the presence of transits of Kepler-19c in the available *Kepler* data.

We present the discovery of the Kepler-19 planetary system, which we first identified from a 9.3-day periodic transit signal in the *Kepler* photometry. From high-resolution spectroscopy of the star, we find a stellar effective temperature $T_{\rm eff}$=5541 ± 60 K, a metallicity [Fe/H]=−0.13 ± 0.06, and a surface gravity log(g)=4.59 ± 0.10. We combine the estimate of $T_{\rm eff}$ and [Fe/H] with an estimate of the stellar density derived from the photometric light curve to deduce a stellar mass of $M_\star = 0.936 \pm 0.040\ M_\odot$ and a stellar radius of $R_\star = 0.850 \pm 0.018\ R_\odot$ (these errors do not include uncertainties in the stellar models). We rule out the possibility that the transits result from an astrophysical false positive by first identifying the subset of stellar blends that reproduce the precise shape of the light curve. Using the additional constraints from the measured color of the system, the absence of a secondary source in the high-resolution spectrum, and the absence of a secondary source in the adaptive optics imaging, we conclude that the planetary scenario is more than three orders of magnitude more likely than a blend. The blend scenario is independently disfavored by the achromaticity of the transit: we measure a transit depth with *Spitzer* at 4.5 μm of 547^{+113}_{-110} ppm, consistent with the depth measured in the *Kepler* optical bandpass of 567±6 ppm (corrected for stellar limb-darkening). We determine a physical radius of the planet Kepler-19b of $R_p = 2.209 \pm 0.048\ R_\oplus$; the uncertainty is dominated by uncertainty in the stellar parameters. From radial-velocity observations of the star, we find an upper limit on the planet mass of 20.3 $M_\oplus$, corresponding to a maximum density of 10.4 g cm^{-3}. We report a significant sinusoidal deviation of the transit times from a predicted linear ephemeris, which we conclude is due to an additional perturbing body in the system. We cannot uniquely determine the orbital parameters of the perturber, as various dynamical mechanisms match the amplitude, period, and shape of the transit timing signal and satisfy the host star's radial velocity limits. However, the perturber in these mechanisms has period $\lesssim 160$ days and mass $\lesssim 6M_{Jup}$, confirming its planetary nature as Kepler-19c. We place limits on the presence of transits of Kepler-19c in the available *Kepler* data.

We present the discovery of the Kepler-19 planetary system, which we first identified from a 9.3-day periodic transit signal in the *Kepler* photometry. From high-resolution spectroscopy of the star, we find a stellar effective temperature $T_{\rm eff}$=5541 $\pm$ 60 K, a metallicity [Fe/H]=-0.13 ± 0.06, and a surface gravity log(g)=4.59 ± 0.10. We combine the estimate of $T_{\rm eff}$ and [Fe/H] with an estimate of the stellar density derived from the photometric light curve to deduce a stellar mass of $M_\star = 0.936 \pm 0.040\ M_\odot$ and a stellar radius of $R_\star = 0.850 \pm 0.018\ R_\odot$ (these errors do not include uncertainties in the stellar models). We rule out the possibility that the transits result from an astrophysical false positive by first identifying the subset of stellar blends that reproduce the precise shape of the light curve. Using the additional constraints from the measured color of the system, the absence of a secondary source in the high-resolution spectrum, and the absence of a secondary source in the adaptive optics imaging, we conclude that the planetary scenario is more than three orders of magnitude more likely than a blend. The blend scenario is independently disfavored by the achromaticity of the transit: we measure a transit depth with *Spitzer* at 4.5 μm of 547^{+113}_{-110} ppm, consistent with the depth measured in the *Kepler* optical bandpass of 567$\pm$6 ppm (corrected for stellar limb-darkening). We determine a physical radius of the planet Kepler-19b of $R_p = 2.209 \pm 0.048\ R_\oplus$; the uncertainty is dominated by uncertainty in the stellar parameters. From radial-velocity observations of the star, we find an upper limit on the planet mass of 20.3 $M_\oplus$, corresponding to a maximum density of 10.4 g cm^{-3}. We report a significant sinusoidal deviation of the transit times from a predicted linear ephemeris, which we conclude is due to an additional perturbing body in the system. We cannot uniquely determine the orbital parameters of the perturber, as various dynamical mechanisms match the amplitude, period, and shape of the transit timing signal and satisfy the host star's radial velocity limits. However, the perturber in these mechanisms has period $\lesssim$ 160 days and mass $\lesssim 6 M_{Jup}$, confirming its planetary nature as Kepler-19c. We place limits on the presence of transits of Kepler-19c in the available *Kepler* data.

We present the discovery of the Kepler-19 planetary system, which we first identified from a 9.3-day periodic transit signal in the *Kepler* photometry. From high-resolution spectroscopy of the star, we find a stellar effective temperature $T_{\rm eff}$=5541 ± 60 K, a metallicity [Fe/H]=−0.13 ± 0.06, and a surface gravity log(g)=4.59 ± 0.10. We combine the estimate of $T_{\rm eff}$ and [Fe/H] with an estimate of the stellar density derived from the photometric light curve to deduce a stellar mass of $M_\star = 0.936 \pm 0.040\ M_\odot$ and a stellar radius of $R_\star = 0.850 \pm 0.018\ R_\odot$ (these errors do not include uncertainties in the stellar models). We rule out the possibility that the transits result from an astrophysical false positive by first identifying the subset of stellar blends that reproduce the precise shape of the light curve. Using the additional constraints from the measured color of the system, the absence of a secondary source in the high-resolution spectrum, and the absence of a secondary source in the adaptive optics imaging, we conclude that the planetary scenario is more than three orders of magnitude more likely than a blend. The blend scenario is independently disfavored by the achromaticity of the transit: we measure a transit depth with *Spitzer* at 4.5 μm of 547^{+113}_{-110} ppm, consistent with the depth measured in the *Kepler* optical bandpass of 567±6 ppm (corrected for stellar limb-darkening). We determine a physical radius of the planet Kepler-19b of $R_p = 2.209 \pm 0.048\ R_\oplus$; the uncertainty is dominated by uncertainty in the stellar parameters. From radial-velocity observations of the star, we find an upper limit on the planet mass of 20.3 $M_\oplus$, corresponding to a maximum density of 10.4 g cm^{-3}. We report a significant sinusoidal deviation of the transit times from a predicted linear ephemeris, which we conclude is due to an additional perturbing body in the system. We cannot uniquely determine the orbital parameters of the perturber, as various dynamical mechanisms match the amplitude, period, and shape of the transit timing signal and satisfy the host star's radial velocity limits. However, the perturber in these mechanisms has period $\lesssim$ 160 days and mass $\lesssim 6M_{Jup}$, confirming its planetary nature as Kepler-19c. We place limits on the presence of transits of Kepler-19c in the available *Kepler* data.

We present the discovery of the Kepler-19 planetary system, which we first identified from a 9.3-day periodic transit signal in the *Kepler* photometry. From high-resolution spectroscopy of the star, we find a stellar effective temperature $T_{\rm eff}$=5541 ± 60 K, a metallicity [Fe/H]=−0.13 ± 0.06, and a surface gravity log(g)=4.59 ± 0.10. We combine the estimate of $T_{\rm eff}$ and [Fe/H] with an estimate of the stellar density derived from the photometric light curve to deduce a stellar mass of $M_\star = 0.936 \pm 0.040\ M_\odot$ and a stellar radius of $R_\star = 0.850 \pm 0.018\ R_\odot$ (these errors do not include uncertainties in the stellar models). We rule out the possibility that the transits result from an astrophysical false positive by first identifying the subset of stellar blends that reproduce the precise shape of the light curve. Using the additional constraints from the measured color of the system, the absence of a secondary source in the high-resolution spectrum, and the absence of a secondary source in the adaptive optics imaging, we conclude that the planetary scenario is more than three orders of magnitude more likely than a blend. The blend scenario is independently disfavored by the achromaticity of the transit: we measure a transit depth with *Spitzer* at 4.5 μm of 547^{+113}_{-110} ppm, consistent with the depth measured in the *Kepler* optical bandpass of 567±6 ppm (corrected for stellar limb-darkening). We determine a physical radius of the planet Kepler-19b of $R_p = 2.209 \pm 0.048\ R_\oplus$; the uncertainty is dominated by uncertainty in the stellar parameters. From radial-velocity observations of the star, we find an upper limit on the planet mass of 20.3 $M_\oplus$, corresponding to a maximum density of 10.4 g cm^{-3}. We report a significant sinusoidal deviation of the transit times from a predicted linear ephemeris, which we conclude is due to an additional perturbing body in the system. We cannot uniquely determine the orbital parameters of the perturber, as various dynamical mechanisms match the amplitude, period, and shape of the transit timing signal and satisfy the host star's radial velocity limits. However, the perturber in these mechanisms has period $\lesssim 160$ days and mass $\lesssim 6M_{Jup}$, confirming its planetary nature as Kepler-19c. We place limits on the presence of transits of Kepler-19c in the available *Kepler* data.

We present the discovery of the Kepler-19 planetary system, which we first identified from a 9.3-day periodic transit signal in the *Kepler* photometry. From high-resolution spectroscopy of the star, we find a stellar effective temperature $T_{\rm eff}$=5541 ± 60 K, a metallicity [Fe/H]=−0.13 ± 0.06, and a surface gravity log(g)=4.59 ± 0.10. We combine the estimate of $T_{\rm eff}$ and [Fe/H] with an estimate of the stellar density derived from the photometric light curve to deduce a stellar mass of $M_\star = 0.936 \pm 0.040\ M_\odot$ and a stellar radius of $R_\star = 0.850 \pm 0.018\ R_\odot$ (these errors do not include uncertainties in the stellar models). We rule out the possibility that the transits result from an astrophysical false positive by first identifying the subset of stellar blends that reproduce the precise shape of the light curve. Using the additional constraints from the measured color of the system, the absence of a secondary source in the high-resolution spectrum, and the absence of a secondary source in the adaptive optics imaging, we conclude that the planetary scenario is more than three orders of magnitude more likely than a blend. The blend scenario is independently disfavored by the achromaticity of the transit: we measure a transit depth with *Spitzer* at 4.5 μm of 547^{+113}_{-110} ppm, consistent with the depth measured in the *Kepler* optical bandpass of 567±6 ppm (corrected for stellar limb-darkening). We determine a physical radius of the planet Kepler-19b of $R_p = 2.209 \pm 0.048\ R_\oplus$; the uncertainty is dominated by uncertainty in the stellar parameters. From radial-velocity observations of the star, we find an upper limit on the planet mass of 20.3 $M_\oplus$, corresponding to a maximum density of 10.4 g cm^{-3}. We report a significant sinusoidal deviation of the transit times from a predicted linear ephemeris, which we conclude is due to an additional perturbing body in the system. We cannot uniquely determine the orbital parameters of the perturber, as various dynamical mechanisms match the amplitude, period, and shape of the transit timing signal and satisfy the host star's radial velocity limits. However, the perturber in these mechanisms has period $\lesssim$ 160 days and mass $\lesssim 6M_{Jup}$, confirming its planetary nature as Kepler-19c. We place limits on the presence of transits of Kepler-19c in the available *Kepler* data.

We present the discovery of the Kepler-19 planetary system, which we first identified from a 9.3-day periodic transit signal in the *Kepler* photometry. From high-resolution spectroscopy of the star, we find a stellar effective temperature $T_{\rm eff}$=5541 $\pm$ 60 K, a metallicity [Fe/H]=-0.13 ± 0.06, and a surface gravity log(g)=4.59 ± 0.10. We combine the estimate of $T_{\rm eff}$ and [Fe/H] with an estimate of the stellar density derived from the photometric light curve to deduce a stellar mass of $M_\star = 0.936 \pm 0.040\ M_\odot$ and a stellar radius of $R_\star = 0.850 \pm 0.018\ R_\odot$ (these errors do not include uncertainties in the stellar models). We rule out the possibility that the transits result from an astrophysical false positive by first identifying the subset of stellar blends that reproduce the precise shape of the light curve. Using the additional constraints from the measured color of the system, the absence of a secondary source in the high-resolution spectrum, and the absence of a secondary source in the adaptive optics imaging, we conclude that the planetary scenario is more than three orders of magnitude more likely than a blend. The blend scenario is independently disfavored by the achromaticity of the transit: we measure a transit depth with *Spitzer* at 4.5 μm of 547^{+113}_{-110} ppm, consistent with the depth measured in the *Kepler* optical bandpass of 567$\pm$6 ppm (corrected for stellar limb-darkening). We determine a physical radius of the planet Kepler-19b of $R_p = 2.209 \pm 0.048\ R_\oplus$; the uncertainty is dominated by uncertainty in the stellar parameters. From radial-velocity observations of the star, we find an upper limit on the planet mass of 20.3 $M_\oplus$, corresponding to a maximum density of 10.4 g cm^{-3}. We report a significant sinusoidal deviation of the transit times from a predicted linear ephemeris, which we conclude is due to an additional perturbing body in the system. We cannot uniquely determine the orbital parameters of the perturber, as various dynamical mechanisms match the amplitude, period, and shape of the transit timing signal and satisfy the host star's radial velocity limits. However, the perturber in these mechanisms has period $\lesssim$ 160 days and mass $\lesssim 6 M_{Jup}$, confirming its planetary nature as Kepler-19c. We place limits on the presence of transits of Kepler-19c in the available *Kepler* data.

We present the discovery of the Kepler-19 planetary system, which we first identified from a 9.3-day periodic transit signal in the *Kepler* photometry. From high-resolution spectroscopy of the star, we find a stellar effective temperature $T_{\rm eff}$=5541 ± 60 K, a metallicity [Fe/H]=−0.13 ± 0.06, and a surface gravity log(g)=4.59 ± 0.10. We combine the estimate of $T_{\rm eff}$ and [Fe/H] with an estimate of the stellar density derived from the photometric light curve to deduce a stellar mass of $M_\star = 0.936 \pm 0.040\ M_\odot$ and a stellar radius of $R_\star = 0.850 \pm 0.018\ R_\odot$ (these errors do not include uncertainties in the stellar models). We rule out the possibility that the transits result from an astrophysical false positive by first identifying the subset of stellar blends that reproduce the precise shape of the light curve. Using the additional constraints from the measured color of the system, the absence of a secondary source in the high-resolution spectrum, and the absence of a secondary source in the adaptive optics imaging, we conclude that the planetary scenario is more than three orders of magnitude more likely than a blend. The blend scenario is independently disfavored by the achromaticity of the transit: we measure a transit depth with *Spitzer* at 4.5 μm of 547^{+113}_{-110} ppm, consistent with the depth measured in the *Kepler* optical bandpass of 567±6 ppm (corrected for stellar limb-darkening). We determine a physical radius of the planet Kepler-19b of $R_p = 2.209 \pm 0.048\ R_\oplus$; the uncertainty is dominated by uncertainty in the stellar parameters. From radial-velocity observations of the star, we find an upper limit on the planet mass of 20.3 $M_\oplus$, corresponding to a maximum density of 10.4 g cm^{-3}. We report a significant sinusoidal deviation of the transit times from a predicted linear ephemeris, which we conclude is due to an additional perturbing body in the system. We cannot uniquely determine the orbital parameters of the perturber, as various dynamical mechanisms match the amplitude, period, and shape of the transit timing signal and satisfy the host star's radial velocity limits. However, the perturber in these mechanisms has period $\lesssim$ 160 days and mass $\lesssim 6 M_{Jup}$, confirming its planetary nature as Kepler-19c. We place limits on the presence of transits of Kepler-19c in the available *Kepler* data.

Transit Curves Fit to Linear Emphemeris

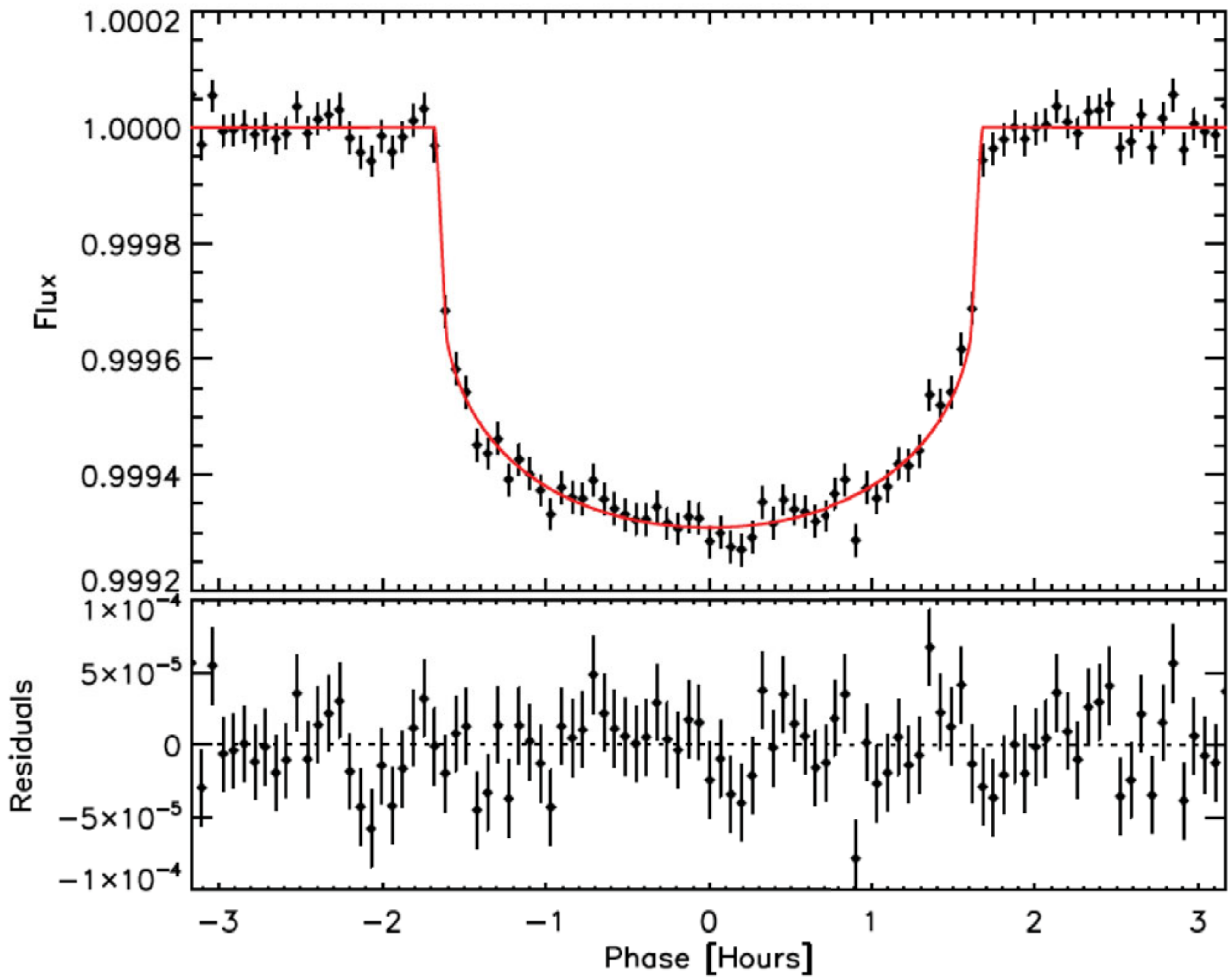

Comparison of Early and Late Transits

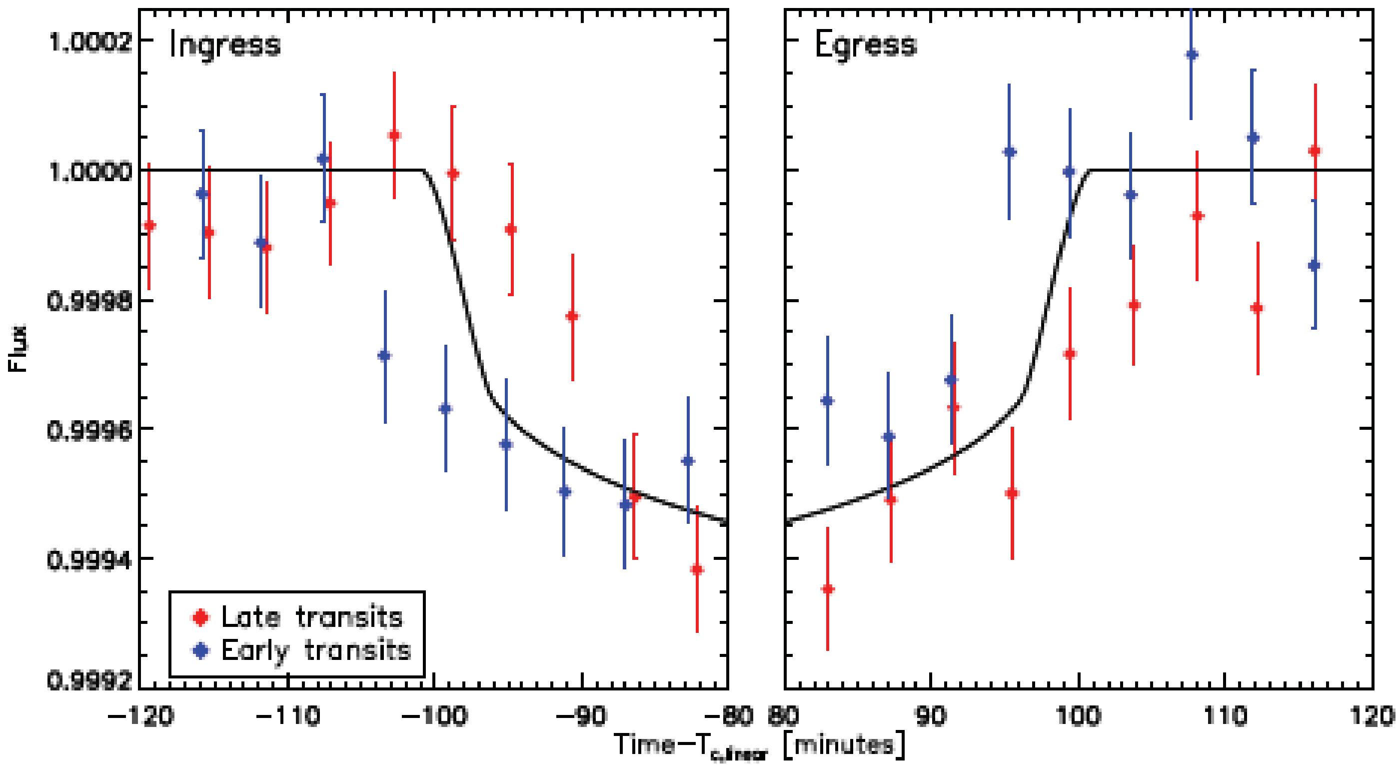

Possible Kepler 19c Orbits

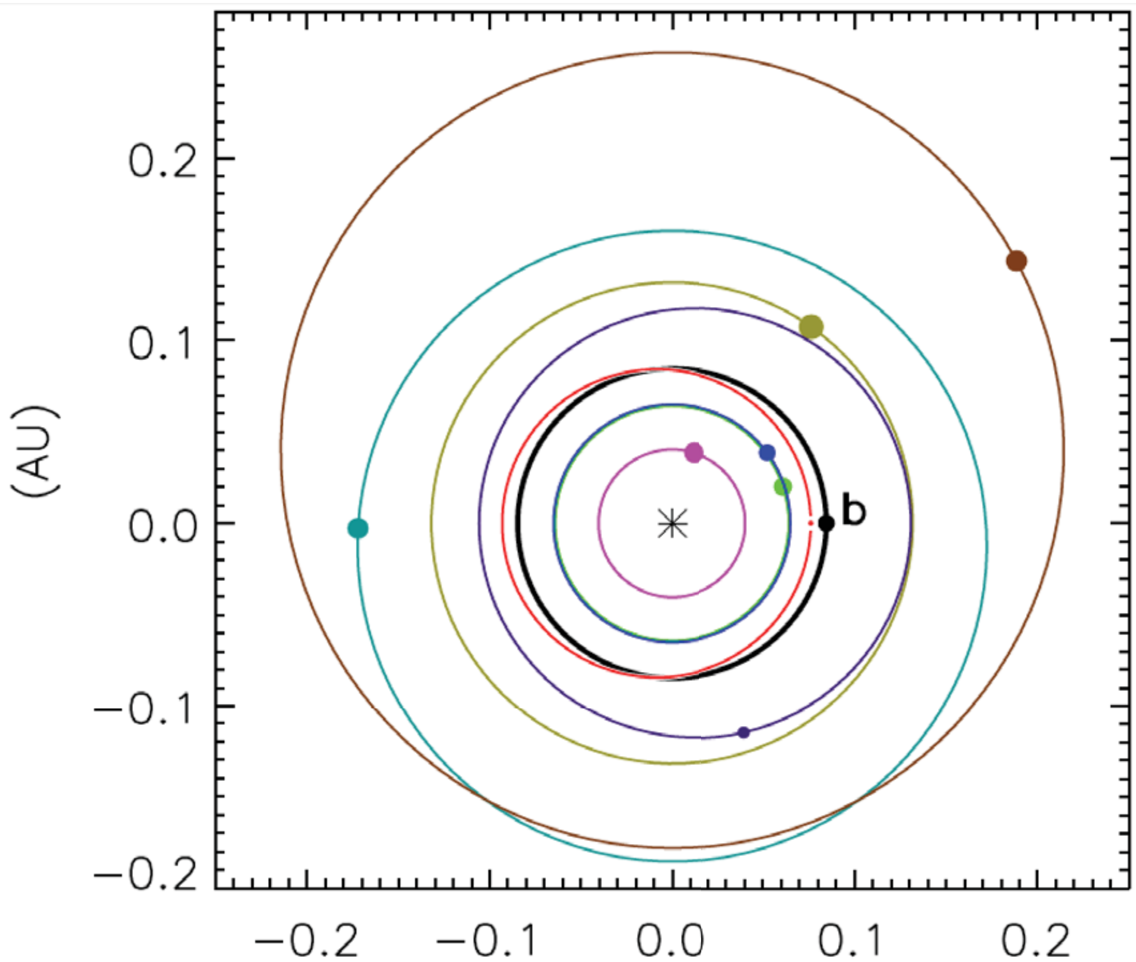

Co-Orbital:
9.287^d
2:3 Resonance:
6.129^d
6.252^d
2:1 Resonance
18.033^d
1:3 Resonance
3.065^d
5:3 Resonance
15.236^d

Transit Timing Variations in a Nutshell

- Transit timing variations (TTV) make it possible to find unseen members of an exosolar system with at least one transiting member.
- May be able to detect planets that are not massive enough to be found with PRV.
- TTVs are hard:
  - The effect is subtle;
  - The data needs to be very high quality − e.g. Kepler;
  - Many models may satisfy the observational boundary conditions;
  - Fairly sophisticated Bayesian modeling required to find the “right” answer;
  - There may be several “right” answers − solutions may be degenerate.
- <u>In some cases, data may be inverted to determine planet system dynamics and constrain masses. But it is very hard.</u>

Microlensing

Some Prominent Microlensing Telescopes

KMTNet

- Network of 3, Southern hemisphere, globally distributed 1.6m optical telescopes.
- Purposed explicitly for detection of microlensing exoplanets.
- Sliding Springs, Australia, South African Astronomical Observatory & Cerro Tololo, Chile.
- Longitude distribution permits continuous temporal coverage of observations (in principle).

WFIRST

- Repurposed surveillance telescope
- Aperture 2.4 m diameter
- NIR (0.76 - 2.0 μ) passband.
- “Wide field” square, 0.53°on a side.
- Cosmology + exoplanet microlensing mission.
- Cancelled in later US Presidential budget (but not dead yet.

The Principle of Gravitational Lensing

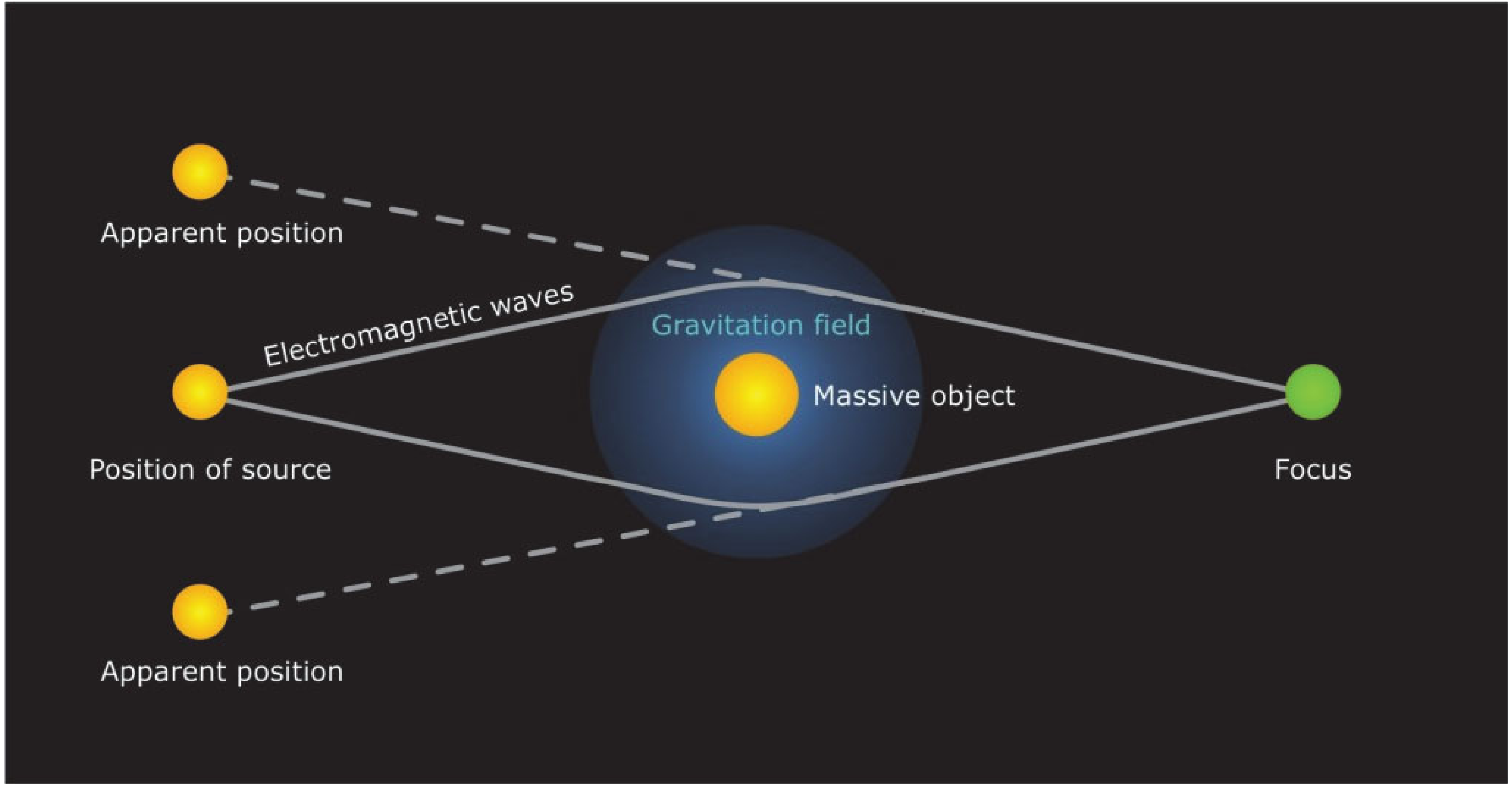

- A mass between the target and the observer bends space.
- The bending focuses the light of the image of the target.
- The target appears brighter to the observer because of this focusing.

Microlensing Often Produces Multiple Images

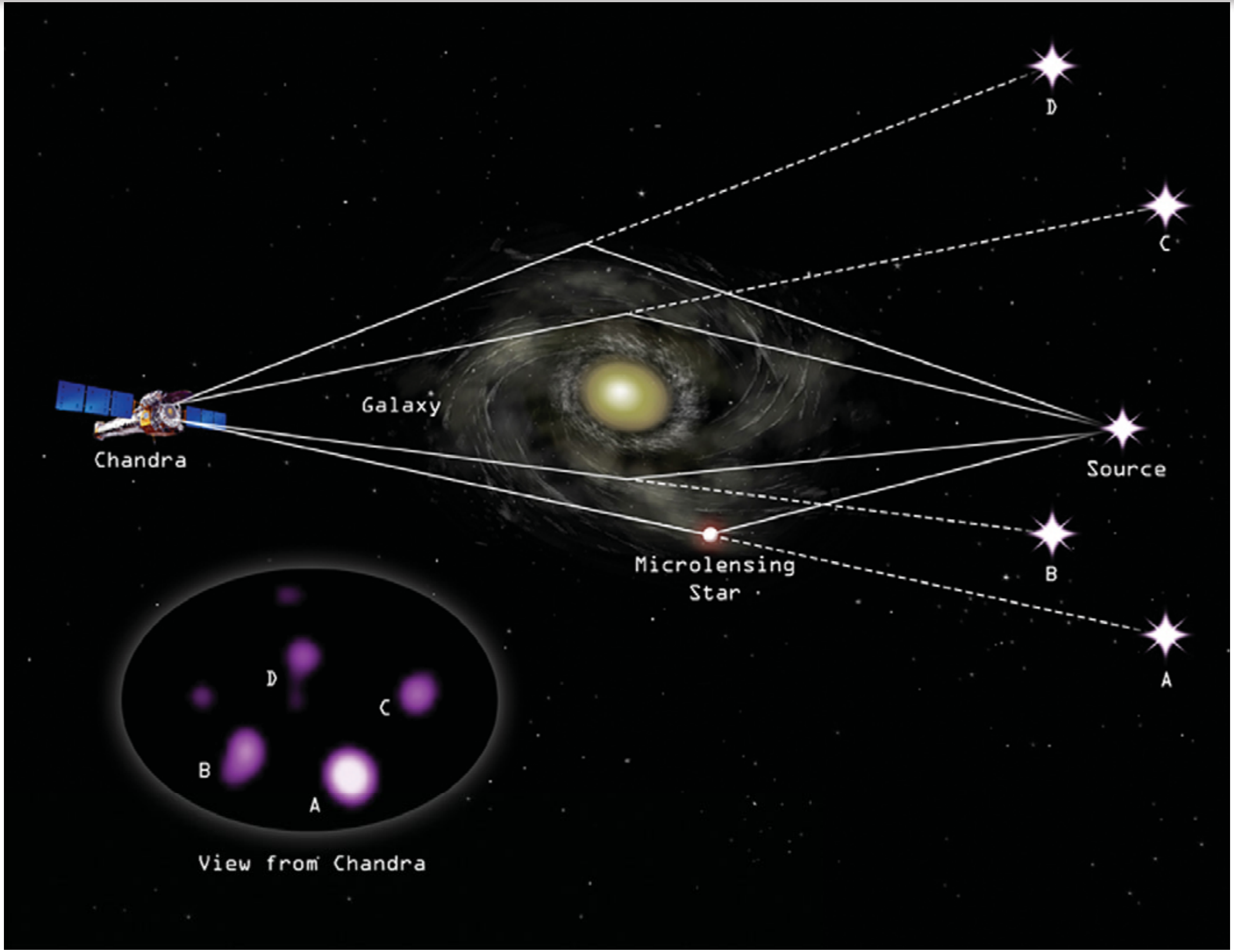

Gravitational Lensing on Cosmological Scale

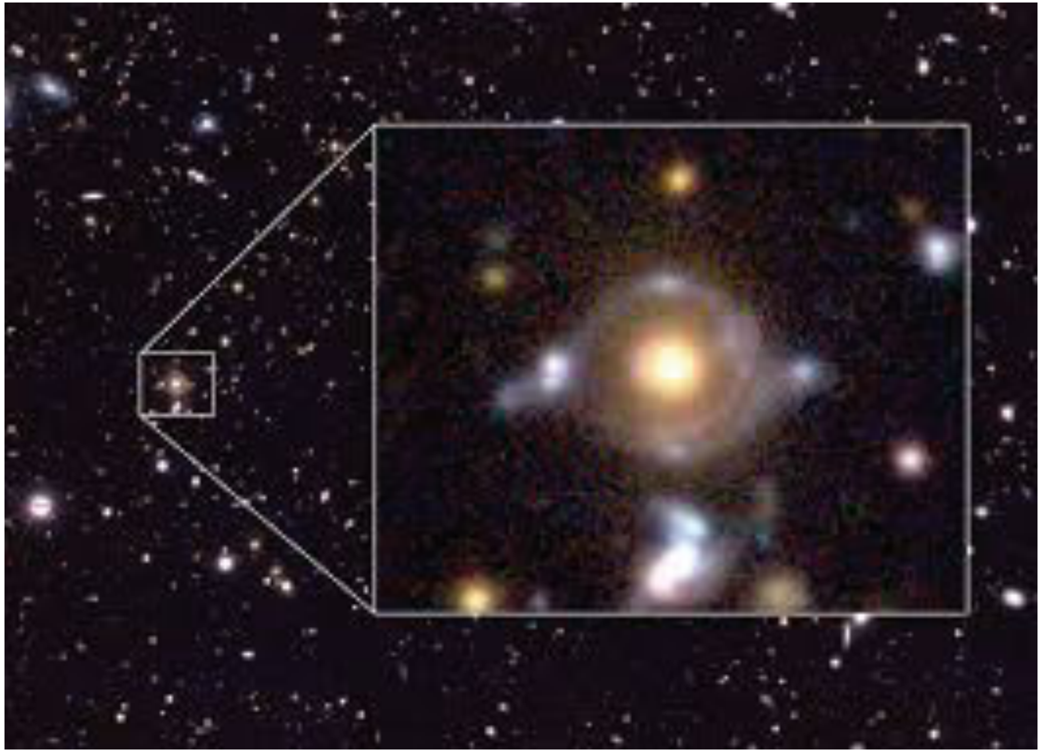

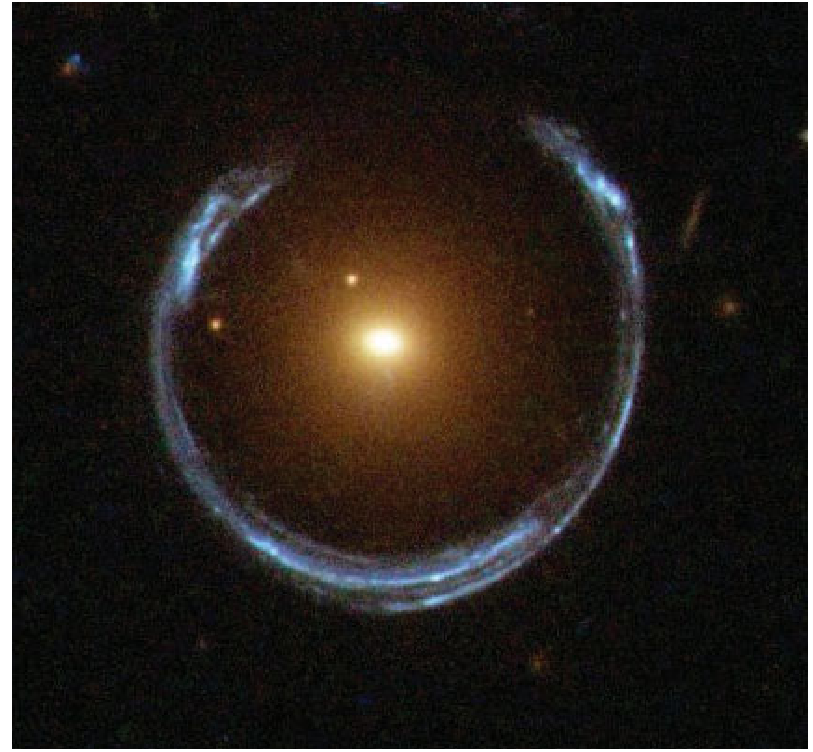

- Foreground galaxies serves as lenses for background galaxies.
- Background galaxies are farther away, farther back in time and rapidly forming stars, hence lensed images are often blue.

Clusters of Galaxies Are Good Gravitiational Lenses

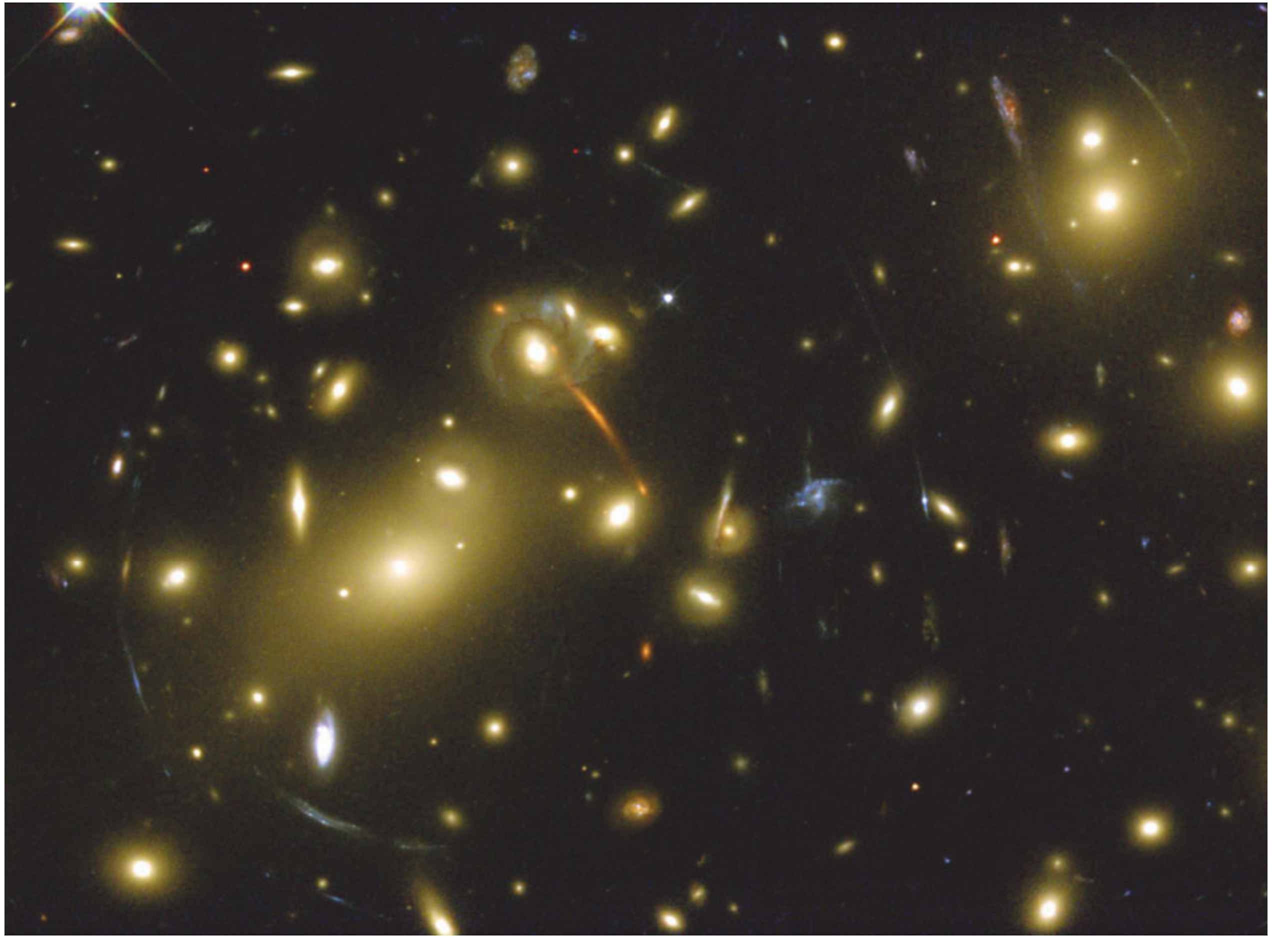

The deep gravitational potential well of cluster of galaxies are good gravitational lenses.

Gravitational Microlensing

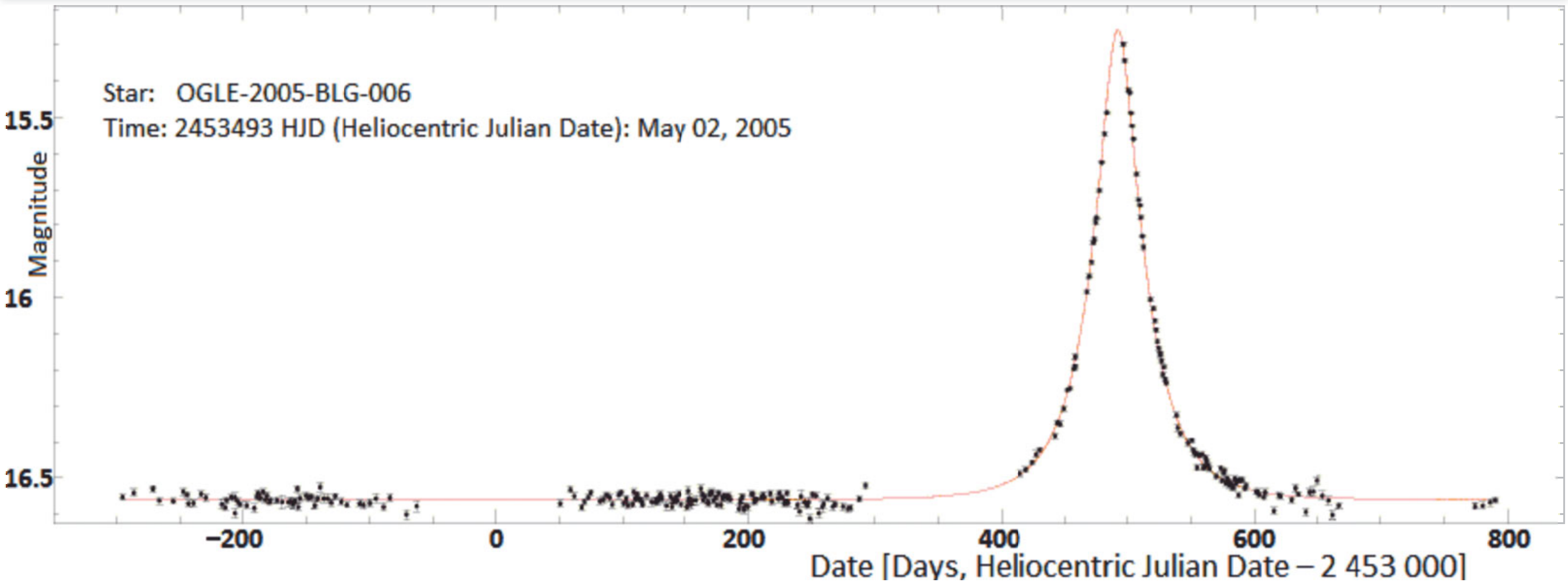

- Microlensing by stars “microlensing first predicted by Paczynski in 1986.
- The first microlensing event was detected in 1989.
- Used to search from Massive Compact Halo Objects.

Microlensing with Exoplanets

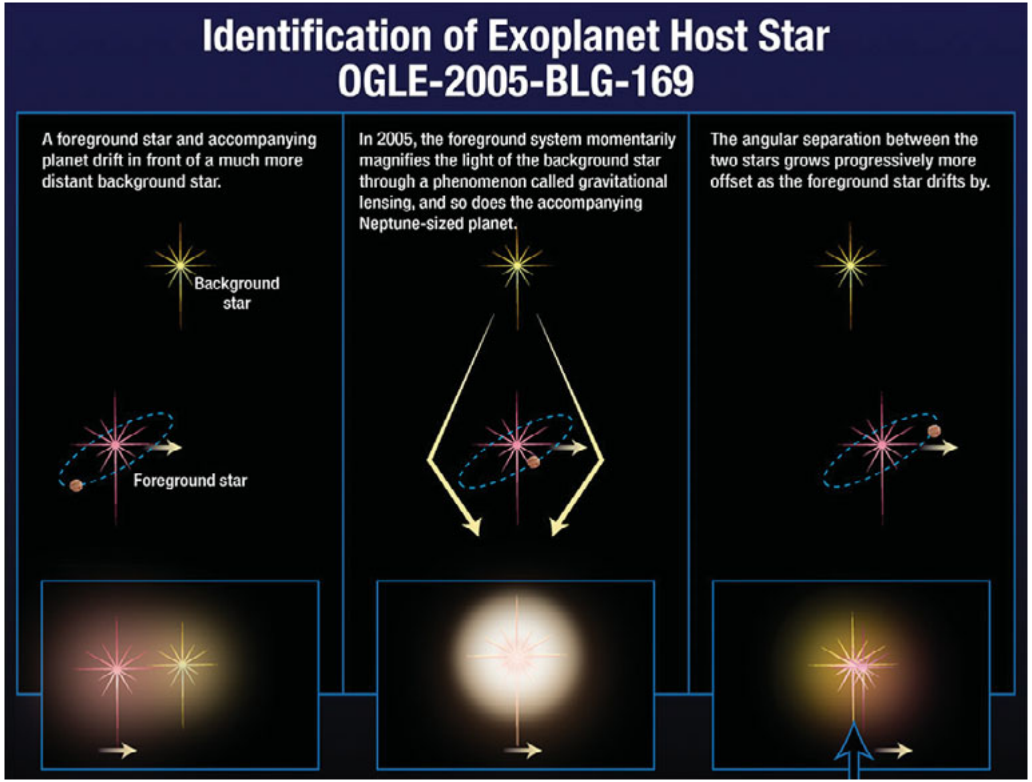

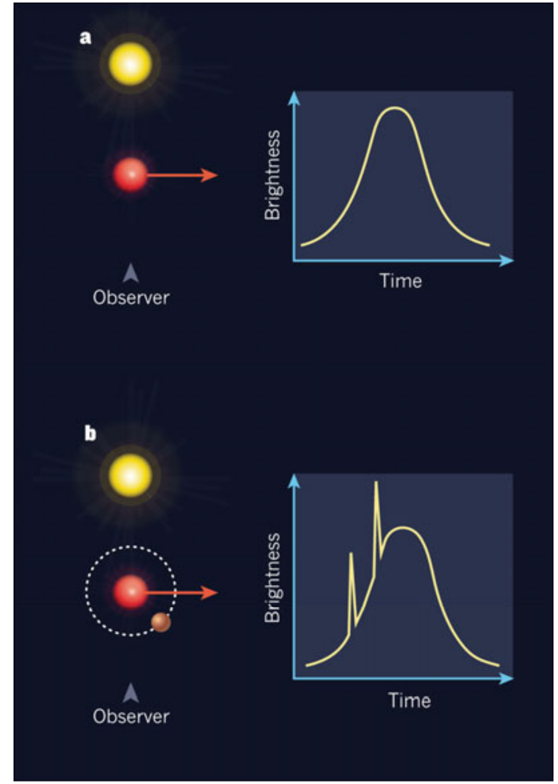

- When there is no exoplanet, the microlensing curve is a smooth curve.
- When a planet orbits the stellar lens, the planet is a lens too.
- It is very small, and moving (oribiting the host star), so the microlensing event is very short.
- The exoplanet is sensed by the “blips” it produce on the stellar microlensing curve.

An Example of a Exoplanet Detected by Microlensing

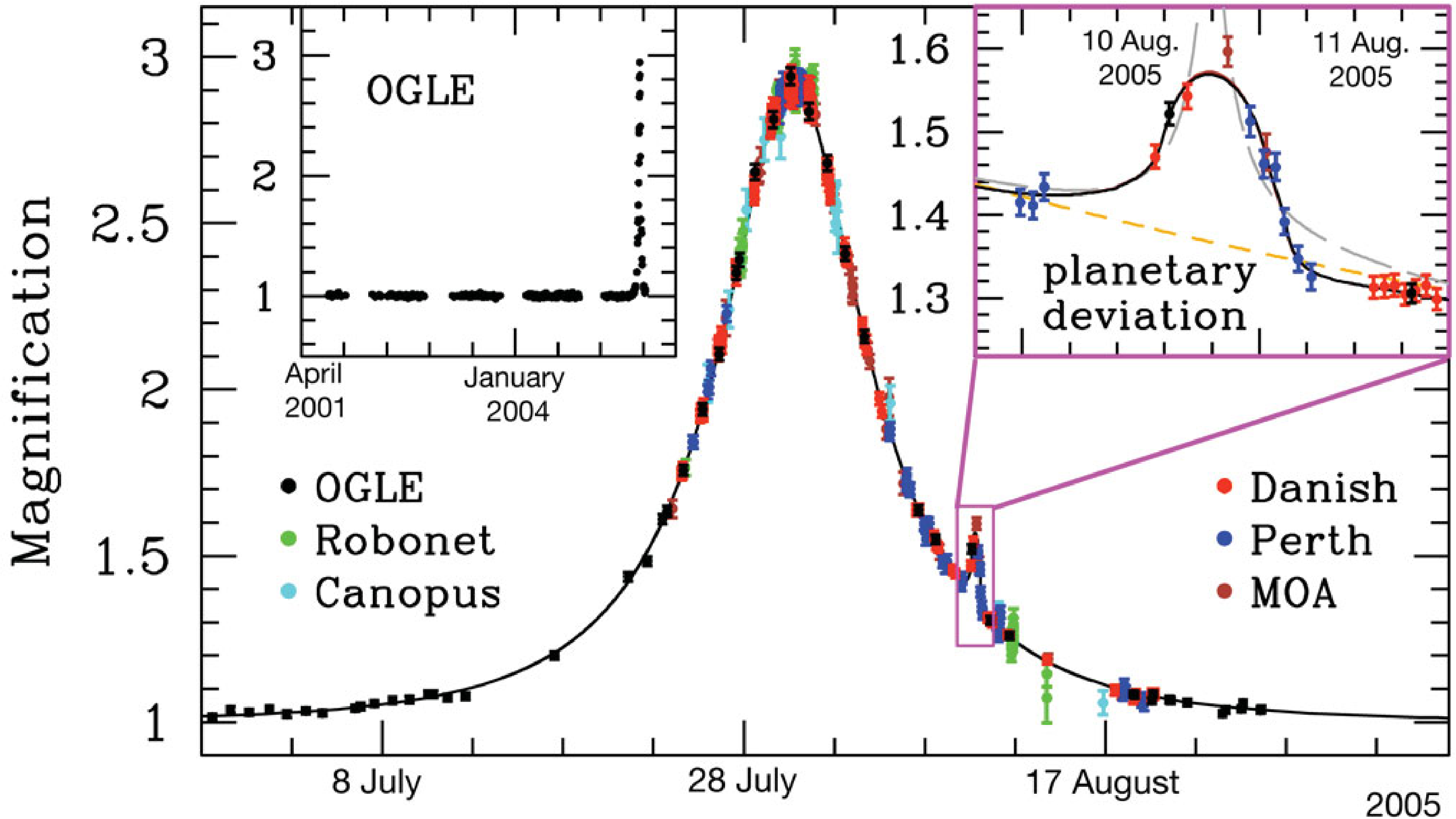

Light Curve of OGLE-2005-BLG-390

Measuring the Absolute Distance to the Exoplanet Microlensing + Parallax

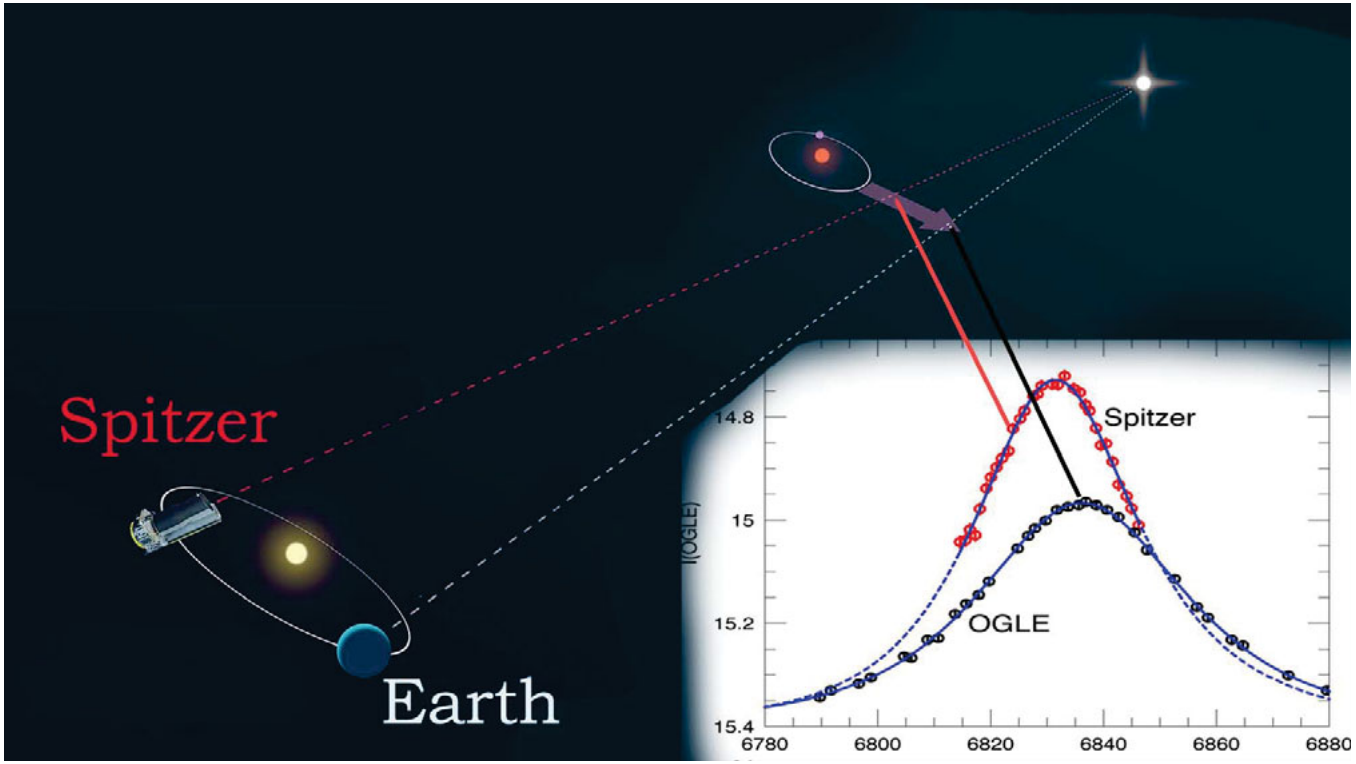

- Spitzer and Kepler (formerly), in Earth trailing orbits, are now very far from Earth.
- This provides two widely separated observing stations.
- It is then possible to make parallax measurement of the lensed exoplanet.
- Parallax provides a direct measurement of the distance to the lens system.

Advantages and Disadvantages of Microlensing

- Microlensing can detect planet with very large semimajor axes.
  - The distance from the star − in a very wide orbit is irrelevant.
  - These planets are very hard do detect by any other methods, except direct imaging (more on this later).
- Microlensing is the best (generally, only) probe of exoplanets at and beyond the snow line in mature exoplanetary systems.
- Stellar noise does not affect microlensing.
- Microlensing measures absolute distances, as long as Spitzer lasts

But ..

- Microlensing can only be done once for any star ⋯ you see it and then it is gone forever.
- It is probably impossible to observe microlensed stars by any other method.
- The exoplanetary system is only measured at one epoch.

Direct Imaging

Taking Direct Images of Exoplanet Requires Sharp Images

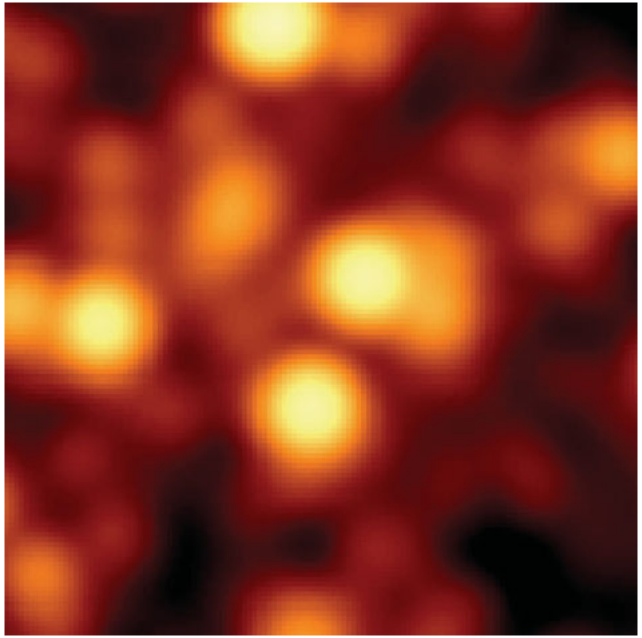

GMT without adaptive optics

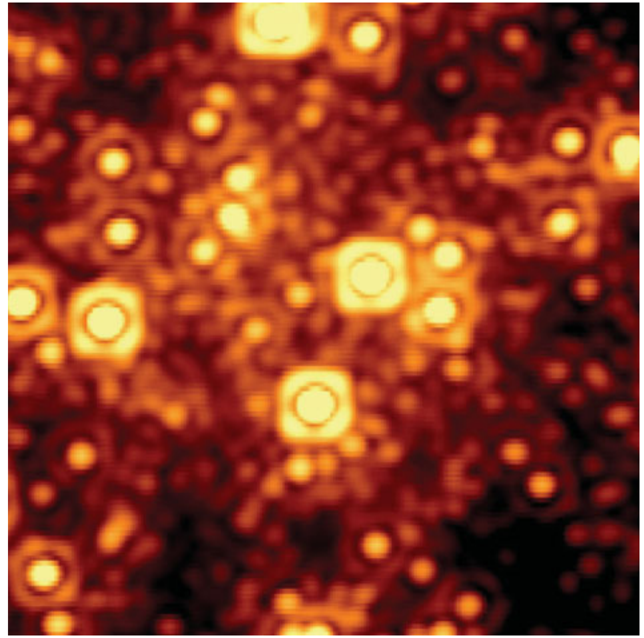

Hubble Space Telescope

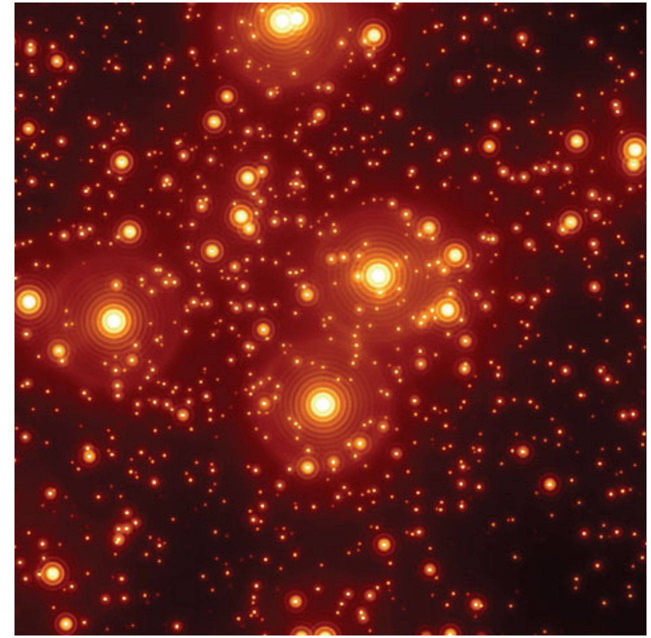

GMT with adaptive optics

Adaptive Optics in a Nutshell

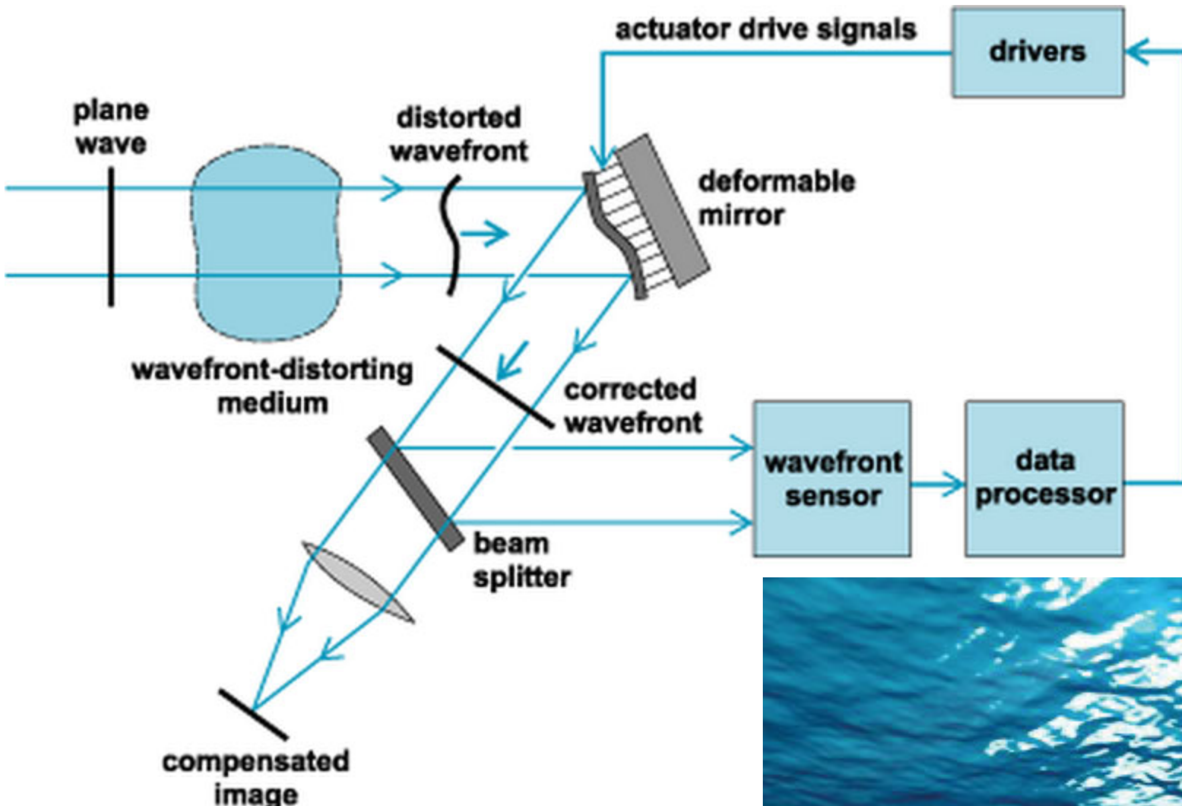

Adaptive Optics Data from the MMT

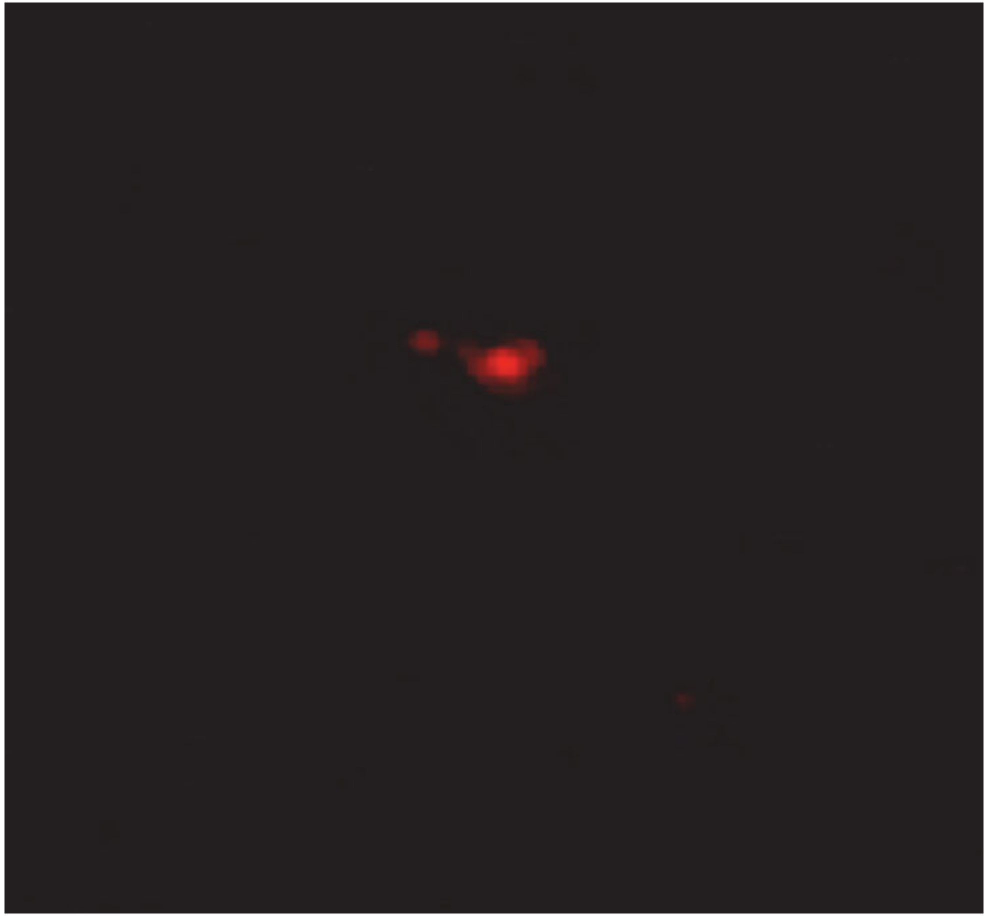

AO On

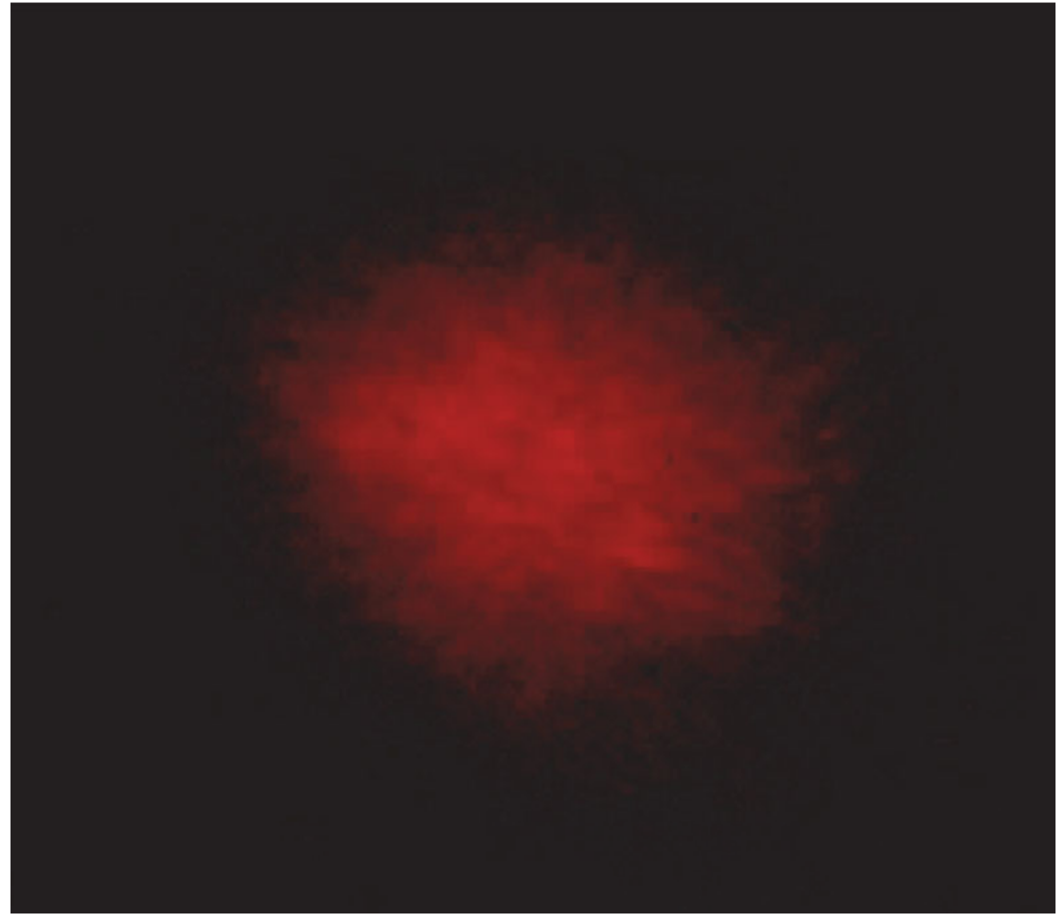

AO Off

Solar Coronagraphy

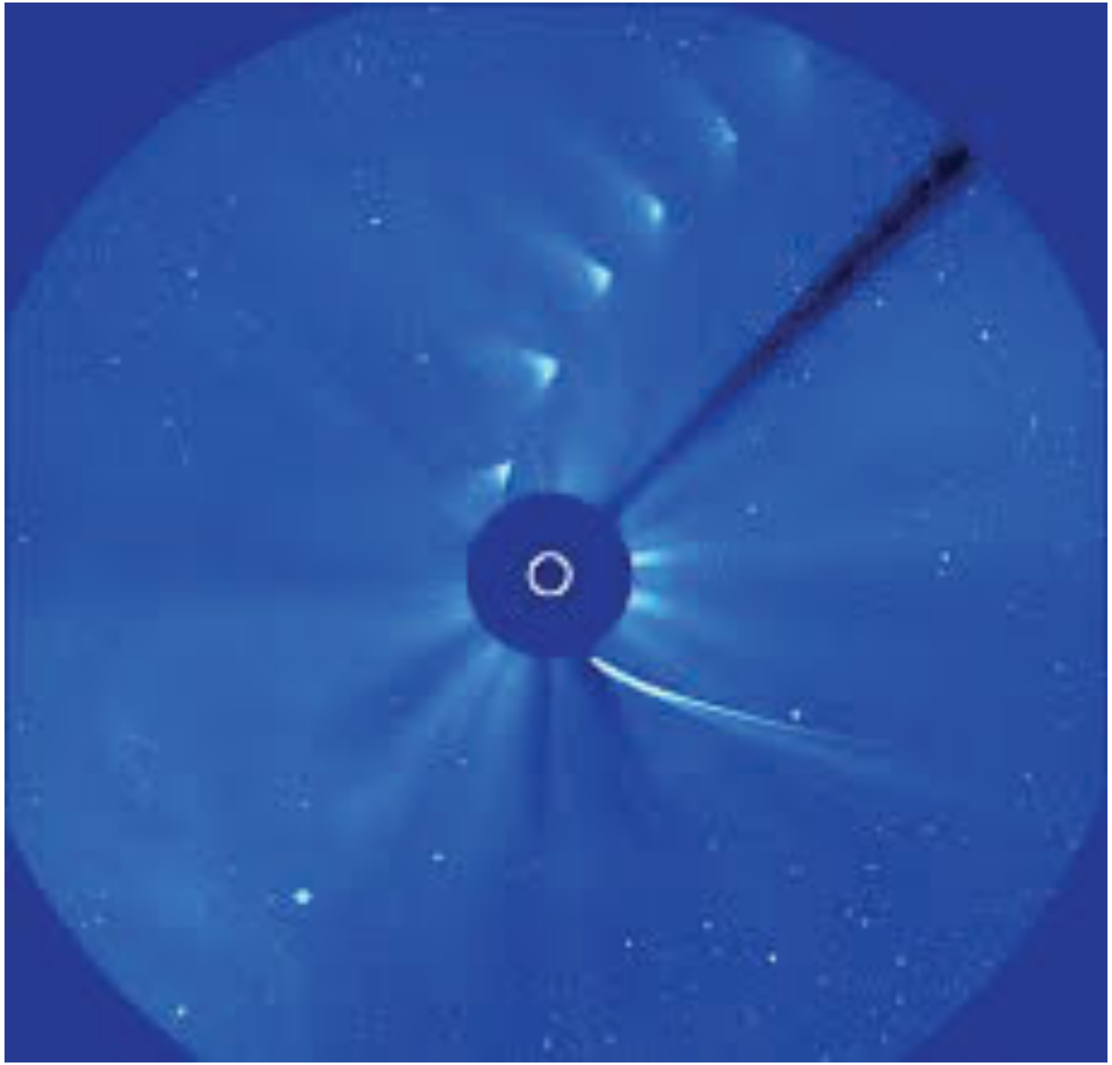

- Stars are bright, solar system objects are not.
- Blotting our the star (or Sun) makes faint, nearby images visible.
- Here Comet ISON passing behind the is observed with the SOHO coronagraph.

The Basic Coronagraph

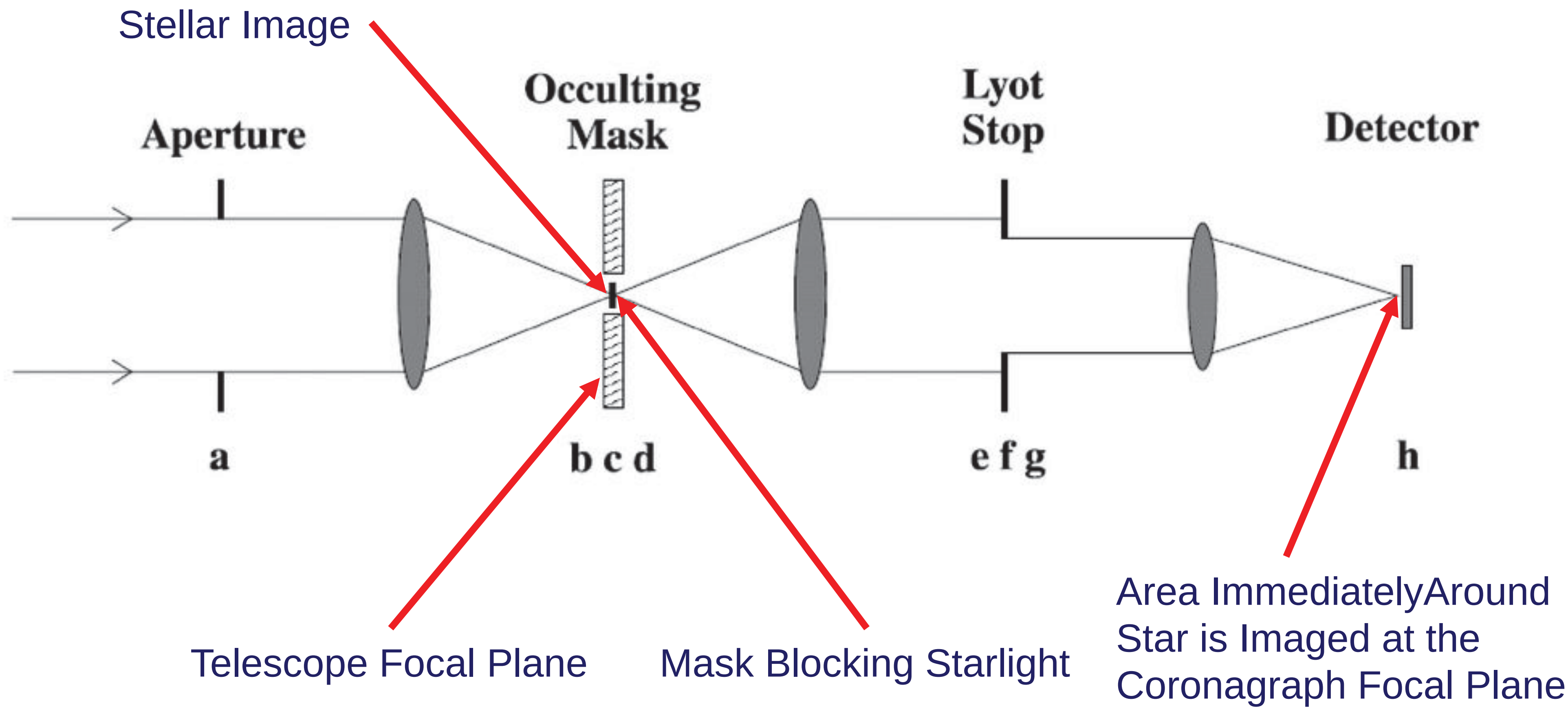

Coronagraphic Direct Image of Fomalhaut

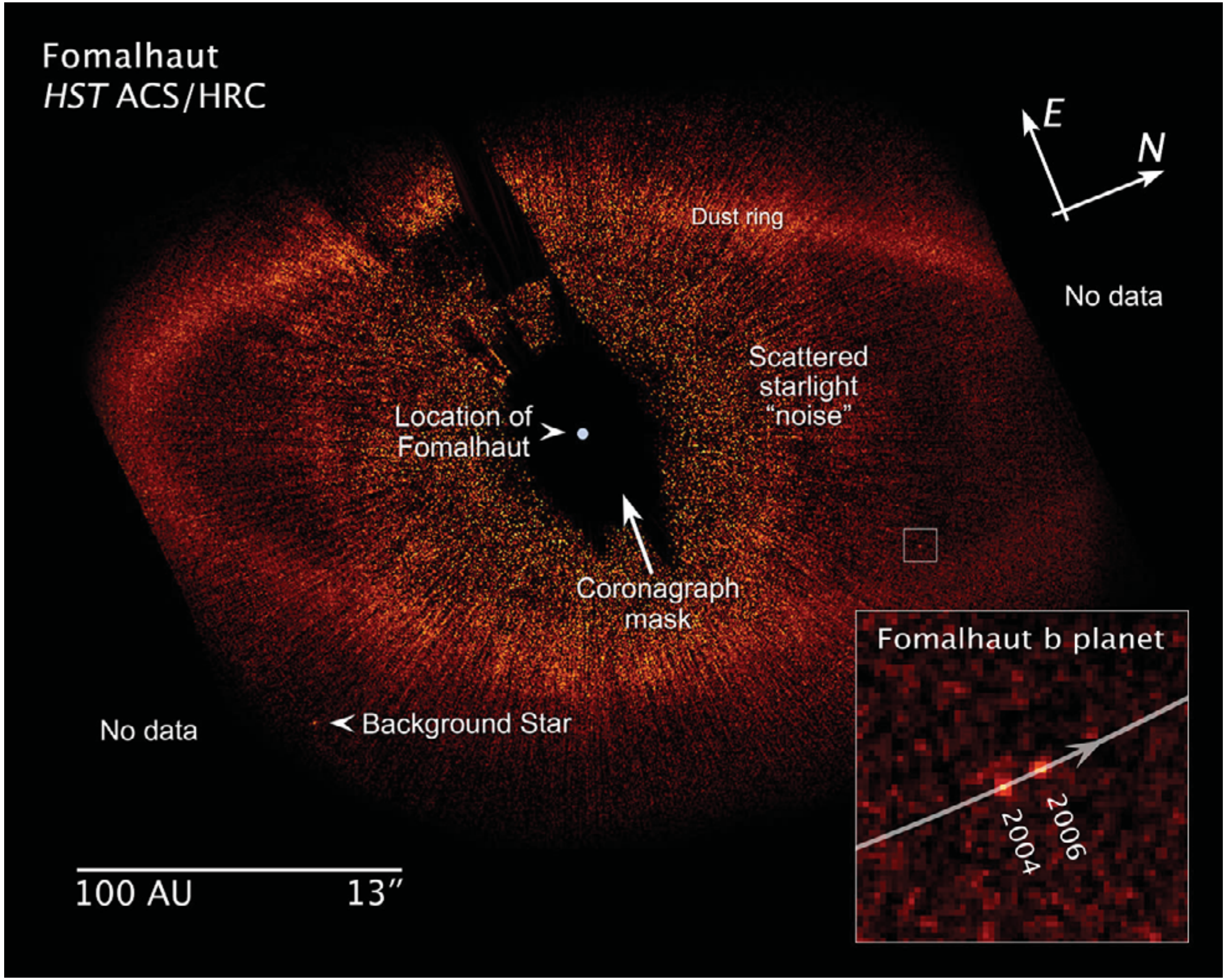

The Fomalhaut System

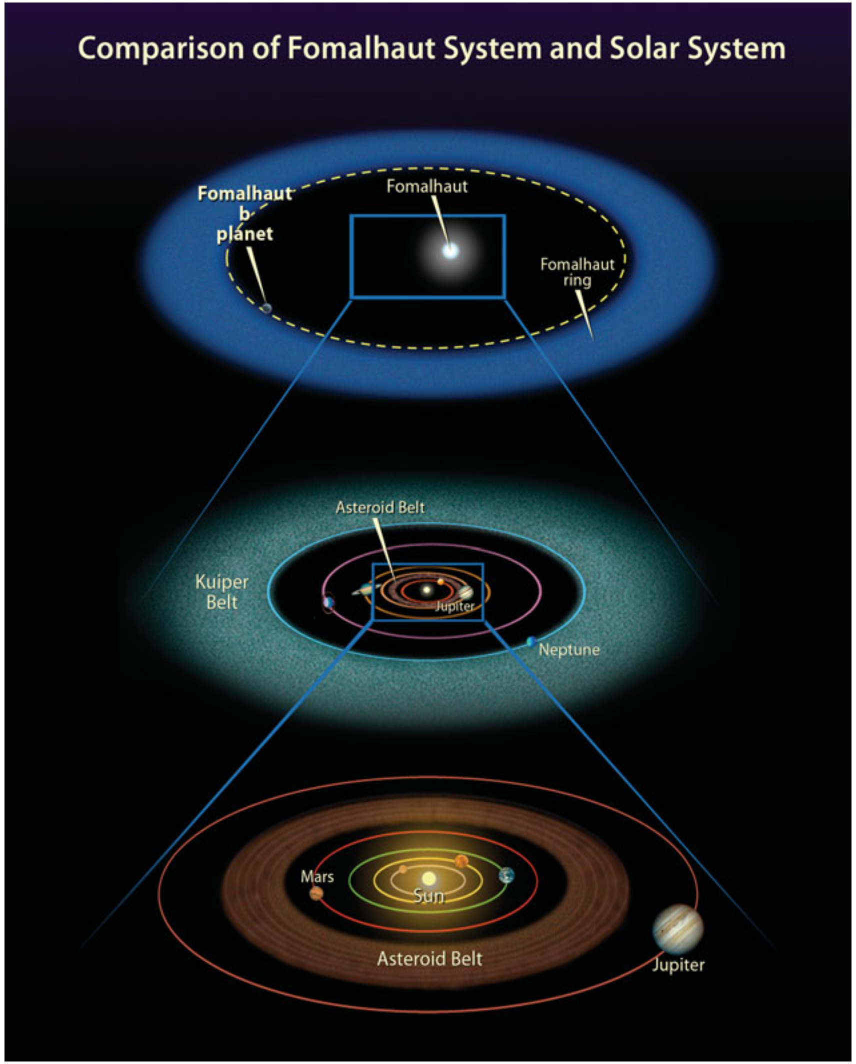

- Fomalhaut is a spectral type A
  - Hard/impossible by PRV
- The orbit is very wide
  - Angular separation is large
  - Star/planet discrimination is easy
- Fomalhaut b is young
  - Hot and self-luminous
  - Bright in the infrared
- Technique not capable of observing “old” system that are not self-luminous
- Available telescope can not discriminate systems as small as the Solar System

What Does the Future Hold for Coronagraphy?

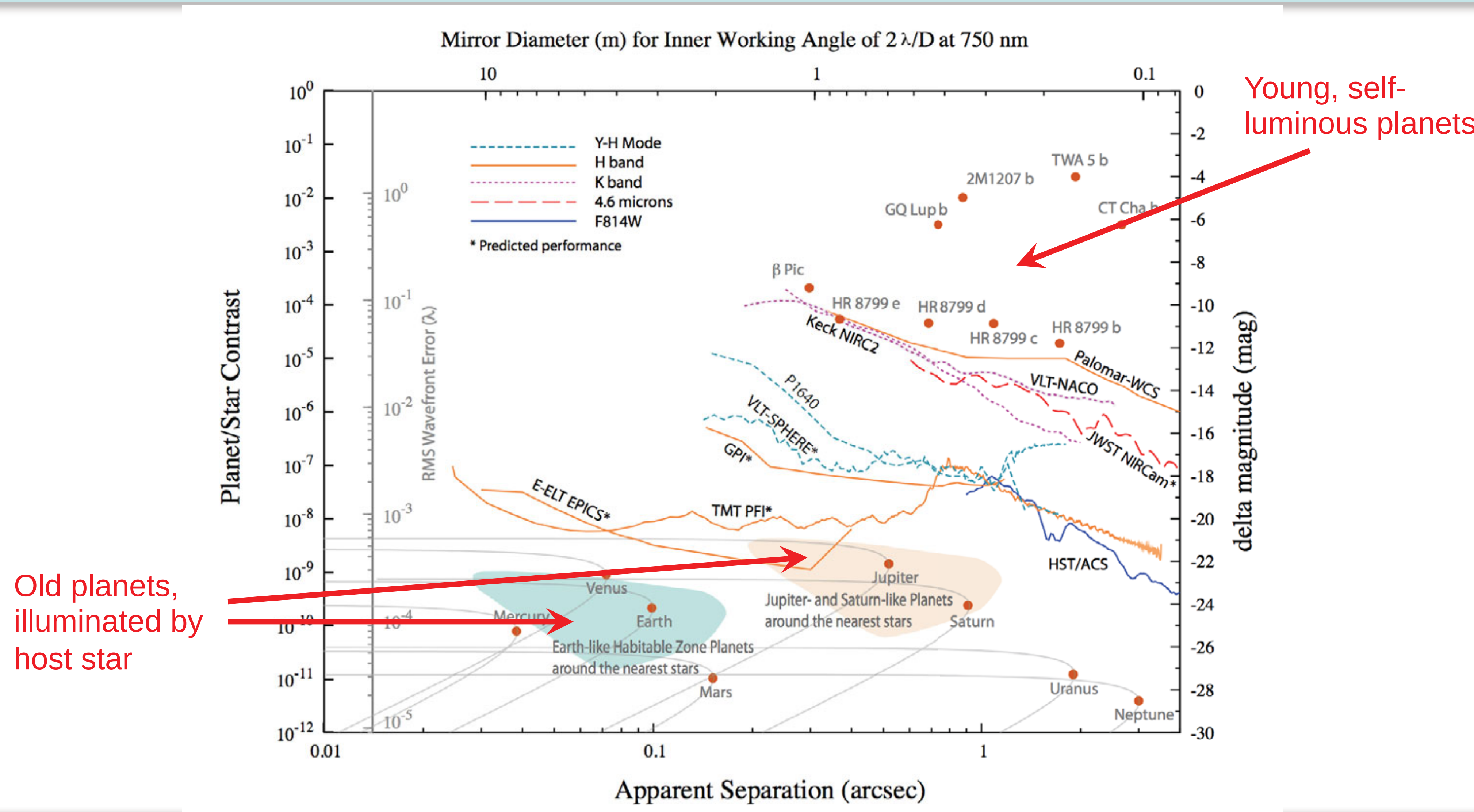

Spectral Dependence of Contrast for Old Planets

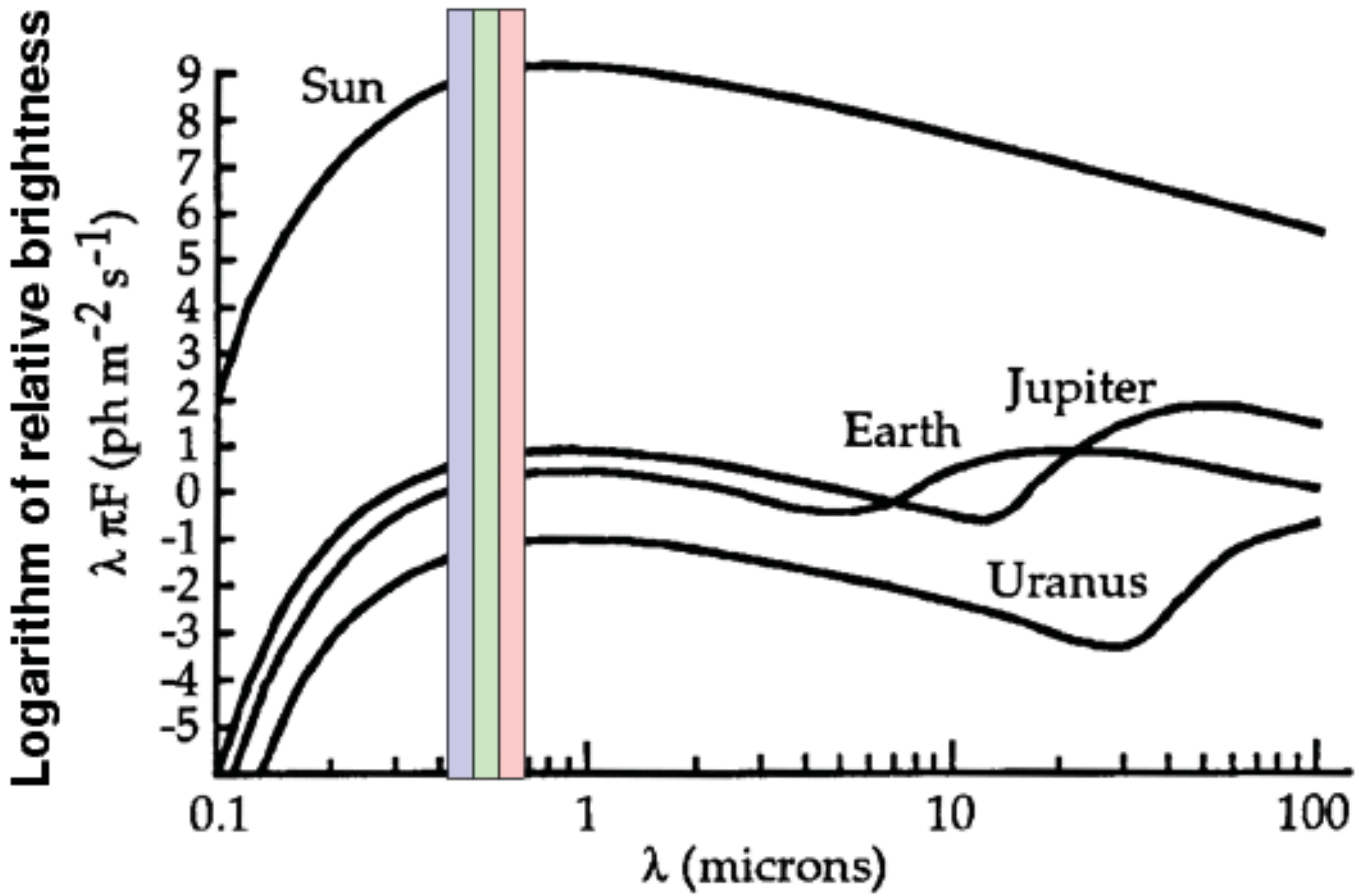

Spectral Dependence of Contrast for Old Planets, in More Detail

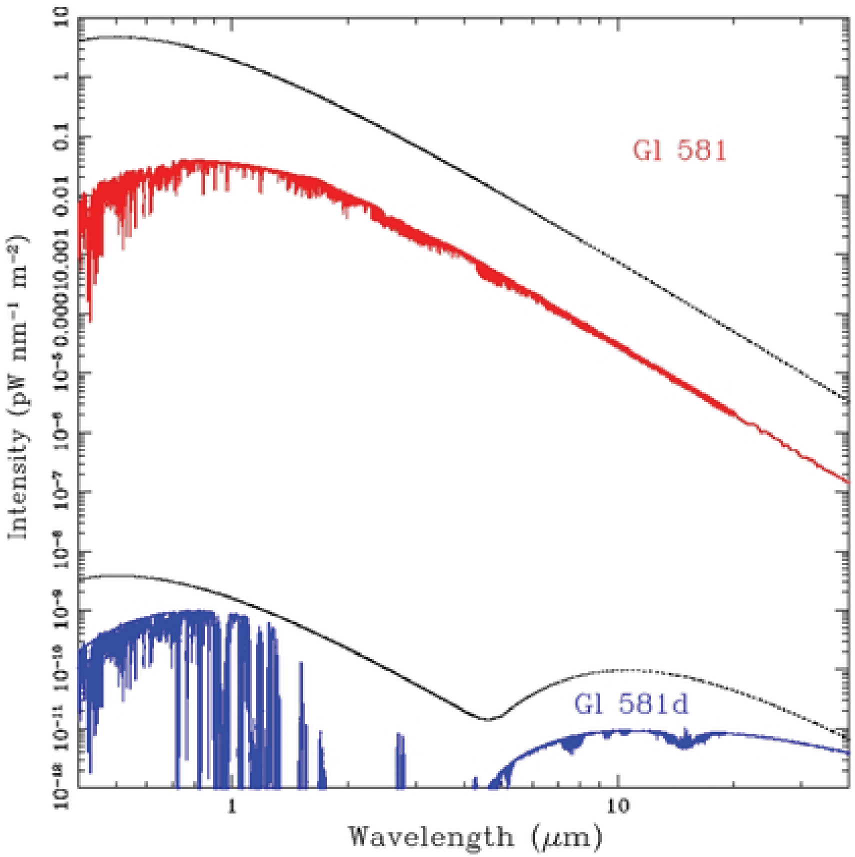

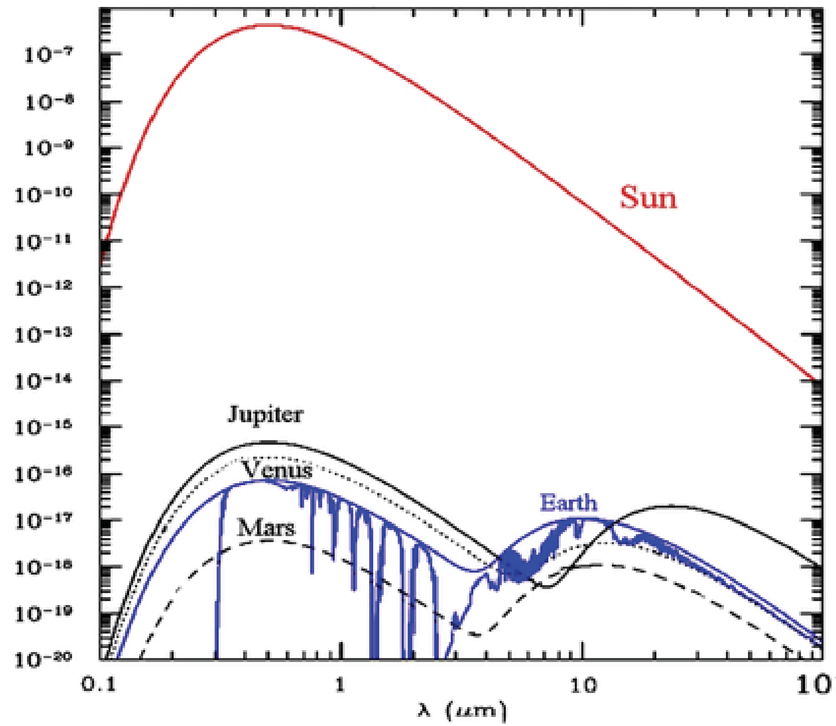

Direct Imaging of Old ExoSolar System Will Be Hard

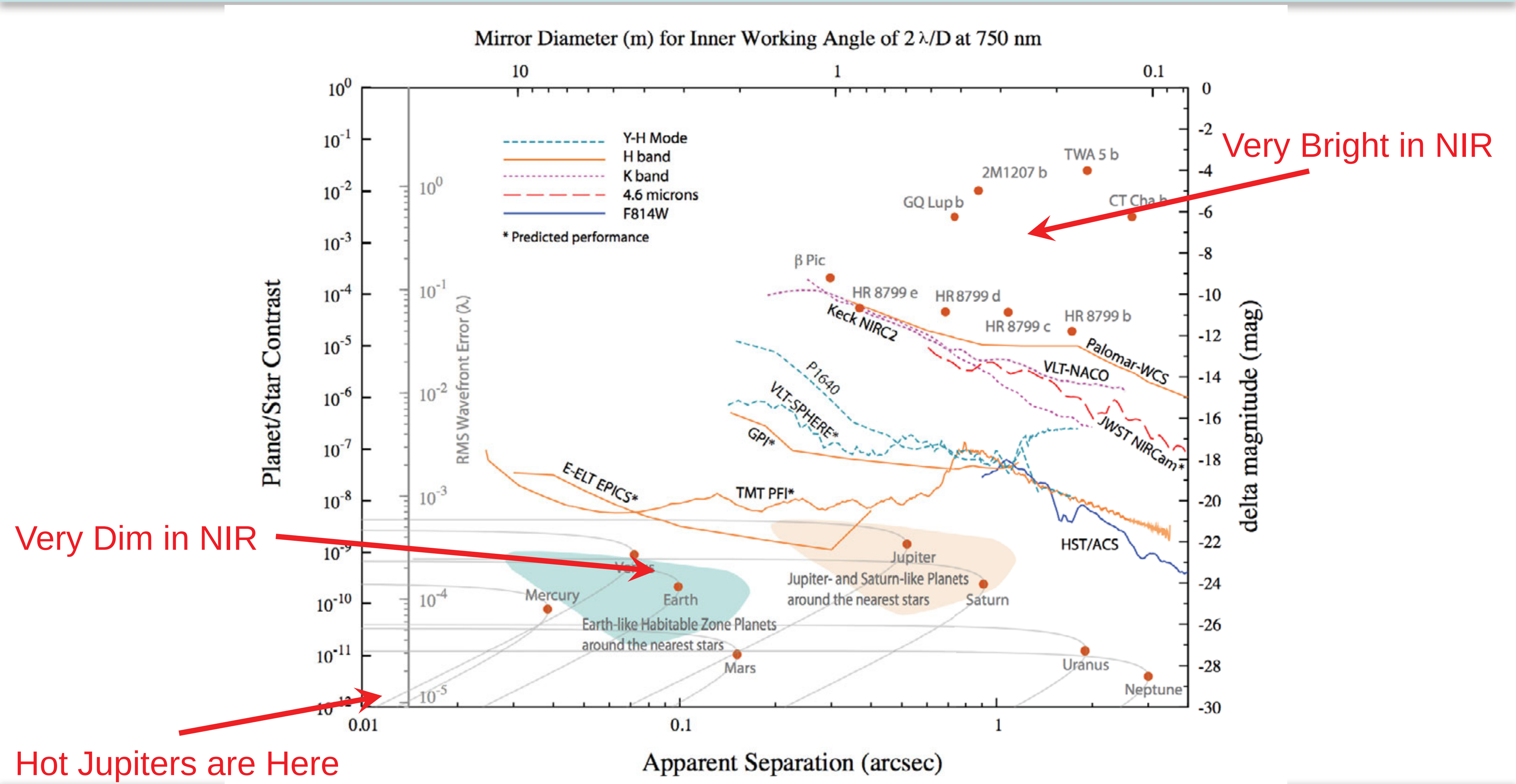

Direct Imaging Summary (With Existing Telescopes)

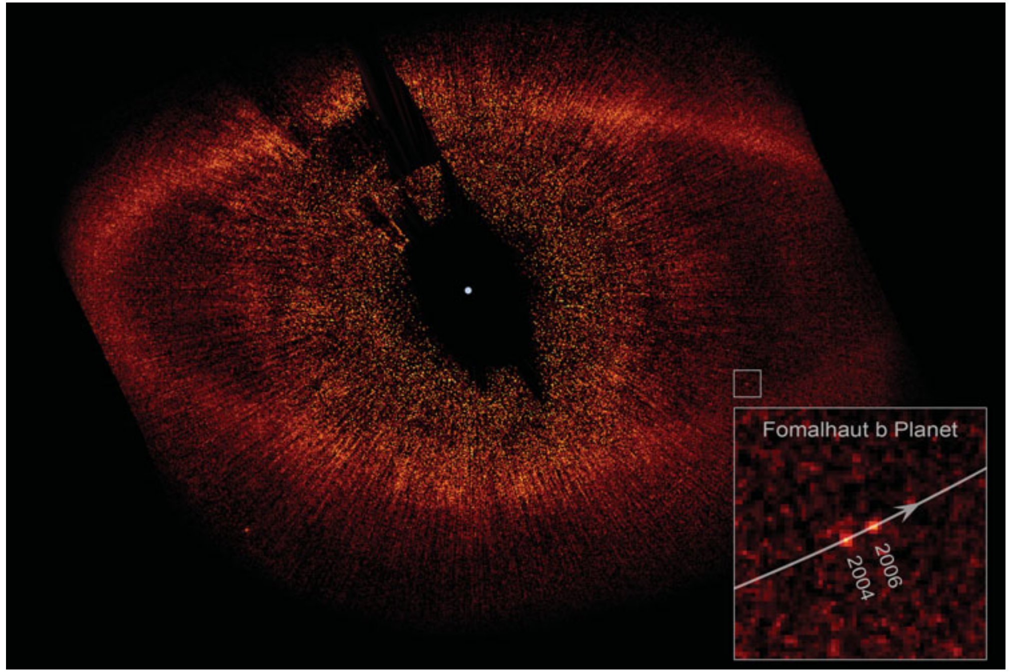

- Triumph of coronographic technique.
- In general, done in near infrared, where AO works best.
- Currently, can only image self-luminous planets, e.g. in debris disks during early formation phase.
- Currently restricted to planets at very large orbital radii, hence long period.
- Access stars more massive than F, where PRV becomes impossible.
- Best for face-on system *Sin i = 0* where PRV does not work.

Astrometry

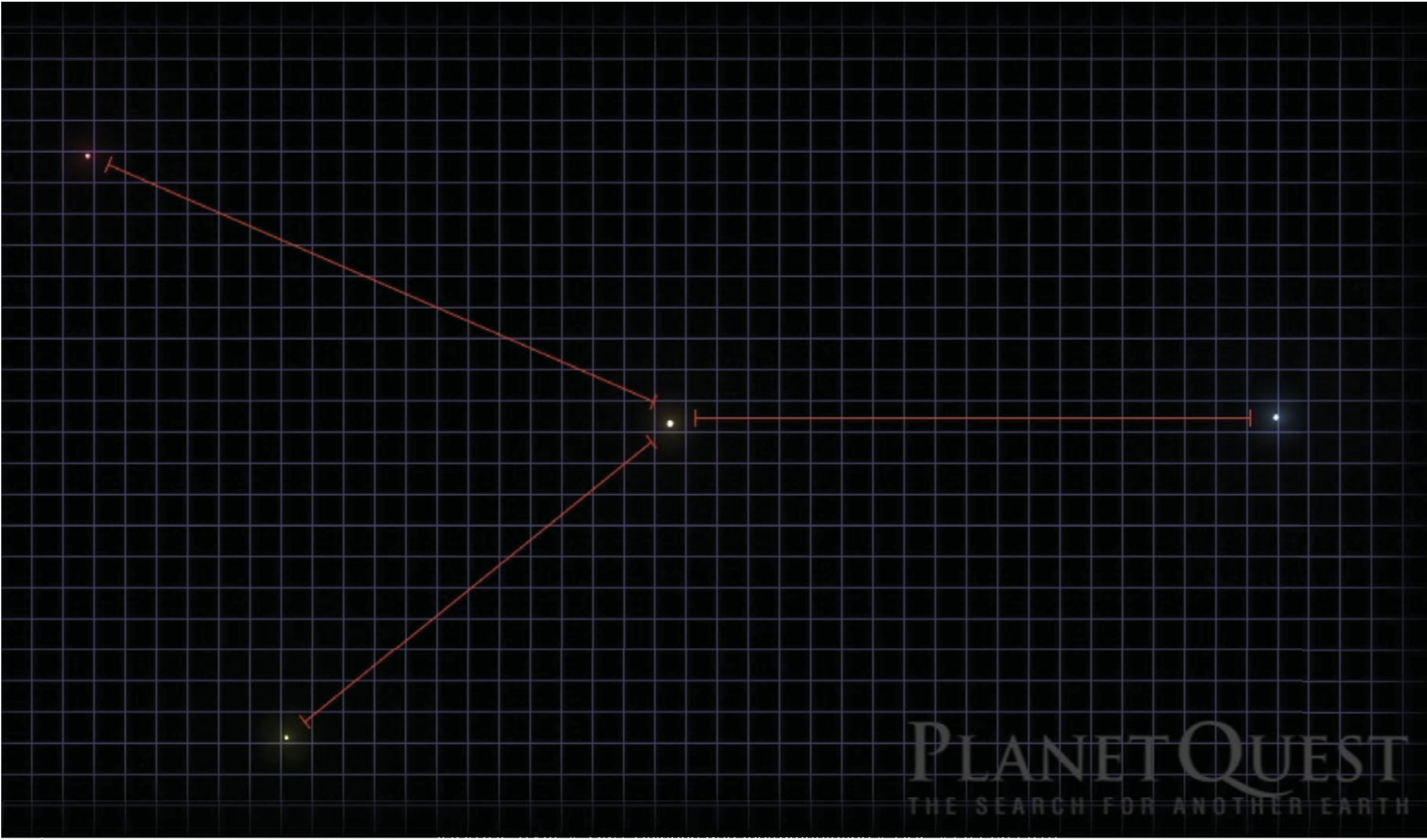
PLANETQUEST
THE SEARCH FOR ANOTHER EARTH

Solar System Influence on the Sun

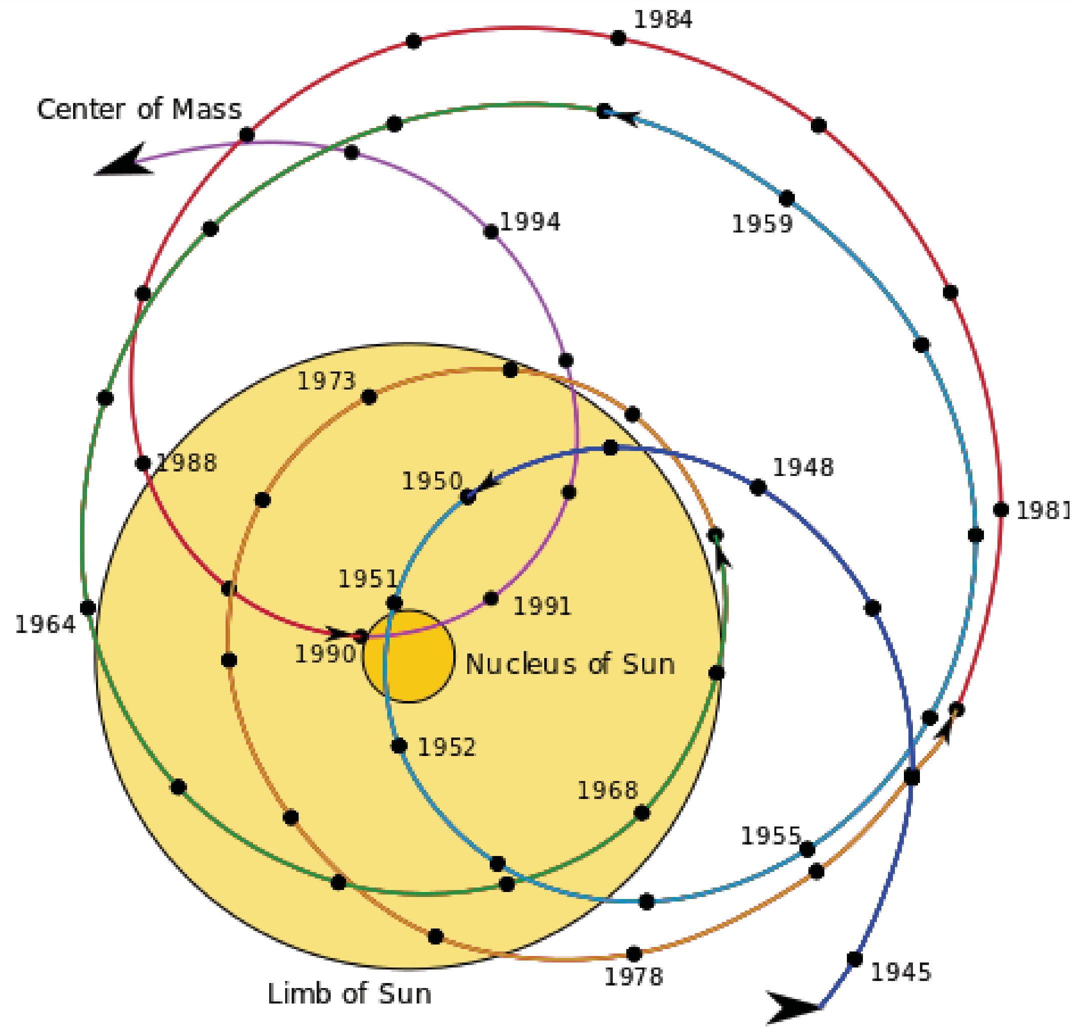

Exoplanet Astrometry Summary

- In 2009, a JPL team claimed detection of VB10b by astrometry;
  - “VB” = Van Biesbroeck;
  - A very, very nearby star.
- PRV did not confirm this result.
- Generally considered to be a null result.
- To date requirements for astrometric detection of exoplanet have exceeded capabilities, i.e. it’s too hard (impossible) to do with existing technology.
- Will probably require space-base (very expensive) interferometers to succeed.
- Measures exoplanet mass for face-on systems.
- When successful, when combined with PRV, will resolve *Sin i* ambuity for non-transiting systems.

Summarizing Existing Exoplanet Detection Methodologies

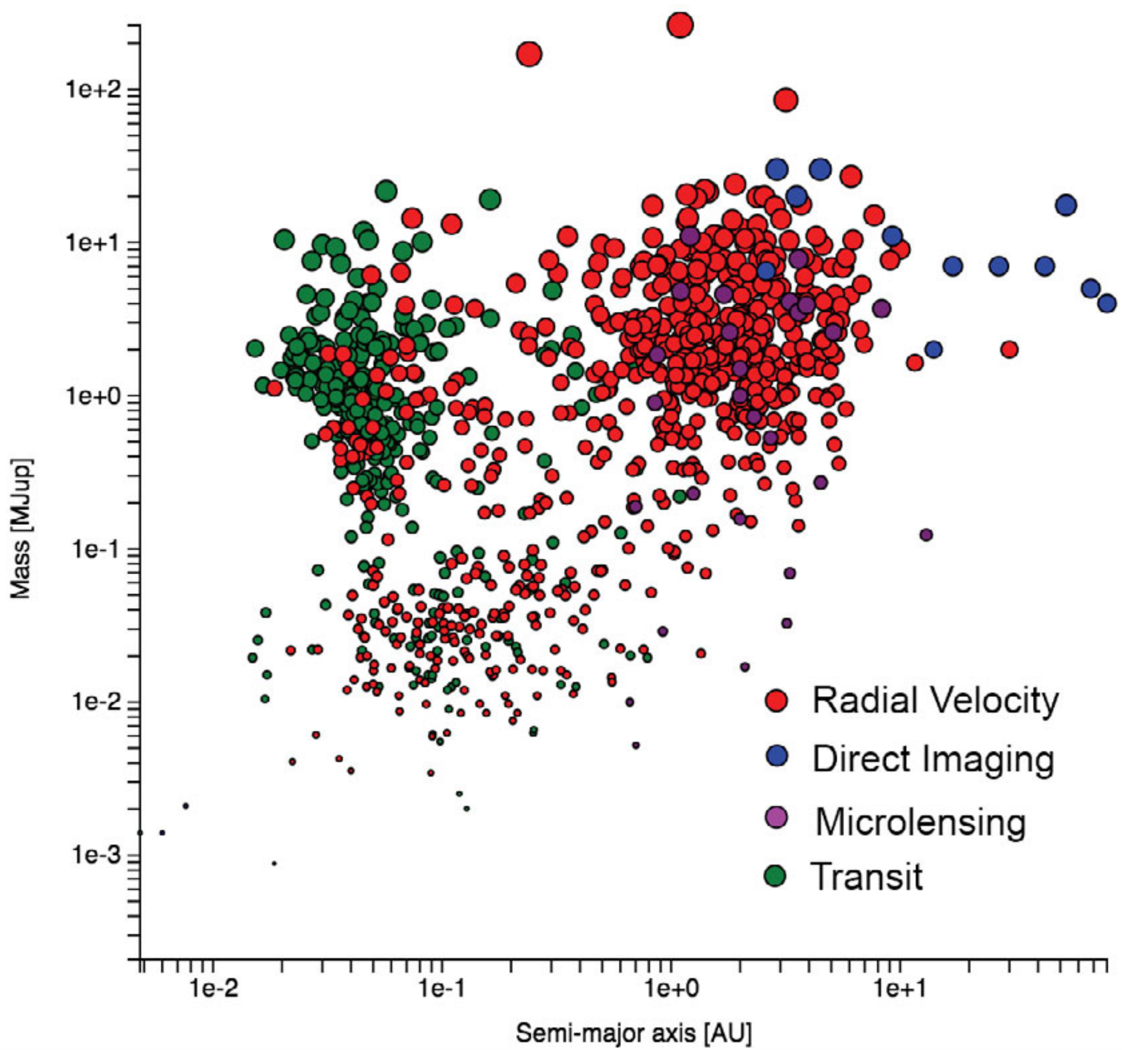

- Direct imaging detect exoplanets in very wide orbit.
- PRV measures broad range mass and eccentricity over broad range of semi-major axis sizes.
- Transit detection selects on short period system.
- Microlensing is very sensitive beyond the snow line for low mass exoplanets.
- More massive, short period exoplanets are easier to detect.

- Transits + PRV yield richest information.

"It's good to be good, better to be good and best to be both."

-Charles Saatchi

The Giant Magellan Telescope: A Tool for Finding Earth 2.0 and Biomarkers

The GMT is a Multi-Mirror Design

Site: Las Campanas, Chile

Optical / IR (0.32–25μm)

25.4 m diameter primary mirror

A mosaic of seven 8.4m mirror

Adaptive optics are intrinsic

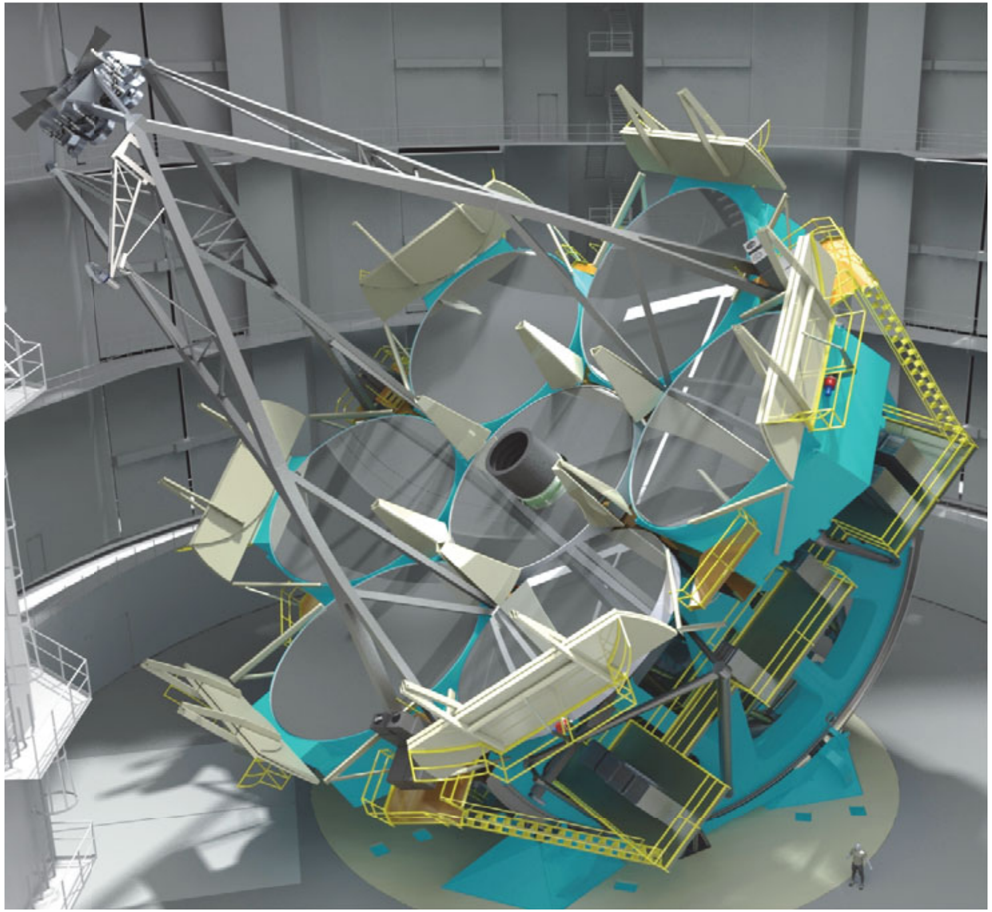

How Big is the GMT?

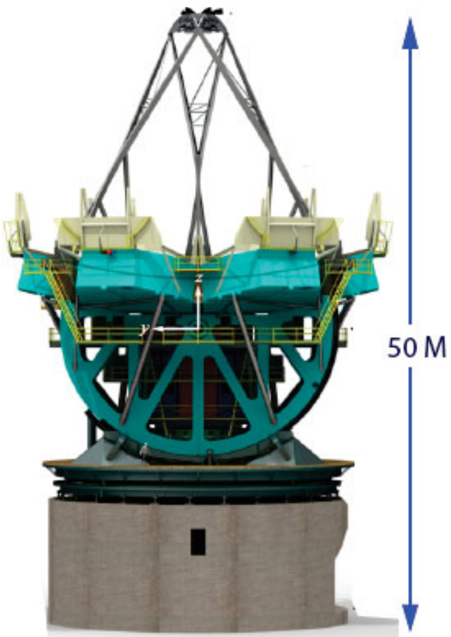

53 M

73 M

50 M
(b.1954)

The GMT-Consortium Large Earth Finder (G-CLEF)

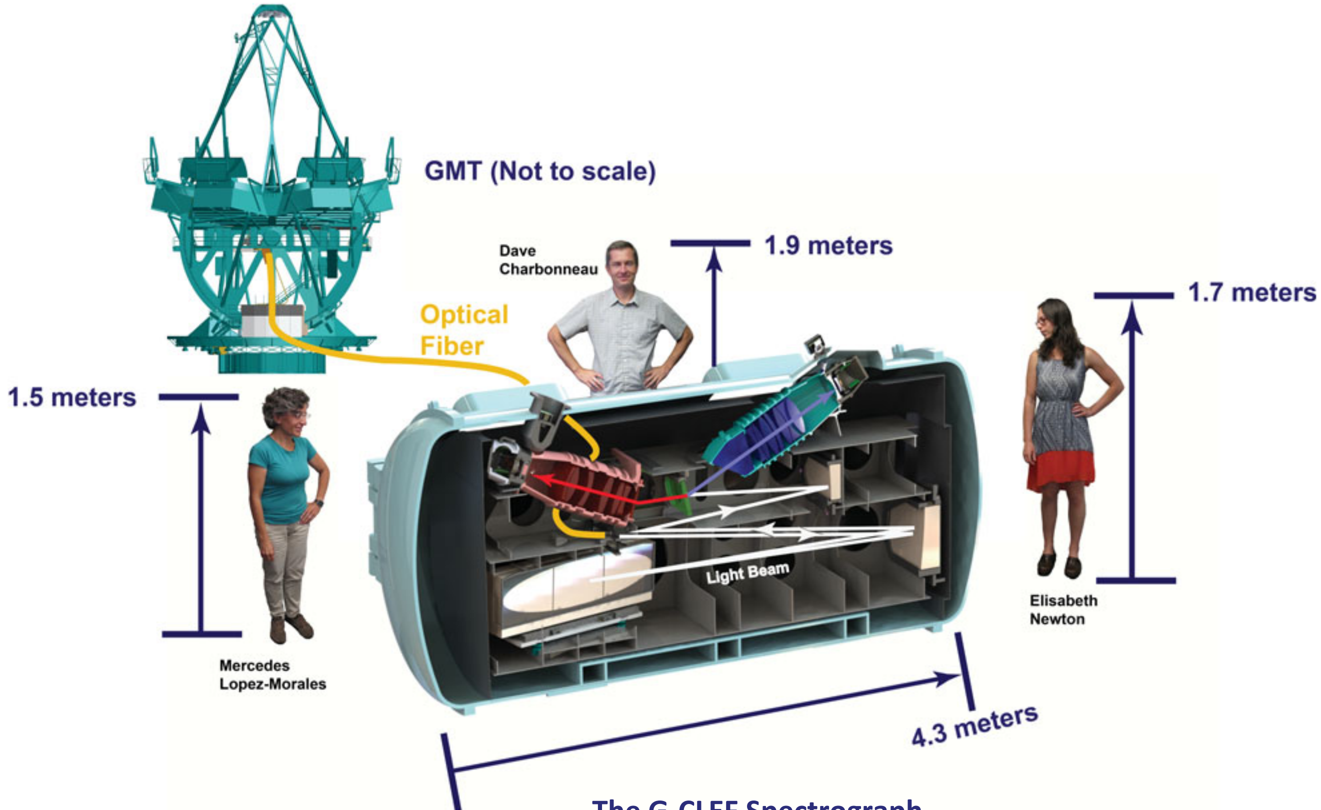

The G-CLEF Spectrograph

G-CLEF is designed to measure the mass of Earth-mass rocky planets orbiting Solar-type stars in the habitable zone.

- Requires 10 cm/sec – 5 time more precise than any existing spectrograph.
- G-CLEF must be more stable than all previous instruments.

The GMT-Consortium Large Earth Finder

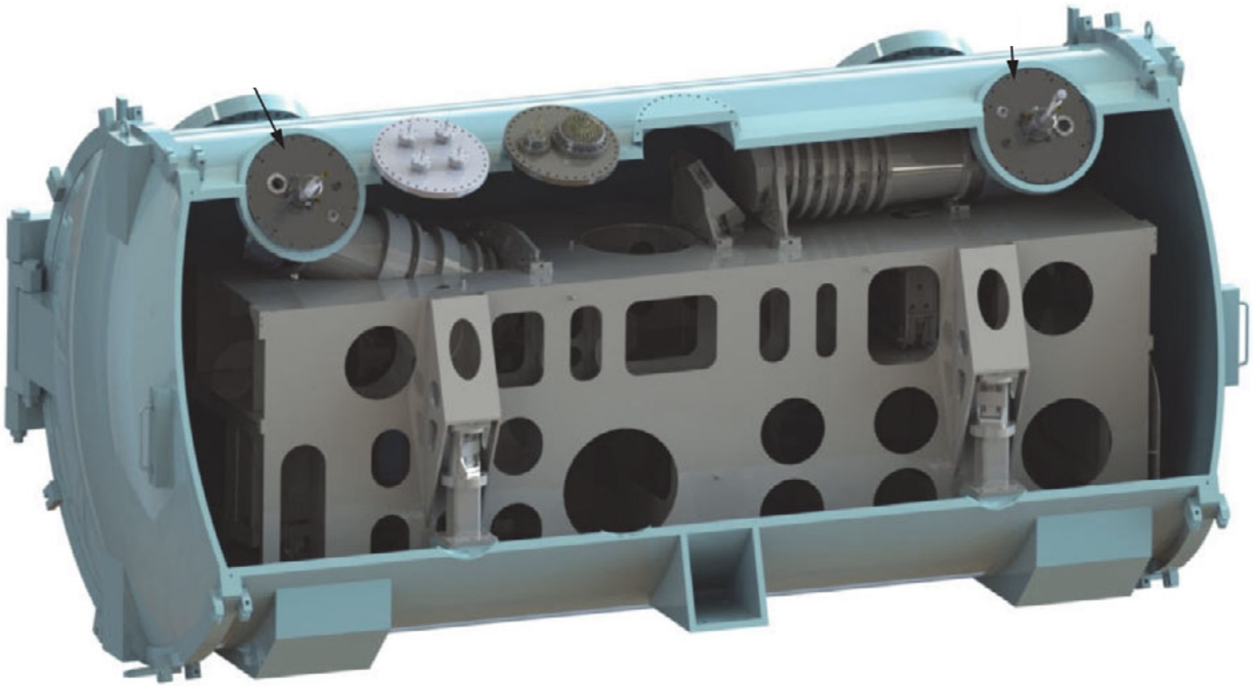

G-CLEF uses new technologies to exceed the performance of previous instruments.

G-CLEF is enclosed in a vacuum chamber, is thermally stabilized and fiber-fed to improve optomechanical stability for RV precision.

G-CLEF Optomechanical Design

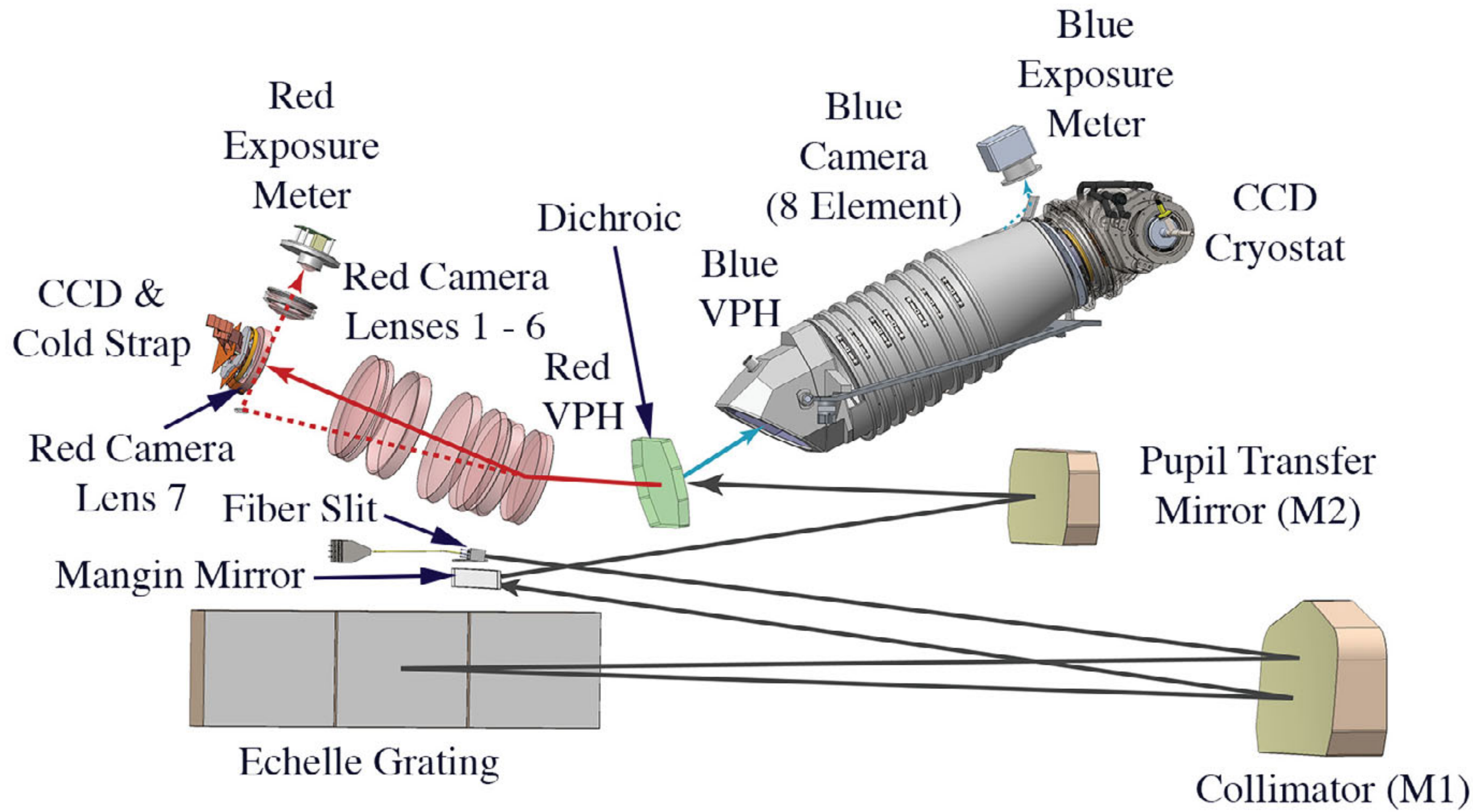

Why do we think we can get to 10 cm/sec?

G-CLEF is Deployed on a Gravity Invariant Location on the GMT

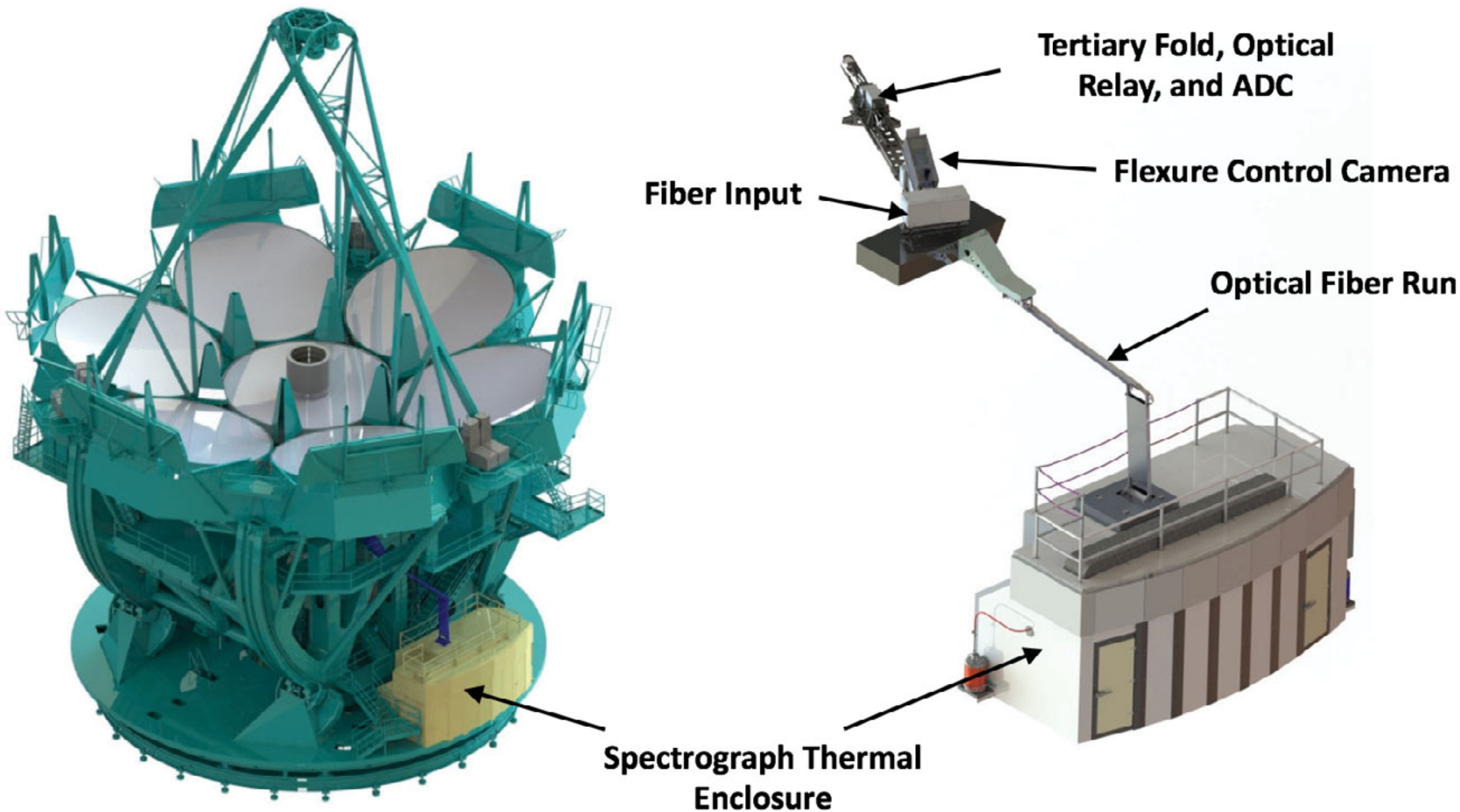

G-CLEF RV Precision Error Contributors are Tracked in a PRV Error Budget

Spectrograph Stability Terms

Values set by interactive analysis/budgeting process

REQUIREMENT BUDGET for PRV Error - Single Measurement Long Term Error (1 sigma)								
	RV ERROR (CM/SEC)							Comments
RV Error from an Observation Program	10							Many measurements with source errors
								(1/4 of single measurement error)
RSS Margin vs. Requirement	15							
Requirement		40						
Current Budget Estimate		37						
Post Calibration Residual Error			32					Formula: Cal error + Calibratable error/10
Calibration process accuracy				30				Based on ThAr source, data from HARPS
Calibratable Error Residual				2				
Calibratable Error Removal Accuracy (% of input)					10.0%			
Instrument Calibratable Errors					23			
Internal Pressure Stability						4		CoDR Analysis of Pressure rise
Spectrograph Mechanical Stability						16		
Acceleration changes							0	Moved to non-claibratable error term
External Pressure Variations							10	Changes in atmospheric pressure acting on housing
Moisture Effects on GREP Bench							10	Moisture Changes on GREP Bench
Material Instability							7	Long term Creep of metals and composites
Spectrograph Thermo-elastic Stability						5		Assuming .001 Degree C Stability
Soak							2.7	Results from October 2014 Quarterly
Lateral Gradient							1.6	Results from October 2014 Quarterly
Vertical Gradient							3.9	Results from October 2014 Quarterly
Detector Mechanical Stability						14		
Piston							6.0	SAO-INST-DOC-00101
XTilt							6.0	SAO-INST-DOC-00101
Ytilt							6.0	SAO-INST-DOC-00101
Lateral IMAD due to temperature							10.0	ALLOCATION pending Study results
Block Stitching Error						3		
Non-calibratable External Errors			10					
Telescope Tracking error				7				10,000 scrambling gain, 69 mas error
On-instrument Tracking error				5				10,000 scrambling gain, 49 mas error
Telescope Focus error				1				.2 mm focus error at 2 degree alignment error
On-instrument focus error				1				.2 mm focus error at 2 degree alignment error
ADC error				5				10,000 scrambling gain, 45 mas error
Non-calibratable Instrument Errors			15					
Stray Light				5				
Detector error				10				
Micro-vibration				0				Averages out per PDR comments received
Telescope Accelerations				4				
Micro-tilt of Azimuth Disk				7				
SW Fitting Error				6				
Barycentric correction error			2					
Custom Formula								
Analysis/Current Practice								
Allocation								
RSS Term								

G-CLEF Vacuum Stability and Base Pressure Are Lower than Previous Instruments

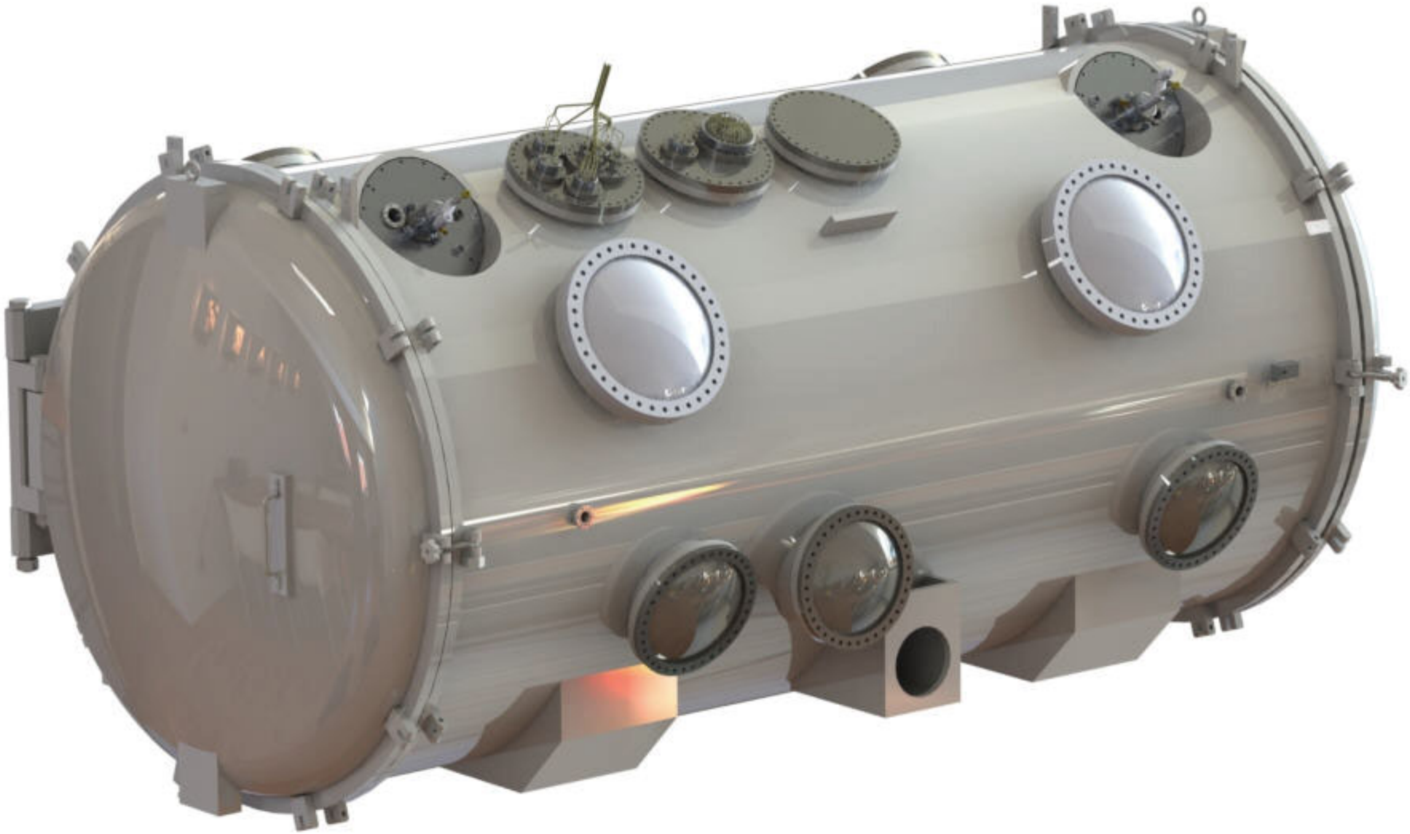

G-CLEF Vacuum Enclosure

STOP Modeling Predicts IMAD Directly

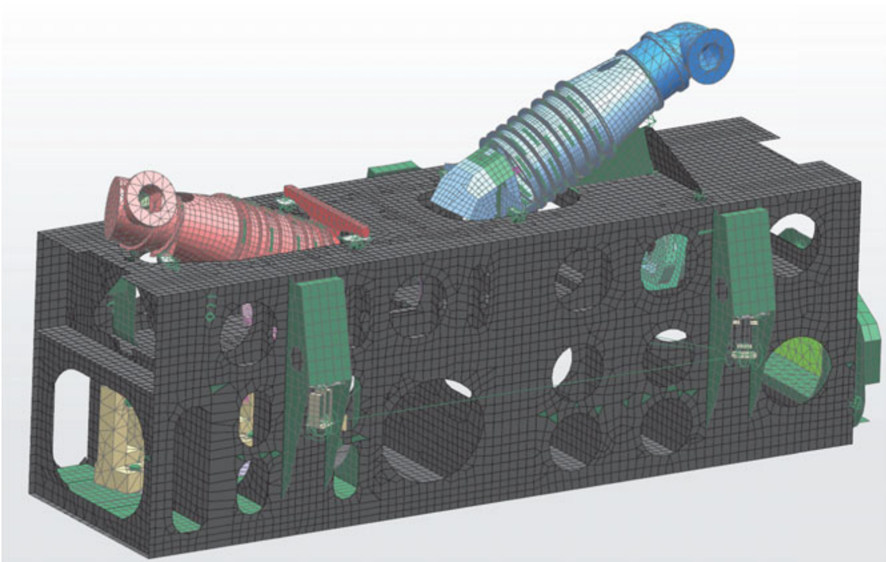

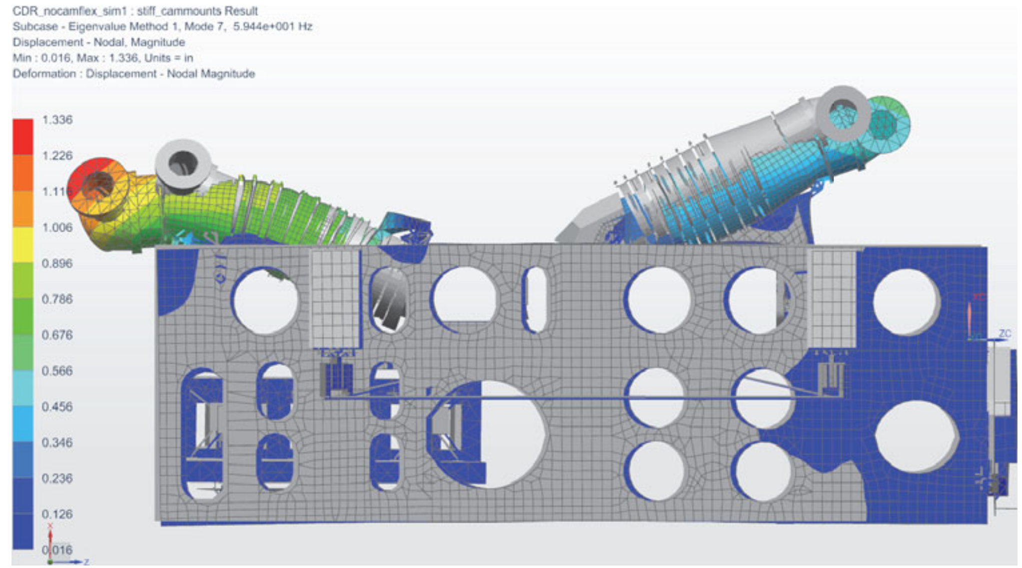

STOP = Structural Thermal Optical Performance

IMAD = Image Motion At Detector

MAD = Mutual Assured Destruction

Optical Bench is Constructed of Lowest Practical CTE Material

Load Case	Optical Bench Material	IMAD, Å Dispersion	PRV Budget	IMAD, % Budget
+0.001ºC Soak	CFRP	1.98	5.4 Å	37%
	Invar	0.68		13%
Vertical Gradient -0.0005ºC/+0.0005ºC	CFRP	1.82	3.2 Å	57%
	Invar	4.18		131%
Lateral Gradient -0.0005ºC/+0.0005ºC	CFRP	5.26	7.8 Å	67%
	Invar	64.4		826%
RSS	CFRP	5.91	10 Å	59%
	Invar	64.5		645%

CFRP CTE = -0.1 ppM/ºC, Invar CTE = 1.3 ppM/ºC
PDR model, red camera optical path

- **Carbon Fiber allows us to meet PRV performance allocation**
- **Invar exceeds PRV performance allocation by 6.5 X**

All precious PRV Spectrograph Optical Benches Constructed of Steel (CTE Steel = 12 ppM°/ C).
Thermal conductivity of CFRP order of magnitude higher than steel.

Spectrograph Thermal Control System Exceeds State of the Art

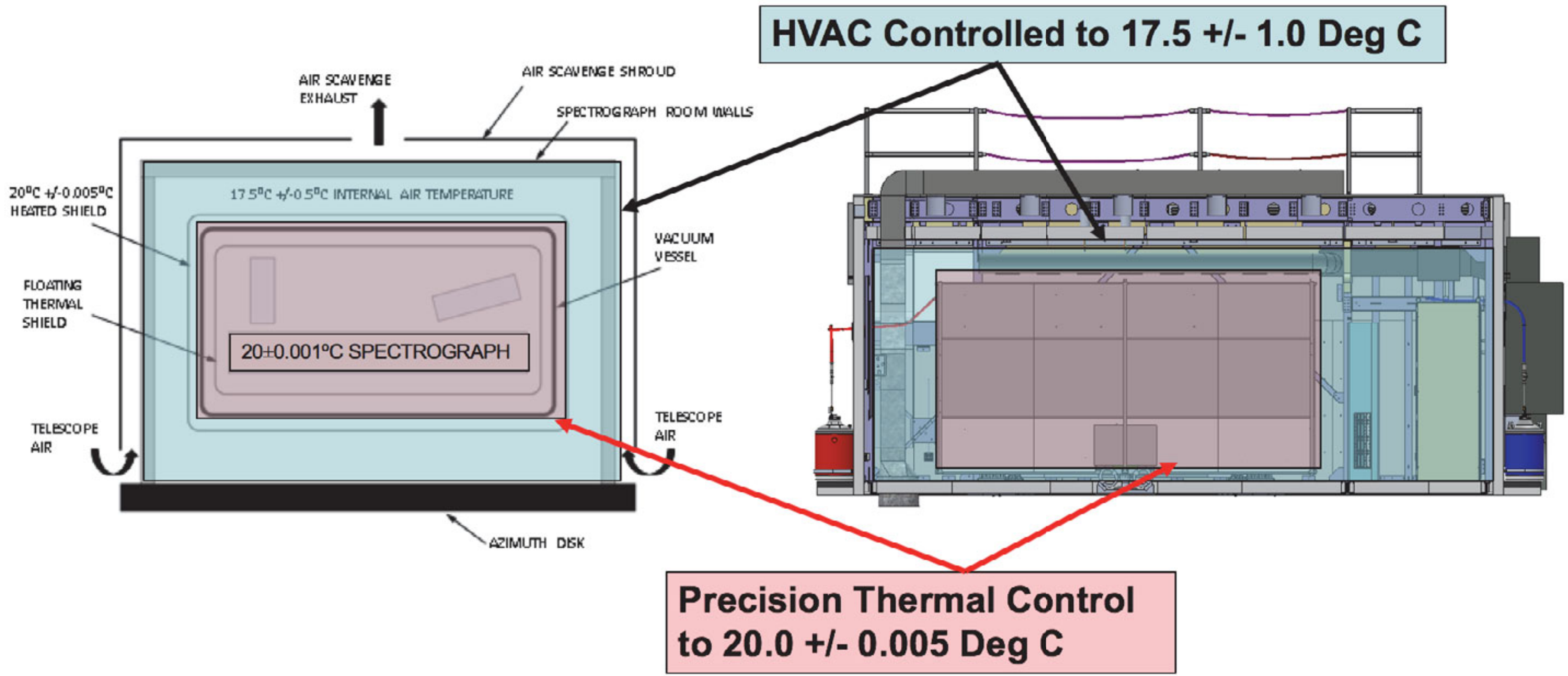

Thermal Control Schematic

Thermal Control Implementation

Thermal control of spectrograph and focal plane have been demonstrated by prototype.

Mechanical Error Allocations Mapped to RV Precision

Budget Term	PRV Allocation	Image Motion Allocation	Performance Solution Image Motion at Detector
Internal pressure variations	4 cm/sec	8 Å	0 Å (ion pumps stabilize operational vacuum)
External pressure variations	10 cm/sec	20 Å	19 Å (maximum daily pressure change of 10 mBar)
Moisture effects on GREP optical bench	10 cm/sec	20 Å	<20 Å (after 33 days initial pump-down)
Long term material creep/instability	7 cm/sec	14 Å	3.3 Å (based on initial CFRP temporal stability)
Spectrograph thermoelastic stability	5 cm/sec	10 Å	9.7 Å (-0.1 to +0.1 ppM/°C CTE bench, 95% confidence)
Detector thermoelastic stability	14 cm/sec	28 Å	8 Å (thermal variation at focal plane, cold finger variation)
Telescope accelerations	4 cm/sec	8 Å	0.5 Å (with self-leveling to 1 μ-radian resolution)
Microtilt of azimuth disk	7 cm/sec	14 Å	0.5 Å (with self-leveling to 1 μ-radian resolution)

PRV: Precision Radial Velocity

G-CLEF May Measure the Mass of an Exo-Mars

Planet	a (AU)	Reflex Velocity (K, m/sec)				
		G2V	M0V	M2V	M4V	M6V
Jupiter (318 M_{Earth})	0.1	89.8	116	136	201	284
Jupiter (318M_{Earth})	1.0	28.4	36.7	42.9	63.6	89.9
Jupiter (318 M_{Earth})	5.0	12.7	16.4	19.1	28.4	40.2
Neptune (17 M_{Earth})	0.1	4.8	6.2	7.2	10.8	15.2
Neptune (17 M_{Earth})	1.0	1.5	2.0	2.3	3.4	4.8
Super Earth (5 M_{Earth})	0.1	1.4	1.8	2.1	3.1	4.4
Super Earth (5 M_{Earth})	1.0	0.45	0.57	0.67	1.0	1.4
Earth	0.1	0.28	0.37	0.43	0.68	0.89
Earth	1.0	0.09	0.12	0.13	0.20	0.28
Mars	0.1	0.03	0.04	0.05	0.07	0.09
Mars	1.0	0.009	0.012	0.014	0.021	0.030

Current state of the art capability

Possible near-term state of the art capability

G-CLEF Spec

G-CLEF Goal

- G2V and M4V are reasonable “archetypes”.
- Habitable zone of M4V has range of periods 4.5 to 70 days.
- Habitable zone of solar type star ~1 year
- Goal of detecting Mars-twins within reach ≤

The GMT Will Trace the Entire (Exo)Planet Life Cycle